

PRESSURE BROADENING IN THE GAMMA-BANDS
OF NITRIC OXIDE

Thesis by

Walter Rollier Thorson

In Partial Fulfillment of the Requirements

For the Degree of

Doctor of Philosophy

California Institute of Technology

Pasadena, California

1957

ACKNOWLEDGEMENTS

I am grateful to Professor Richard M. Badger for his guidance, sound advice, and patient encouragement, especially at critical points in the work. He suggested the investigation and has consistently helped me to clarify my understanding of the problem.

I should also like to acknowledge the valuable discussions I have had with Dr. Oliver R. Wulf, Dr. Saul S. Penner, Dr. Dwight Weber, and Dr. Verner Schomaker.

I am very thankful to the United States Government for two National Science Foundation Predoctoral Fellowships. I wish also to thank the California Institute of Technology for financial assistance in the form of an Institute Scholarship and a graduate teaching assistantship, and E. I. Du Pont de Nemours and Co. for a summer research fellowship.

"Man shall not live by bread alone, but by every word that proceedeth out of the mouth of God."

ABSTRACT

The pressure broadening in the γ -bands of nitric oxide, which has been the subject of considerable controversy in the literature, has been studied quantitatively with the Cary Ultraviolet Spectrophotometer. The behavior of the optical density, as a function of total pressure and of the amount of gas in the path, has been investigated for the $\gamma(1,0)$ and $\gamma(0,0)$ bands. Both the nitric oxide self-broadening and the broadening by nitrogen were studied. The classical theory of Lorentz gives an adequate description of the effect. Curves of growth computed from a model of the spectrum near the band head of $\gamma(0,0)$ have been used to analyze the pressure effect quantitatively. Without recourse to absolute intensity data it is not possible to do more than show that the collision diameter is less than 9 Å. The recent measurements of intensity made by Weber and Penner permit the collision diameter to be estimated as 3.8 Å. By this criterion the pressure broadening cannot be called "abnormal."

The photographic work of Naudé on the pressure effect has given support to the suggestion of a large pressure broadening. A photograph taken by him shows no fine structure at a pressure of 450 mm Hg, and this was attributed to a broadening of the lines into one another. A photograph taken in this laboratory under the same conditions is in strong disagreement with his results, showing very clear fine structure. There exists

at present no other evidence on pressure broadening in the γ -bands which cannot be harmonized with the interpretation given above. It may be concluded that there is no evidence from the pressure broadening effect for a pressure-induced predissociation in these bands of nitric oxide.

TABLE OF CONTENTS

PART	PAGE
ACKNOWLEDGEMENTS	ii
ABSTRACT	iii
TABLE OF CONTENTS	v
LIST OF TABLES	vi
LIST OF FIGURES	vii
I. INTRODUCTION	1
II. EXPERIMENTAL	8
A. PREPARATION OF GASES AND SAMPLES FOR ANALYSIS	8
B. SPECTROSCOPIC TECHNIQUES	19
III. GENERAL FEATURES OF THE PROBLEM	28
IV. EXPERIMENTAL RESULTS	42
V. THEORETICAL CALCULATIONS	64
VI. ESTIMATE OF THE COLLISION DIAMETER	91
VII. ERRORS	97
VIII. PHOTOGRAPHIC INVESTIGATION OF EARLIER RESULTS	104
IX. CONCLUSIONS AND DISCUSSION	110
APPENDIX, PART I: DATA TABLES A AND B	117
APPENDIX, PART II: CALCULATION OF THE CORRELATION FACTOR BETWEEN THEORETICAL AND EXPERIMENTAL OPTICAL PATHS	133
REFERENCES	136
PROPOSITIONS	138
REFERENCES FOR PROPOSITIONS	142

LIST OF TABLES

TABLE	PAGE
1. Slit Widths and Spectral Widths in the Cary Spectrophotometer	23
2. Nitric Oxide Band Model	67
3. Results of the Calculation Based on Lorentz Contour	70

LIST OF FIGURES

FIGURE	PAGE
1. Nitric Oxide Potential Energy Curves	2
2. Nitric Oxide Generator	9
3. Nitric Oxide Purifying Train	10
4. Vacuum Manifold	11
5. Cell Manifold and Cell Construction	12
6. N ₂ Purifying Train	13
7. Spectrophotometer Optical System	24
8. Typical Spectrophotometer Tracings	26
9. Optical Density Versus Pressure of NO in Nitric Oxide Self-Broadening	45
10. Optical Density Versus Pressure of NO in Nitric Oxide Self-Broadening	46
11. Optical Density Versus Cell Path, Nitric Oxide Self-Broadening	47
12. Optical Density Versus Cell Path, Nitric Oxide Self-Broadening	48
13a. True Pressure Effect in Nitric Oxide Self- Broadening	51
13b. True Pressure Effect in Nitric Oxide Self- Broadening	52
14-20. Nitrogen Broadening of Nitric Oxide	55
21. Optical Density Versus Cell Path and Half-Width, for Calculation Based on Lorentz Contour	71

LIST OF FIGURES--Continued

FIGURE	PAGE
22. Theoretical Growth Curves for Combined Doppler-Lorentz Broadening	87
23. Theoretical Growth Curves for Both Calculations	89
24a. Collision Diameter Estimate	94
24b. Collision Diameter Estimate	95
25. SO ₂ Self-Broadening	113

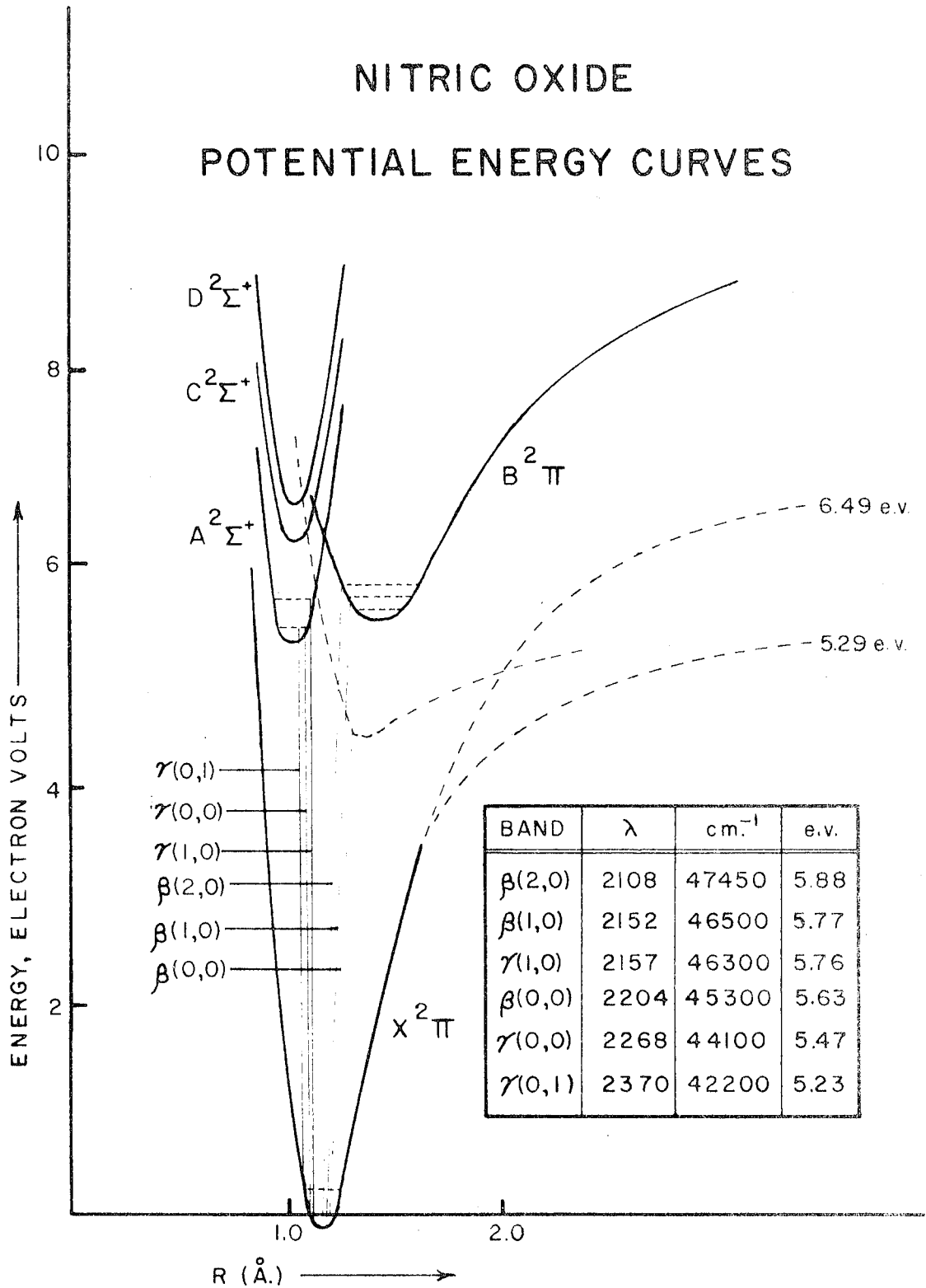
PLATE	PAGE
I. $\gamma(0,0)$ Band of Nitric Oxide	108

I. INTRODUCTION

The ultraviolet absorption bands of nitric oxide, especially those above 2000 Å, have been the subject of a number of investigations and considerable discussion (2-7). Most interest has been in the question of the apparent pressure broadening in the $\gamma(1,0)$ and $\gamma(0,0)$ bands at λ 2159 and λ 2268, respectively, and the $\beta(2,0)$ band at λ 2108. This question is of interest because the phenomenon may relate to the values of the dissociation energies of nitric oxide and nitrogen, which are of course tied together by thermal data and the known value of $D(O_2)$.

The term diagram for NO is shown in Figure 1. The ground state is $X^2\Pi$, with a doublet separation of 120 cm^{-1} , the $^2\Pi_{3/2}$ state lying the higher (normal order). The ground state curve has been extrapolated to two limits, corresponding to the two disputed values for $D(NO)$, 5.29 e.v. and 6.49 e.v. The known excited states in order of increasing energy are $A^2\Sigma^+$, $B^2\Pi$, $C^2\Sigma^+$, $D^2\Sigma^+$, ... In addition, Mulliken (1) predicted a number of other states, one of which, a $^4\Pi$ state, is of especial importance to the problem being considered, and is indicated by a dashed line in the diagram. The γ -band system, which is the most prominent in absorption, involves transitions to the $A^2\Sigma^+$ state; the β -band system, to the $B^2\Pi$ state. It will be noted that the upper levels involved in the $\gamma(1,0)$ and $\gamma(0,0)$

FIGURE 1:



bands are 5.76 and 5.47 e.v., respectively, above the ground state, and are intermediate between the two proposed dissociation limits. For this reason any abnormal behavior in these bands might be of significance in determining the dissociation limit; and just the kind of abnormality one might expect was reported early in the study of NO.

The ${}^4\Pi$ state as predicted by Mulliken crosses the $A^2\Sigma^+$ state near its lower vibrational levels, but never intersects the $B^2\Pi$ state. If the lower value for $D(\text{NO})$ were correct, a radiationless transition into this ${}^4\Pi$ level from the $A^2\Sigma^+$ state would bring about a dissociation of the molecule. This would be an intercombination, and is therefore forbidden, but under the influence of external field perturbations during collisions with other molecules the selection rules could be sufficiently altered to permit a "pressure-induced predissociation." This explanation was put forward by Wulf (5) to account for the observations made by Lambrey (2) and Naudé (6). On the other hand, even if the higher value for $D(\text{NO})$ were correct, the possibility still remains that radiationless transitions into the ${}^4\Pi$ state could take place. The probability of such transitions would tend to be less than for transition to a continuum, and would tend to be non-uniform for different lines, because of the discrete character of the levels of the ${}^4\Pi$ state, but if the state has a very broad minimum, the situation would more and more closely approximate that of a continuous distribution of energy levels. Consequently,

while a strong pressure broadening effect may be interpreted as arising because of an induced predissociation, it is not in itself an unambiguous indication that the energy levels showing such broadening are above the dissociation limit.

In any case, the purpose of this investigation was not to consider the theoretical problem of interpreting the pressure broadening, but rather to quantitatively describe that broadening. Lambrey (2), who was the first to report any anomalous behavior, studied the absorption spectrum above $\lambda 2000$ by photographic methods over a range of pressures from 4.6 to 650 mm Hg total pressure, and cell paths from 0.4 to 2 m long. He also studied the effect of added inert gas on the spectrum. His results demonstrate that the optical density in the $\gamma(1,0)$ and $\gamma(0,0)$ bands varies as a function of $(lp)P^{0.8}$, where l is the cell path, p the partial pressure of NO, and P the total gas pressure. However, Lambrey incorrectly concluded that the density was proportional to $lpP^{0.8}$. Because of this, his results have sometimes been disregarded. Lambrey also studied the much weaker band $\beta(2,0)$ and found no such pressure effect. Naudé (6) observed the qualitative effect of about 440 mm of added nitrogen on the spectrum of the $\gamma(1,0)$ band, in a path 90 cm long filled with NO at 21 mm Hg. He found that lines separated by an Angstrom appeared distinct initially, but upon addition of the nitrogen "every rotational line is broadened so much that absorption becomes complete between them." Mayence (3) made

a study of these bands and others in the vacuum ultraviolet region with low resolution. She disagreed with Lambrey's conclusions, but corroborated his results for the γ -bands. However, she found that the β -bands and δ -bands in the vacuum ultraviolet also show the same pressure effect as the γ -bands. Her conclusions were that the optical density, d , can be expressed as follows:

$$d = c\sqrt{\lambda p P}$$

However, her data alone do not conclusively demonstrate this. Gaydon and Fairbairn (7), having found no apparent anomalies in the emission spectrum of NO, studied absorption bands $\gamma(1,0)$ and $\gamma(0,0)$ with a cell path of 15 cm and pressure p of 2.0 mm NO, and one atmosphere of added nitrogen. They were able to resolve the fine structure quite clearly, and dispute the question of whether there really is a significant broadening of the lines at all. Marmo (4) has studied the vacuum ultraviolet absorption spectrum of NO with a photoelectric recording spectrophotometer, with fairly good resolution (up to 0.2 Å), and has found "apparent absorption coefficients" (Section III) for most of the region $\lambda 1050$ to $\lambda 2272$, at various pressures with a cell 4.70 cm long. An apparent pressure effect was observed by him in all systems. He also observed a true pressure effect in the $\gamma(4,0)$, $\delta(0,0)$, and other bands, by observing the effect of adding methane, but he has published no quantitative data about it. Without recourse to the results

of Lambrey, it is not possible to determine conclusively if the apparent pressure effect is actually partly due to line broadening or is only the result of incomplete resolution, since Marmo did not have any means of studying the variation of optical density with cell path, in order to isolate effects due to incomplete resolution from the true pressure effects.

The investigation reported here consists of three parts. The first is experimental, and consists of a study of the $\gamma(1,0)$ and $\gamma(0,0)$ bands at various pressures and three cell paths, using an ultraviolet spectrophotometer with good resolution. Both nitric oxide alone and nitric oxide pressure-broadened by nitrogen were studied. The dependence on the optical density at the peaks of the spectrum upon the pressure and cell path has been obtained. The $\beta(2,0)$ band was studied qualitatively, but was too weak for reliable results. The results agree substantially with those obtained by the workers mentioned, and prove conclusively that there is a measurable pressure effect. The second part consists of theoretical calculations on a model of the spectrum; the results obtained are in agreement with the experimental behavior, and provide a method of estimating the collision diameter for the molecule in the $A^2\Sigma^+$ state. The third part is a photographic reinvestigation of the experiments of Naudé and of Gaydon and Fairbairn; our results disagree with those of Naudé, showing very clear fine structure in the region where he concluded

that the lines are broadened completely into one another. It has further been shown by this investigation that nitrogen is just as effective as NO itself in causing line broadening in these bands.

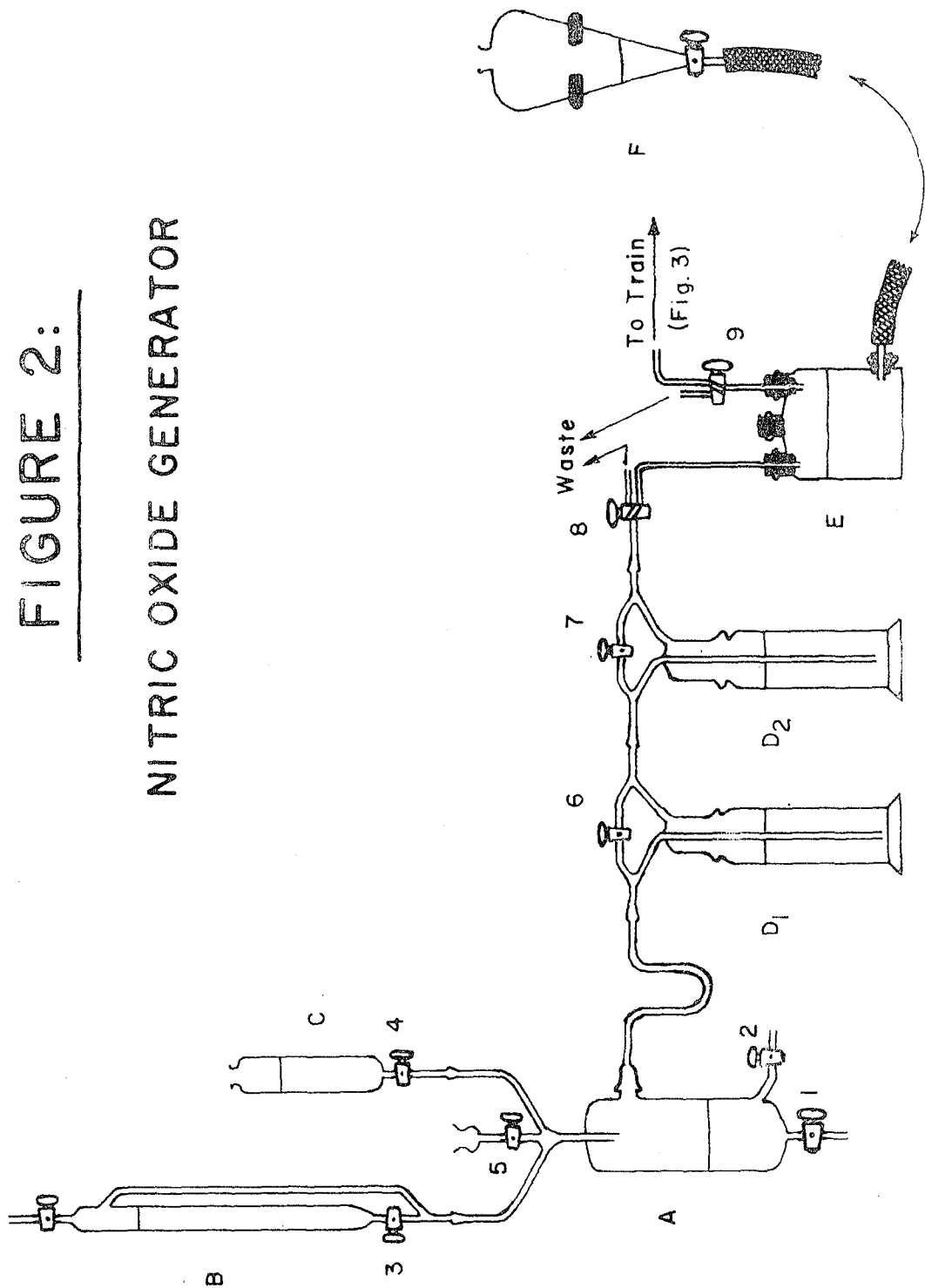
II. EXPERIMENTAL

A. PREPARATION OF GASES AND SAMPLES FOR ANALYSIS

Nitric oxide was generated in the apparatus shown in Figure 2, by filling the generator A, which had a capacity of about 500 cc, with approximately 150 cc of a solution containing 167 g KI and 333 g KNO_2 per liter, and adding 50% H_2SO_4 dropwise from the feeder B. Additional iodide-nitrite solution could be added from the feeder C. Before the generator was started, the whole train as far as the transfer bottle E was flushed with pure nitrogen. The gas evolved was passed through a washing bottle D_1 filled with 94% sulfuric acid, and then through one D_2 containing a 50% solution of KOH; these two scrubblings removed iodine and much of the NO_2 . The rate of evolution was difficult to control because of poor mixing in the generator. The gas was collected in the transfer bottle, displacing the dibutyl-phthalate which was used as a level control, until about 300 cc was accumulated; then the two-way stopcock #8 was switched so that the generator discharged into the waste line. The gas collected in the transfer bottle was discarded until it formed NO_2 upon discharge into the air; subsequent batches were cautiously transferred via stopcock #9 through a calcium chloride drying tube and into the primary collecting trap H (see Figure 3), which was cooled in a liquid nitrogen bath. Both the drying tube

FIGURE 2:

NITRIC OXIDE GENERATOR



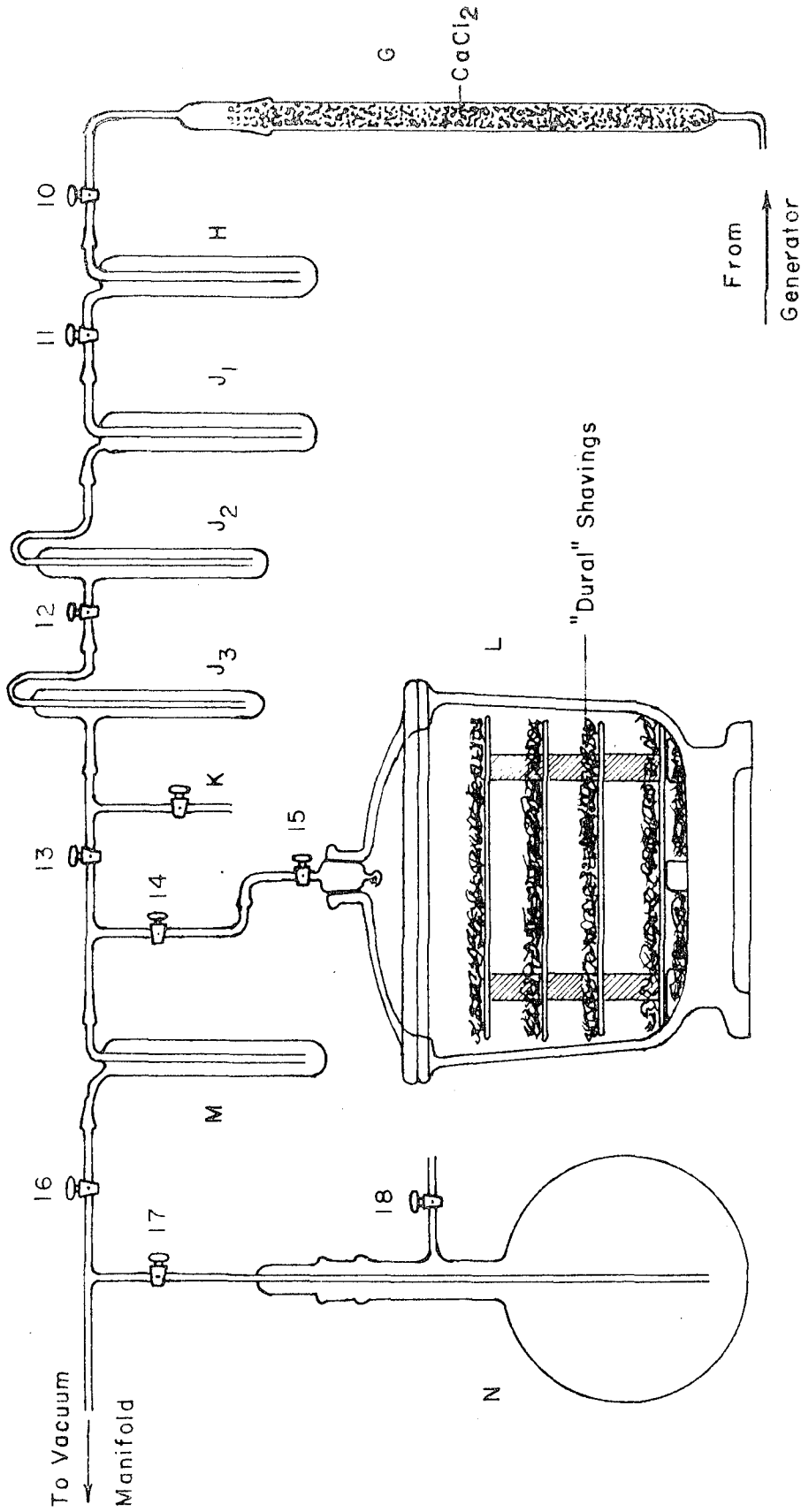


FIGURE 3:
NITRIC OXIDE PURIFYING TRAIN

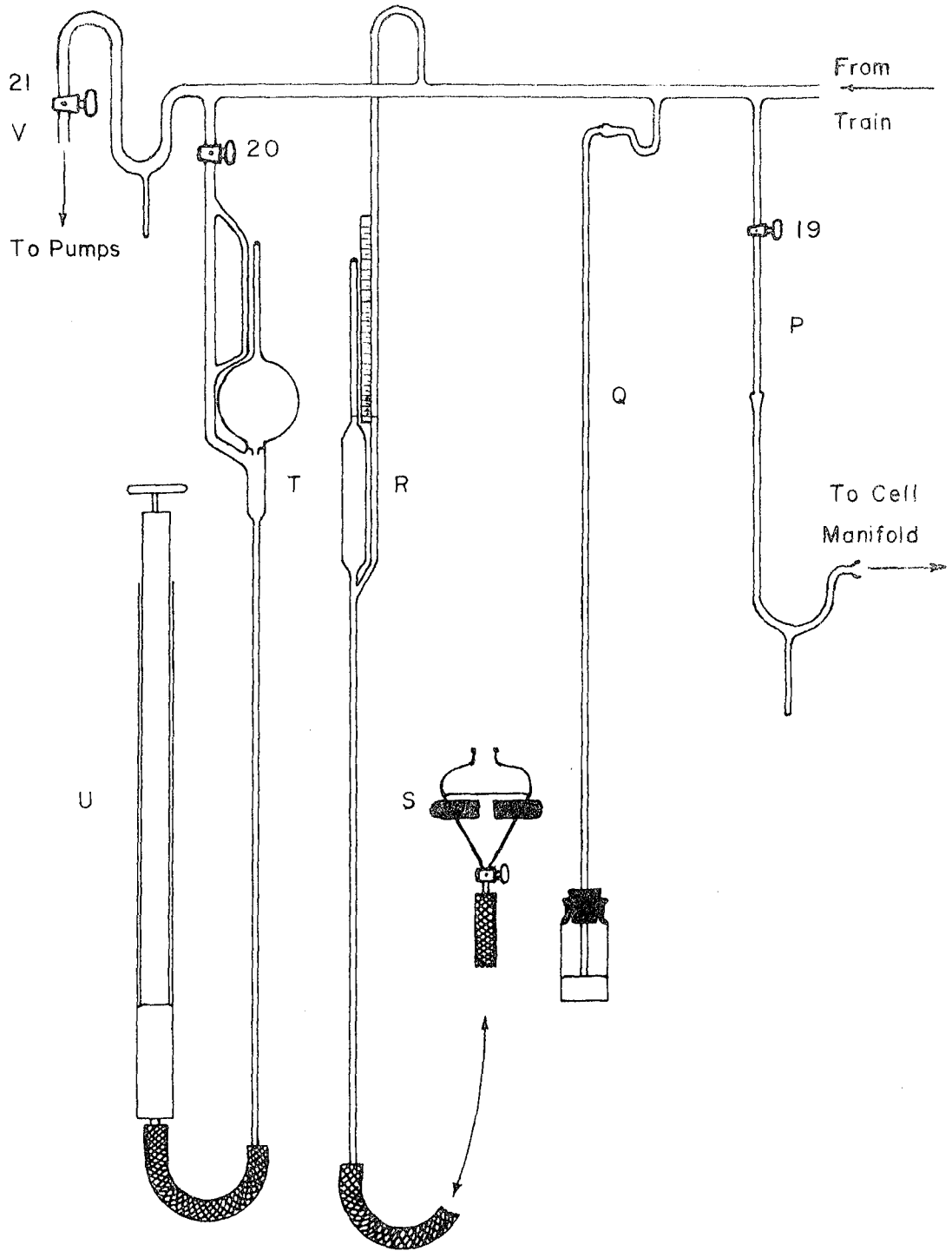


FIGURE 4:
VACUUM MANIFOLD

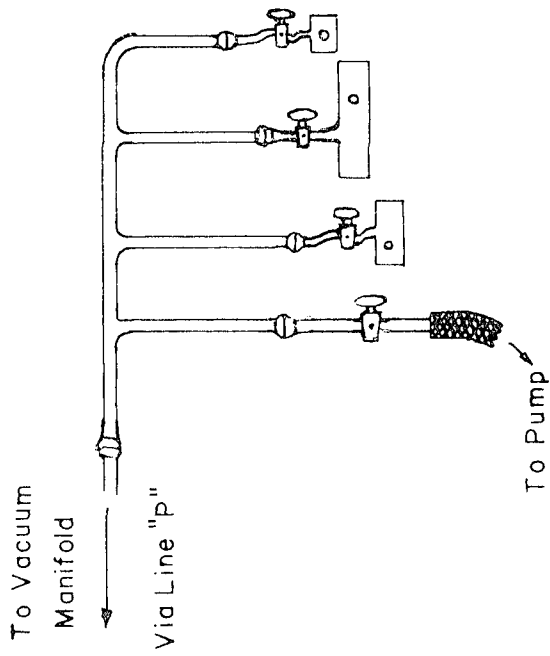
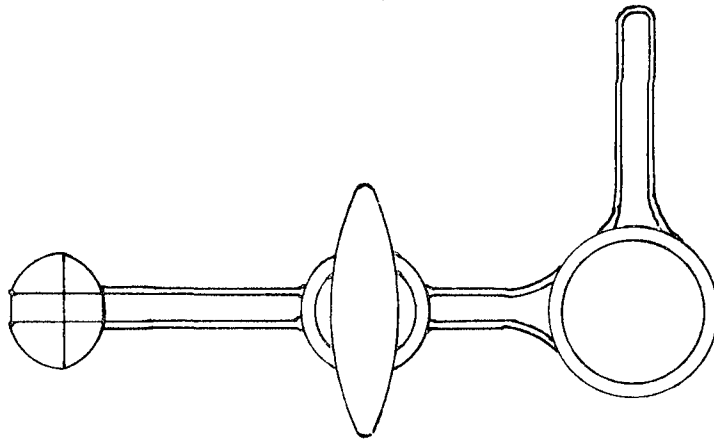


FIGURE 5:

CELL MANIFOLD & CELL CONSTRUCTION

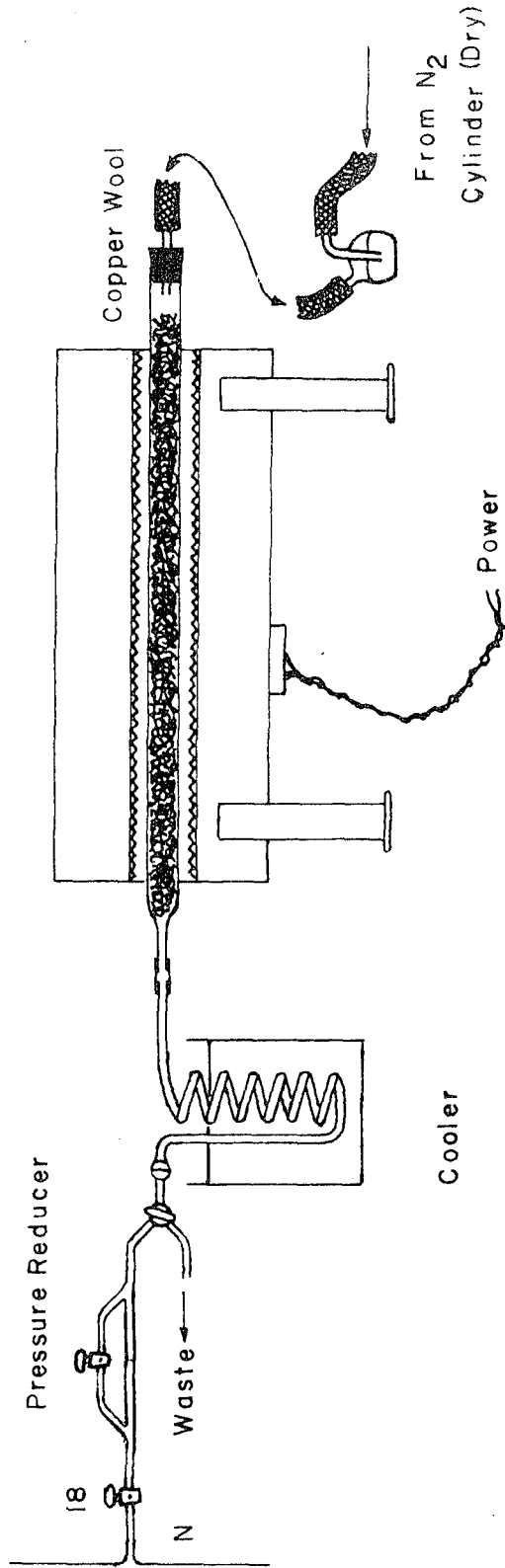


FIGURE 6:

N₂ PURIFYING TRAIN

and the trap were initially evacuated. When the contents of the transfer bottle had been shifted to H, then stopcock #9 was closed and the generator line again opened at stopcock #8. By this method the nitric oxide was collected in batches of 300 cc at atmospheric pressure, and each batch transferred to the collecting trap. The process was continued until about 10 g of solid NO had been condensed in the trap H. The use of dibutyl-phthalate in the transfer bottle showed no observable effect on the gas; however, in time a yellow color was imparted to the dibutyl-phthalate, apparently from its action on the "Koroseal" tubing which connected the transfer bottle to the leveling reservoir F.

The NO thus condensed in the trap H had intense brown, blue, and green colorations, due to water and nitrogen dioxide impurities. It was purified by simple distillations through the three traps J_1 , J_2 , J_3 , the last fractions being discarded through the waste outlet K. The resulting product collected in the trap M was a grayish-white solid, a light blue-green liquid. At this point the gas thus purified was evacuated while frozen, to remove the nitrogen collected from the generator train; then it was evaporated into the evacuated storage tank L, a large vacuum desiccator which had been packed with "Dural" alloy and aluminum shavings, and stored there permanently. The aluminum apparently reacts with NO_2 , because if impure NO stands for about two weeks over it, it no longer will have any green coloration when condensed, but becomes the light

blue reported in the literature, and the ultraviolet absorption spectrum is freed from NO_2 or N_2O_3 absorption. The reaction quite probably produces nitrogen, since a small pressure of non-condensable gas always resulted after impure NO had been stored inside. The reaction is most likely catalyzed by small amounts of water on the surface of the metal.

Although the cobalt indicator in the drying tube showed that the drying capacity of the calcium chloride had not been exhausted, it would probably be more effective to use phosphorus pentoxide as a drying agent.

To fill cells for the photographic work, the cell, which was fitted with a ball joint, was attached directly to the cell-filling line P (see Figure 4), gas was admitted from the trap into the evacuated line until the desired pressure was attained, and the pressure was measured with a scale attached to the open-end manometer Q. Then the cell was closed, and the excess nitric oxide was re-condensed in the trap M before detaching the cell.

To fill the cells for the NO self-broadening experiments, a cell manifold (see Figure 5), was constructed so that several cells could be filled simultaneously, and this manifold was attached to the filling line. Instead of a fourth cell, if desired a bypass line to the forepump could be attached to the manifold. Then the part of the system which included the pressure gauges, the filling manifold, and the attached

cells was evacuated; for this purpose, it was found that the mechanical pump was adequate to remove any significant amounts of oxygen. At the same time, NO was being condensed from the storage tank into the trap M; when sufficient had been collected, the stopcock #14 was closed, and the trap was opened through the stopcock #16 to the vacuum line to remove non-condensable gases. After pumping for a short while, the pump was cut off at stopcock #21, the liquid nitrogen bath was removed from M, and nitric oxide was evaporated into the system until the manometer indicated the desired approximate pressure. Then #16 was closed again, and the liquid nitrogen bath replaced at M. The pressure of NO was measured with the calibrated gauge R if the pressure were less than about 60 mm Hg, and with the manometer if it were greater (the gauge R worked basically on the same principle as a McLeod gauge). After measurement of the pressure, the cell stopcocks were closed, the stopcock #16 was opened to recover the excess NO, and then closed again. Next the stopcock #19 on the filling line P was closed, and finally the cells were detached and the spectra taken immediately. After the spectra were taken, the cells were re-attached, to the manifold, but not opened, and the manifold and gauge lines were evacuated as before. The cells were opened to the manifold at the time when NO was being added from the trap M. Subsequent procedure was a cyclic repetition of the above; in this way a series of spectra at steadily increasing pressures was ob-

tained.

After the nitric oxide self-broadening experiments, a sufficient amount of NO was prepared and stored in the storage tank, and the generator and purifying train were removed to make room for other apparatus.

Nitrogen for the nitrogen-broadening experiments was purified in the apparatus shown in Figure 6. Linde Pure "Dry" Nitrogen was bubbled through a mercury rate indicator and thence into a fused quartz tube packed with copper wool, which had been previously cleaned with concentrated ammonium hydroxide, dried and heated to about 400°C with nitrogen passing through it. The tube was inside a tube furnace operated at about 400°C . The hot gas then passed into an ice-water cooler and then through a stopcock and pressure-reducing device to the storage tank N, which was attached to the vacuum system through stopcock #17. The storage tank was initially evacuated, while the best operating pressure in the purifying line was about atmospheric pressure. In spite of the pressure-reducing device, it proved extremely difficult to maintain steady flow rates with such a drop in pressure. By constant supervision, however, it was finally possible to fill the 5-liter storage tank with nitrogen at one atmosphere. When the nitrogen had been purified, the reservoir was sealed off at stopcock #18 and the apparatus was dismantled.

The following procedure was employed to fill the cells for studying the pressure broadening by nitrogen:

1. A definite amount of nitric oxide was added to the cells, and the partial pressure of NO measured. Then the spectrum was taken of this initial sample.

2. The cells were next re-attached to the cell manifold, and the small side-arms provided on each cell were immersed in liquid nitrogen. (The cell stopcocks remained closed). The vacuum manifold and cell manifold were evacuated thoroughly.

3. After the side-arms had been immersed in the liquid nitrogen baths for a sufficient time to freeze out the nitric oxide present in the cells, operations to add nitrogen to the cells were begun: the vacuum line was closed off by means of stopcock #21, then by opening stopcock #17 nitrogen was admitted to the system until the manometer Q indicated approximately the desired pressure, and then #17 was closed.

4. The cell stopcocks were opened in cyclic order and then immediately closed in the same order. Then the liquid nitrogen baths were removed, and the pressure in the vacuum manifold was measured with the gauge R, or with the manometer, if the pressure exceeded about 45 mm Hg.

5. Stopcock #19 was closed, the cells removed and the spectra obtained. Care was taken to warm the cell side-arms to room temperature before taking the spectra.

6. After the spectra were obtained, the cells were again attached to the cell manifold and the side-arms placed in the liquid nitrogen baths. The pump bypass shown in Figure 5 was employed to remove air from the cell manifold. Then the pump

stopcock was closed, and stopcock #19 was opened. Subsequent procedure beginning at step 3 was a cyclic repetition of the above, with steadily increasing pressure of nitrogen added in each cycle. A given series of such measurements at a constant partial pressure of NO is designated a "series" in the tabulated data of Appendix, Data Table B.

B. SPECTROSCOPIC TECHNIQUES

Two basic methods of studying the pressure broadening were employed: A photographic method similar to the procedure used by Lambrey, and a method using a direct-reading ultraviolet spectrophotometer, which gave tracings of optical density versus wavelength.

1. Lambrey carried out his experiments in the following way: Cells of several different path-lengths were used, and in each cell the partial pressure of nitric oxide was adjusted so that the product of cell path and partial pressure, (lp), was a constant. Under these circumstances he found that the optical density in the γ -bands increases markedly with pressure, while the optical density in the β -bands remains about the same. Further investigation of the γ -bands showed that the optical density of these bands for pure nitric oxide remains constant if the quantity ($lp^{1.8}$) is kept constant. Lambrey also studied the pressure broadening of NO by argon and nitrogen, and found that the optical density of the γ -bands

can be expressed as a function of $(lpP^{0.8})$, where P is the total gas pressure. A serious question regarding the validity of Lambrey's comparison of the behavior of the γ -bands and β -bands arises from the fact that the intensities, and thus the optical densities at the same optical path, of the two bands are widely disparate. The γ -bands, it is now known, are of the order of one-hundred times as strong as the β -band in question. The first experiments were designed to overcome this objection, by comparing the γ - and β -bands, at the same total pressure and partial pressure of NO, but at cell paths correlated with the relative intensities, so that the optical densities would be comparable. For this purpose a double cell, made of two parallel and interconnecting tubes of the proper lengths, was constructed.

The source used was the molecular emission spectrum of hydrogen, produced by a discharge lamp operating under continuous pumping at about 2 to 4 mm Hg, and a 1200-volt, 60-cycle a.c. power supply. Quartz optics were used throughout, crystal quartz in the lenses, and fused quartz for the lamp and cell windows. The spectrograph was a Bausch & Lomb Medium Quartz instrument, with a dispersion of 4.6 Å/mm at $\lambda 2200$. Eastman-Kodak "Orthochromatic DK-50" plates were used; these are somewhat insensitive in the region of interest, but can be sensitized by the application of a coating of fluorescent material. For this purpose, it was found most satisfactory to dip the plates before use into a solution of

petroleum jelly in ligroin (40° - 60° C), which had been warmed to dissolve all the solute, and then to withdraw them quickly to insure uniformity of coating. The grease was removed before development by a thorough rinse in acetone. The resulting plates were satisfactorily sensitive, but more care in the procedure would be necessary to obtain plates suitable for photometry. It is important, for instance, that the coating of fluorescent material be as thin as possible and still secure sensitization, because of the fact that the fluorescence is re-radiated in all directions, and this will produce a loss of definition in the fine structure of a band spectrum.

The lengths of the two cells in the double cell originally were 100 cm and 27 cm; this ratio was suggested by crude data gathered from two sources, and is totally incorrect. The γ -band $\gamma(0,0)$ at such a path ratio is still very much stronger than the $\beta(2,0)$ band. (The $\beta(1,0)$ band overlaps the $\gamma(1,0)$ band, and therefore it is preferable to compare the isolated bands $\gamma(0,0)$ and $\beta(2,0)$.) Doubling the long path was still inadequate, and it is probable that a more correct equivalent path, for a 1-meter path for the β -band, would be less than 4 mm for the γ -band. The major difficulty is that the β -band is so weak that it is impossible at low pressures to record anything except the head of the band. Due to the unavailability of the proper focal length in a quartz lens, it proved impractical to use the 2-meter cell, since much of the light was scattered, and exposures necessary became excessively long.

There remains, of course, the alternative of increasing the pressure of nitric oxide in the cells; but there are two objections to this: first, the experiments must be conducted at a low pressure in order to demonstrate a significant abnormality; roughly, this would limit the maximum "low" pressure to about 100 mm Hg. Secondly, and more stringent, is that the γ -bands degrade toward the violet, while the β -bands degrade toward the red, and the fine structure from $\gamma(1,0)$ encroaches and covers the fine structure from $\beta(2,0)$, making it impossible to be accurate in distinguishing them at pressures above about 40 mm.

Because of the unsatisfactory character of results being obtained by the above method, attention was turned to a new approach to the band spectrum problem: namely, instead of attempting to compare the γ -bands with the β -bands, to attempt an analysis of the behavior of the γ -bands in themselves, and to try to deduce values for the line parameters from indirect information obtained with incomplete resolution. This second procedure proved so successful that the photographic method was abandoned and all the data used for quantitative estimations have been obtained by it. It now seems likely, as will be more fully discussed later, that any procedure based on a comparison of the two bands would be inconclusive.

2. The second method involved the direct measurement of optical density versus wavelength setting, at several path-lengths, and a range of pressures, with a double-beam double-

monochromator ultraviolet spectrophotometer, a commercial instrument made by the Applied Physics Corporation of Pasadena, California, called the Cary Spectrophotometer, Model 11M. This uses a hydrogen discharge as source, and has a split-beam system with balanced photoelectric detectors. A diagram of the optical system of the spectrophotometer is shown in Figure 7. Tracings of optical density of the bands were made at two resolutions; slit widths in mm and effective spectral widths for the two band-heads $\gamma(1,0)$ and $\gamma(0,0)$ are shown for each setting used, in Table 1, below:

Table 1.

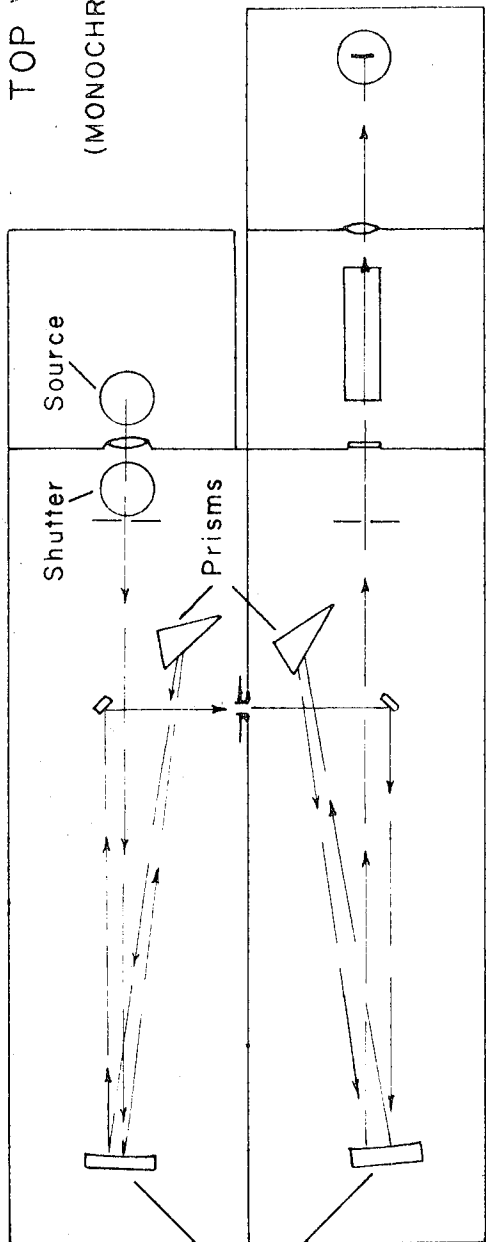
Slit Widths and Effective Spectral Widths

Resolution	Wavelength	Slit Width, mm	Effective Width A cm ⁻¹	
Higher Setting	$\lambda 2268$	0.037	0.32	14.1
	$\lambda 2157$	0.087	0.57	26.4
Lower Setting	$\lambda 2268$	0.068	0.59	26
	$\lambda 2157$	0.167	1.10	51

Narrower slits were available, but the signal-to-noise ratio was too small to give reliably reproducible results, and the highest setting used above was a sort of compromise between the desired high resolution and the difficulty mentioned.

TOP VIEW

(MONOCHROMATOR)



Collimating
Mirrors

SIDE VIEW
(DOUBLE BEAM
SYSTEM)

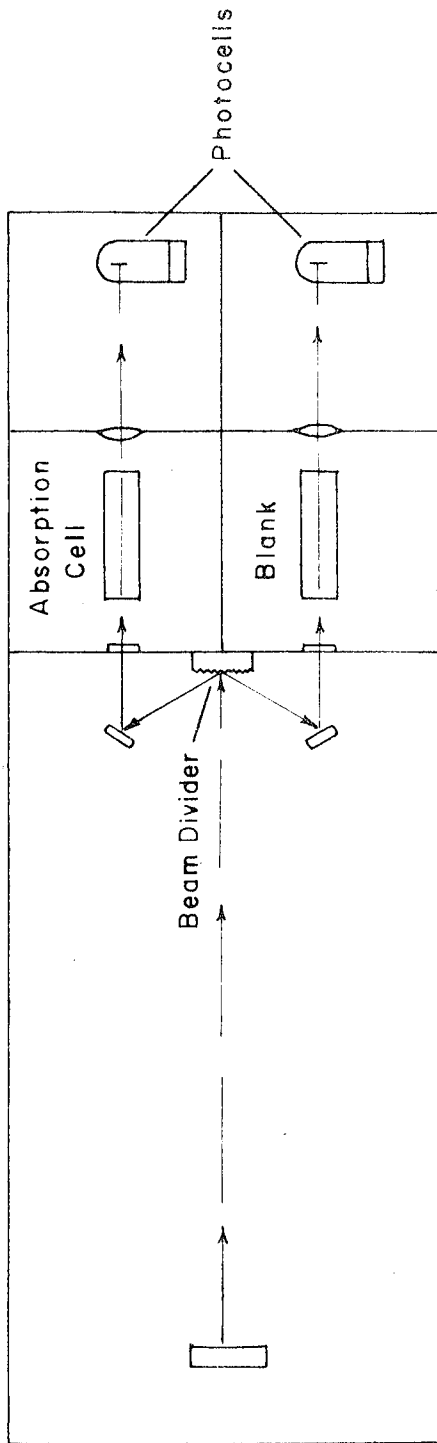


FIGURE 7: SPECTROPHOTOMETER OPTICAL SYSTEM

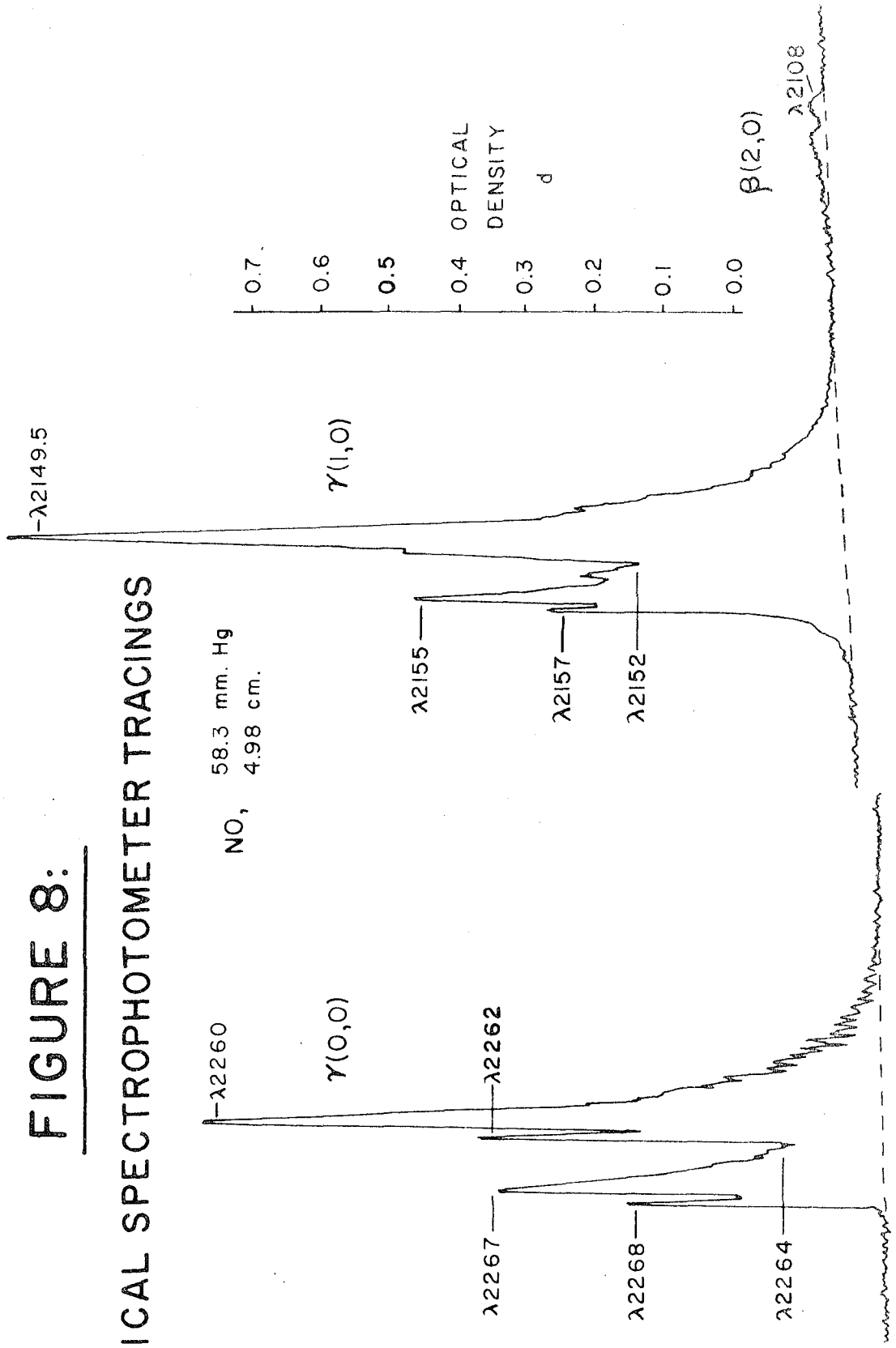
The absorption cells were made of pyrex glass, and were fitted with 2 mm stopcocks and ground ball joints. Their diameter was about 20 mm, and the cells designated CI, C, B, and A had respective lengths 11.48, 9.95, 4.98, and 2.38 cm. Quartz windows were sealed to the ends with red sealing wax for the NO self-broadening studies. When they were properly sealed, there was no observable leak over a period of two weeks. The transmission of the windows, as observed through the evacuated cells, was good over the whole range from $\lambda 2000$ to the visible region; although for two of the windows a gently sloping absorption continuum began at $\lambda 2150$ and increased toward $\lambda 2000$, it could easily be extrapolated under the $\gamma(1,0)$ band (see Figure 8). When the nitrogen-broadening experiments were carried out, a short side-arm of 6 mm tubing was attached to each cell for condensing out the NO as described earlier, so that the nitrogen for pressurizing could be added without any escape of NO from the cell. The freezing-out process caused the rest of the cell to become very cold by conduction, and the sealing wax on the windows cracked, producing leaks. This difficulty was circumvented by the use of "Araldite," a furane-base resin cement, able to withstand very low temperatures, but removable by heat or by treatment with hot chromic acid cleaning solution.

Care was taken that in the nitrogen-broadening experiments the cells were brought approximately to room temperature, by warming them with the hands, and then allowing them to

FIGURE 8:

TYPICAL SPECTROPHOTOMETER TRACINGS

NO, 58.3 mm. Hg
4.98 cm.



stand briefly (about 5 minutes). Results were normally reproducible, so that complete re-mixing of the NO appeared to have been achieved by this process.

Typical tracings for each of the bands are shown in Figure 8. Measurements were made at the points marked, and are designated in the tabulated data (Tables A and B) according to the indication used in the drawings.

An attempt was made to study the $\beta(2,0)$ band at $\lambda 2108$, but it was far too weak throughout almost the entire range of pressures studied; and as has been already mentioned, the tail from the $\gamma(1,0)$ band strongly overlaps it at higher optical paths.

For the nitric oxide self-broadening experiments, pressures from 1.04 to 501 mm Hg of NO were employed; for the nitrogen broadening, partial pressures of NO from 4.19 to 27.2 mm Hg, and added nitrogen pressures from zero to 500 mm Hg, were used. Data obtained are tabulated in Tables A and B.

III. GENERAL FEATURES OF THE PROBLEM

The purpose of this section is to discuss the relationship of the quantities which may be studied experimentally to the physical parameters of the molecule and its spectrum. The general significance of spectral line widths in the case under consideration will be first considered, followed by technical definitions of useful quantities and a formulation of the general problem involved in a theoretical analysis of the experimental data.

The shape of a spectral line is a statistical indication of the conditions under which measurement of the energy difference of two states has been made. From a study of the particular contour of a line, it may be possible to ascertain what processes limit the stability of the excited state, and to calculate the values of certain of the quantum mechanical parameters of the system. There are five main processes which affect the width of a spectral line: natural decay or "radiation damping," quantum mechanical resonance effects, Van der Waals or simple collision broadening, field perturbations by permanent dipoles, and the Doppler broadening (8). In a more general sense, the first three of these effects are similar, in that they may be understood in terms of the Heisenberg uncertainty principle. The lifetime of an excited state may be limited by its own instability with respect to

emission, or by collision deactivation with another molecule, or yet again by the possibility of exchanging a quantum of energy with an identical molecule nearby. Consequently, each of these effects will produce an uncertainty in the energy, ΔE , which is of the order of magnitude given by the requirement that $\Delta E \Delta t \geq \hbar$, where Δt is the average lifetime of the excited state.

The fourth cause of line broadening may be thought of as arising from a statistical average of the Stark or Zeeman shifts induced by the electric or magnetic fields of permanent dipoles in the gas. This problem was first treated by Holtsmark (9), and the results applied to the broadening of the Balmer series lines in the hydrogen atomic emission spectrum at great pressures. An exact second-order calculation leads to asymmetric line contours, which are in fact observed in such a case. In infrared spectra, line asymmetry has occasionally been observed at fairly high pressures, notably in the case of HCl. However, in our experiments this very interesting phenomenon probably contributes nothing to the line shape, since (1) the pressures were always low compared to those in the cases mentioned above, (2) NO has a very small electric dipole moment, and magnetic effects would not be noticeable at such small pressures, and (3) nitrogen, which has no dipole moments, has been observed to be just as effective in broadening the lines in the γ -bands as nitric oxide itself. Quadrupole field effects are of course far too small to be observed

in any case.

There remains the Doppler broadening, which is simply an average of the Doppler effect over the Maxwellian velocity distribution in the gas.

A brief derivation of the line contours which these effects produce will now be given:

(A) Doppler broadening: According to the Doppler effect, systems with velocity v_x in the direction of propagation will absorb a frequency

$$\nu = \nu_0 (1 - v_x/c)$$

The number of atoms in a velocity range dv_x at v_x is given by the Maxwell distribution:

$$dn = n \left(\frac{M}{2\pi RT} \right)^{1/2} \exp\left(-\frac{Mv_x^2}{2RT}\right) dv_x.$$

M is the molecular weight, n is the number of atoms or molecules per cc. The fraction dn/n is also the relative intensity in the frequency range $d\nu$ at ν :

$$\frac{f_t(\nu)}{F_t} d\nu = \left(\frac{Mc^2}{2\pi RT\nu_0^2} \right)^{1/2} \exp\left[-\frac{Mc^2}{2RT\nu_0^2}(\nu - \nu_0)^2\right] d\nu$$

Thus a Gaussian distribution arises whose "half-width" is seen to be:

$$\alpha_D = 2(\ln 2)^{1/2} \left(\frac{2RT}{Mc^2} \right)^{1/2} \nu_0$$

It follows that the "Doppler half-width" is increased with temperature, and it is usually the predominant factor determining line contour in the optical region, being of greater magnitude than most natural line widths. It will be noted that the Doppler width is independent of gas density.

(B) Natural line width and collision broadening: As has been mentioned, the basic explanations of both these phenomena are similar, and the treatment for each case results in an identical form for the line contour. Detailed and refined quantum mechanical treatments of these phenomena have been made, and the results agree in their outward form for the line contour with what is obtained from simpler classical considerations. Natural decay corresponds to the classical problem of an oscillator damped by its own radiation energy losses; collision broadening, or Van der Waals interaction, to the problem of a monochromatic oscillator interrupted at random by collisions in the gas. Only in the latter analogy is there much true physical correspondence in the classical picture, and it is also the one which has remained to the present day as a useful concept in treating the problem. The quantum mechanical treatment of the collision broadening problem has been done by Karplus and Schwinger (10); a useful discussion of the general nature of collision broadening has been made by Van Vleck and Weisskopf (11). The basic form of the line contour, however, was derived a long time ago by H. A. Lorentz, and for that reason it is called the

"Lorentz contour." A brief outline is given here for the derivations based on classical "radiation damping" and on collision broadening:

In the case of radiation damping, one considers the rate of energy loss by an harmonically oscillating charge; this loss rate is proportional to the square of the instantaneous acceleration. If one supposes that damping is small compared to the amplitude of oscillation, the result is that an envelope for the amplitude is obtained which falls off exponentially with time,

$$A(t) = A_0 e^{-t/\tau}$$

The Fourier analysis of this damped wave train gives a frequency distribution:

$$\frac{f}{F} = \left(\frac{A_0^2 C^2}{4} \right) \left[\frac{1}{\frac{4\pi^2(\nu - \nu_0)^2}{C^2} + \left(\frac{1}{\tau C} \right)^2} \right]$$

Here $\frac{2}{\pi\tau C}$ is the half-width, is related to the charge of the electron, its mass, etc., and is a constant for all emitters on a wavelength scale; it is at this point that the classical picture is inadequate, since there is actually a great variation in the natural widths of lines.

The treatment of collision broadening is also simple: one imagines an oscillator of frequency ν_0 to emit monochromatic radiation for a time t , at the end of which it is interrupted by a collision. A Fourier analysis of this finite

wave train is made; and then the contributions to the spectrum are averaged over all times t between collisions with the probability factor $e^{-t/\tau}$, where τ is the mean time between collisions. Again the Lorentz curve is the result.

Therefore in the case of nitric oxide in the ultra-violet, it will be necessary to consider two basic contours: the Gaussian line shape, which is due to the Doppler effect, and the Lorentz contour, involving those effects which limit the lifetime of the molecule in the excited state. It can be shown that the half-widths for natural line width and collision broadening are additive (8); and therefore one may treat them as a single parameter, the Lorentz half-width α_L . The combination of the Doppler effect and the Lorentz contour, however, is complicated, and cannot be put in closed form in the general case, except as an integral. However, for special cases, certain approximations are valid. It is clear, for instance, that at any reasonably large distance from the line center, the Doppler contribution is very small, and the line shape in the wings is essentially a Lorentz contour. Even for intermediate cases, it will always be meaningful to speak of a parameter related to the contribution of Lorentz broadening to the line contour.

The consequence of the Lorentz theory of collision broadening is that the half-width or related parameter of a collision-broadened line is related directly to the gas density and the molecular dimensions by the kinetic theory of

gases:

$$\alpha_L = \frac{2}{\pi \tau c}$$

where $\frac{1}{\tau}$ is the mean number of collisions per second.

From the kinetic theory, for a homogeneous Maxwellian gas composed of hard elastic spheres of diameter σ ,

$$\frac{1}{\tau} = \sqrt{2} \pi n_0 \bar{v} \sigma^2 \quad ; \quad n_0 = \frac{p}{RT} \cdot \frac{\tilde{N}}{760} ,$$

where n_0 is the number of molecules per cc, \bar{v} is the mean speed, and σ is called the collision diameter. Thus the half-width is proportional to the total pressure in the Lorentz pressure broadening theory. An expression for \bar{v} may also be obtained from kinetic theory:

$$\bar{v} = \sqrt{\frac{8RT}{M\pi}} = \frac{2\sqrt{2\pi kT}}{\pi \sqrt{m}}$$

from whence we may deduce that

$$\sigma^2 = \frac{\pi \alpha_L \sqrt{M} c}{4 n_0 \sqrt{\pi k T}} = \frac{\alpha_L c R (760) \sqrt{\pi M T}}{4 \tilde{N} p R}$$

This leads to the result at $T = 300^\circ\text{K}$:

$$\sigma = 3.80 \times 10^{-6} \sqrt{\frac{\alpha_L}{P}} \text{ cm.} \quad \begin{array}{l} \alpha_L \text{ in cm}^{-1} \\ P \text{ in mm Hg} \end{array}$$

At 300°K, use of the formula for the Doppler half-width and the molecular weight of NO, gives $\alpha_p = 0.10 \text{ cm}^{-1}$ at $\lambda 2268$.

Therefore if it were possible to ascertain the value of the Lorentz half-width parameter for some pressure, assumption of the Lorentz theory would immediately provide a value for the "optical collision diameter." Since many gases which do not have large electric dipole moments give results from their infrared or microwave spectra which are of the same order of magnitude as those obtained by viscosity or other standard kinetic measurements of size, the value of the collision diameter σ for the molecule in these bands would afford some criterion of abnormality.

It will be useful to define a few quantities of interest in the tabulation of data and in the interpretation of results:

(1) The observed spectrum results from the contributions of many absorption lines, of different center frequencies, intensities, and shapes. These superpose on one another to produce a function $f_t(\nu)$, which we shall call the true absorption coefficient. If one could observe the spectrum with infinite resolving power and an infinitesimal layer of absorber, the curve $f_t(\nu)$ vs frequency ν could be obtained.

(2) The length of absorbing path is designated by l ; the partial pressure of the absorber by p ; the total gas pressure by P . In addition we shall define a quantity x , called the "optical path," which is the product (lp) in the units cm-mm Hg.

(3) A quantity $A_t(\nu)$, called the true absorption, is defined as follows: Let monochromatic radiation of frequency ν and intensity I traverse an optical path dx of absorber; then the change in intensity, dI , is given by the equation

$$dI = -f_t(\nu) I dx$$

Integration leads to the well-known Beer-Lambert law,

$$\frac{I_T}{I_0} = \exp[-f_t(\nu)x]$$

where I_T is the transmitted and I_0 the incident intensity of light passing through the optical path x of absorber with true absorption coefficient $f_t(\nu)$. The true absorption, $A_t(\nu)$, is then defined by the equation

$$A_t(\nu) = 1 - \frac{I_T(\nu)}{I_0(\nu)} = 1 - \exp(-f_t(\nu)x).$$

(4) In actual observation, resolving power is never great enough to observe $A_t(\nu)$ directly; instead, the spectrometer admits a band of radiation containing contributions from frequencies centered around the frequency of observation, ν_0 , with a weighting function, $\rho(\nu - \nu_0)$. It has been shown that this function can be satisfactorily represented by a Gaussian curve, whose width is the effective resolution of the instrument (13). What one may observe, then, with an

actual instrument, is the observed absorption,

$$A_o(z_o) = \frac{\int_{-\infty}^{\infty} \rho(\nu - z_o) A_t(\nu) d(\nu - z_o)}{\int_{-\infty}^{\infty} \rho(\nu - z_o) d(\nu - z_o)}$$

(5) A quantity which is analogous to the true absorption coefficient $f_t(\nu)$, is designated $k_o(z_o)$, and is called the apparent absorption coefficient; it is defined by the equation

$$A_o(z_o) = 1 - \exp(-k_o(z_o)x)$$

(6) Finally, a quantity d , called the optical density, is defined by

$$d(z_o) = -\log_{10}(1 - A_o(z_o)) ; \quad d = \frac{k_o(z_o)x}{2.303}$$

(7) To facilitate discussion of the spectrum, it will be well at this point to set down for reference a few relationships, so that the significance of the experimental variables to the quantum mechanical parameters of the system will be clear. For a single spectral line (dipole radiation), if we integrate $f_t(\nu)$ over the line contour, the following relation is true:

$$\int_{n', n''} f_t(z) = \frac{h\nu_j}{c} B_{n'n''} [N_{n''} - N_{n'}]$$

Here ν_j is the center frequency of the line in question, $N_{n'}$ and $N_{n''}$ are the numbers of molecules per cc in the upper and lower states, respectively, of the transition giving rise to the line, and $B_{n'n''}$ is called the Einstein absorption coefficient. The Einstein coefficient is

$$B_{n'n''} = \frac{2\pi}{3\hbar^2} \left[|\mu_{x_{n'n''}}|^2 + |\mu_{y_{n'n''}}|^2 + |\mu_{z_{n'n''}}|^2 \right]$$

where $\mu_{x_{n'n''}}$ is the quantum mechanical dipole matrix element between the two states,

$$\int \psi_{n'}^* \mu_{x_i} \psi_{n''} dVol.$$

(7) Assuming the lines to have symmetry about their centers, a number of parameters for the lines will be defined:

ν_j is the central frequency of the jth line.

α_j is called the half-width of the line, and is defined by the condition that the absorption coefficient of the line have one-half its maximum value at the frequencies $(\nu_j \pm \alpha_j/2)$. The maximum value of $f_j(z)$ will be called F_j .

The interpretation of observed spectra in terms of the true line contour and line width is difficult because of the analytical problem arising from incomplete resolution by the spectrometer. The problem essentially is to compute the integral:

$$\int_{-\infty}^{\infty} \rho(z-z_0) [1 - \exp(-\chi f_{\xi}(z))] dz$$

For the case where $f_{\xi}(z)$ is a single line with Lorentz contour, Ladenburg and Reiche (12) computed the "integrated absorption" with a uniform constant weighting function,

$$\int A_0(z_0) dz_0$$

and found that over a considerable range of x and α_L it is proportional to the square root of x and of α_L . Dennison (13) has shown that the absorption of a single Lorentz line at its center is proportional again to $\sqrt{x\alpha_L}$. Elsasser (14) has computed the integrated absorption for an infinite series of equally intense equidistant lines, all of Lorentz contour with equal half-widths, and has found that over a wide range of x and α_L it is proportional to the square root of $(x\alpha_L)$ also. More recently, Penner and Tsien (15) have shown that for arbitrary intensities and random spacing, but with no overlapping of lines, the integrated absorption is still proportional to $\sqrt{x\alpha_L}$. Behavior of the optical density roughly parallels that of the integrated absorption.

The above results are valid over a wide intermediate range of x and α_L , but it is fairly obvious that at low values of optical path x the observed integrated absorption must become a linear function of x , while at high optical paths it must eventually reach a maximum. On the other hand, for low values of half-width, the contour must approach Doppler form, and qualitative considerations will make it evident that for small α_L , a change in the Lorentz half-width will not greatly alter the integrated absorption.

While the general behavior of the optical density as a function of the line width and the optical path may be thus predicted if the Lorentz theory is correct, the quantitative form of the curves for optical density, as a function of the half-width, for various values of optical path, the so-called "curves of growth," will depend more critically upon the details of the spectrum. In order to make an analysis which will permit an estimate of the collision diameter, it will be necessary to obtain curves of growth and correlate them with experimental curves of optical density versus pressure at constant optical path, at the same frequency and optical path. In order to make the correlation it is almost absolutely necessary to know the absolute intensity of the γ -bands; without that information one may only hope to guess at an approximate correlation based upon the behavior of the individual curves for different optical paths.

Because the experimental results justify the assumption

of Lorentz broadening, detailed calculations were carried out to obtain complete curves of growth for two optical paths. The results of the calculations show a very clear "break" in each curve of growth, in a region where the Lorentz half-width becomes a significant contributor to the increase of optical density. It was initially hoped that the half-width at which this "break" occurred would not depend critically upon the optical path, but this turned out not to be the case. Fortunately, however, an estimate of the absolute intensity of the γ -bands has become available through the work of Penner and Weber (22).

The next section presents an analysis of the experimental results on a qualitative basis, and shows the correctness of the Lorentz theory as a description of pressure effects observed. The section following gives an account of the theoretical calculations of the growth curves.

IV. EXPERIMENTAL RESULTS

The spectrophotometer tracings gave the optical density on a linear wavelength scale for the two absorption bands $\nu(1,0)$ and $\nu(0,0)$. Figure 8 shows the appearance of these bands at the higher resolution employed, and contains a key to the Data Tables A and B. As will be noted, there is fine structure indicated by the appearance of the $\nu(0,0)$ band toward its short wavelength side. The two double-headed sub-bands characteristic of a ${}^2\Sigma^+ - {}^2\Pi$ transition are clearly seen, the main splitting being due to the spin splitting in the ground state, the doubling of the sub-bands to the P- and Q-type heads.

At higher pressures in the NO self-broadening studies, a very weak continuum was observed underneath the $\nu(1,0)$ band, which increased in strength as the pressure increased. The absorption did not change with time, so that it was not due to leakage of air into the cell, with consequent formation of N_2O_3 . It is unknown whether this continuum was a part of the NO spectrum, which seems unlikely as it has not been previously reported, or due to a trace of N_2O_3 or other contaminant. The transmission of the quartz cell-windows seemed to be slightly different for the various cells, and some absorption by them in this region was noted as a contributor to the background in the case of the 11.48 cm cell (CI). In any

case, it was always possible to accurately extrapolate the continuum as a monotonic background underneath the $\gamma(1,0)$ band. Many of the cases in which a strong background could be seen were discarded for quite another reason: namely, the high optical density of the bands at higher optical paths. When the optical density at the peaks in the bands became greater than about 1.5, it began to deviate systematically downward from the expected behavior, and became erratic, often decreasing with increasing pressure. The explanation of this is simply that at high optical densities, very little light is transmitted, and accuracy is limited by the reliability of the photocell response to progressively weaker signals. Therefore in the data tabulated, no values of \underline{d} are extended beyond about 1.5; and downward deviations of these high densities from behavior predicted by obvious extrapolation are not considered significant.

The collected data for NO self-broadening are shown in Table A, Data Tables; the data for nitrogen broadening are in Table B. In addition, Figures 9-20 show the dependence of \underline{d} as a function of the variables \underline{l} , \underline{p} , and \underline{P} .

The higher resolution used in the experiments was comparable to that attained by Marmo, and therefore a comparison can be made with his quantitative data on self-broadening in the $\gamma(1,0)$ and $\gamma(0,0)$ bands. He used a single cell 4.70 cm long, and has recorded the values of $k_o(z')$, the apparent absorption coefficient, at various pressures and several

wavelengths. He observed that the value of k_0 decreased as the inverse-square-root of the pressure, $k_0 \propto \frac{1}{\sqrt{p_{NO}}}$. This phenomenon he correctly attributed to incomplete resolution.

In order to compare his data with our values of optical density versus pressure, it is necessary to multiply the k -values from his tabulation by $x/2.303$ (x is the optical path, ℓp). Figures 9 and 10 show some values of $\text{Log}_{10}(d)$ versus $\text{Log}_{10}(p)$. Marmo's data are represented by the open circles and dashed lines. It is thus evident that Marmo's data are in moderate agreement with values obtained in our experiments.

It will be observed that the curves of $\text{Log}_{10}(d)$ versus $\text{Log}_{10}(p)$ increase in slope as p increases, and reach a linear dependence upon p , at pressures above about 20 mm Hg. This in itself is not necessarily a significant fact, since in the limit of strong absorption, when the lines are completely absorbed out and merge into one another, one would obtain this result (Beer's law). However, aside from any discussion, as to whether these conditions hold, which might be based on the intensity of the absorption, the phenomenon above may be demonstrated to be a true pressure effect by the dependence of $\text{Log}_{10}(d)$ on $\text{Log}_{10}(\ell)$, which is shown for various pressures and two wavelengths in Figures 11 and 12; namely, at pressures above 20 mm, the dependence of d upon p is significantly different from that of d upon ℓ , under identical conditions of optical path and total pressure.

The slope of a plot of $\text{Log}_{10}(d)$ versus $\text{Log}_{10}(p)$ or $\text{Log}_{10}(\ell)$

FIGURE 9:

NITRIC OXIDE SELF-BROADENING

$\text{Log}_{10}(\text{Optical Density})$ vs. $\text{Log}_{10}(p_{\text{NO}})$

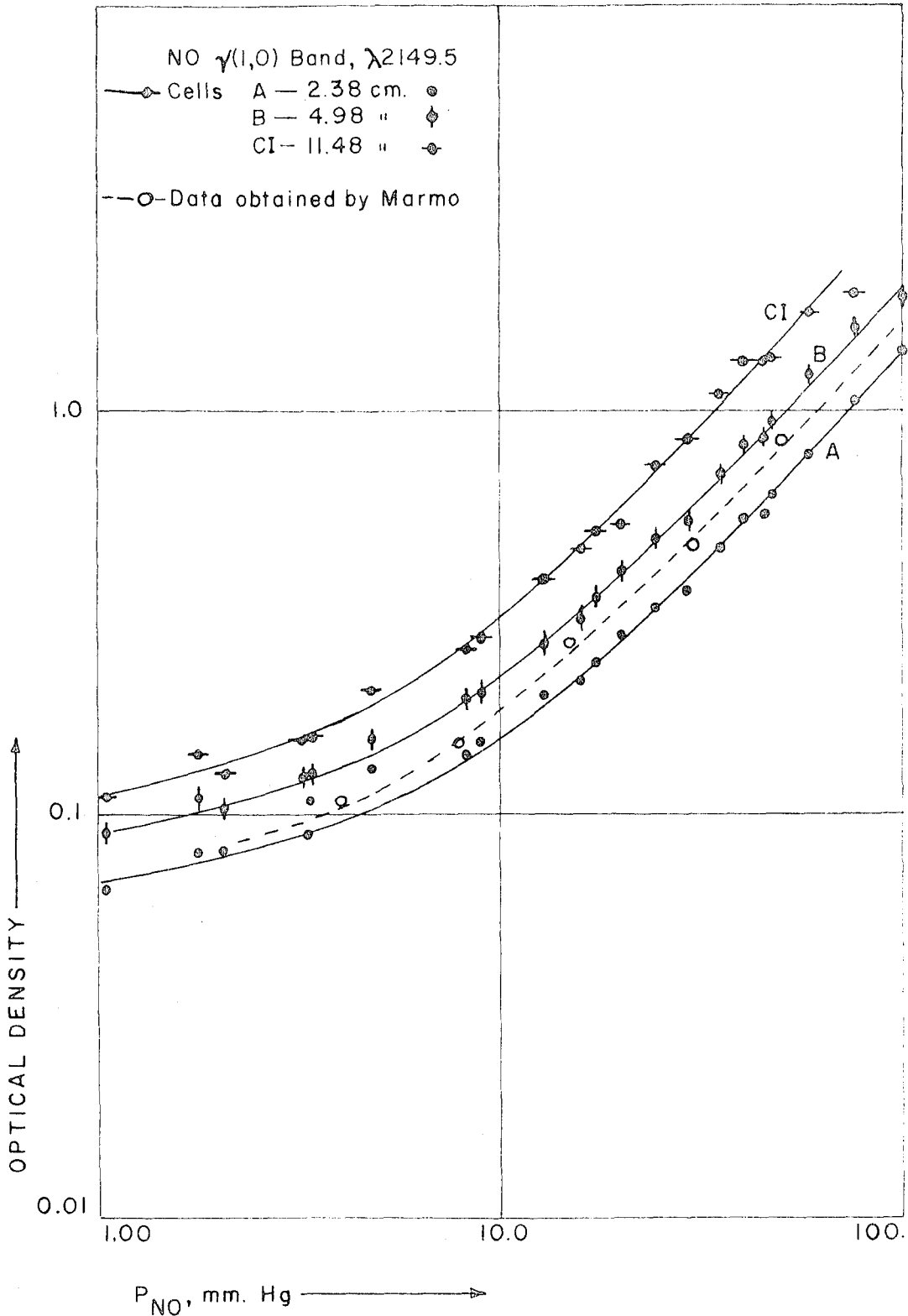


FIGURE 10:
NITRIC OXIDE SELF-BROADENING

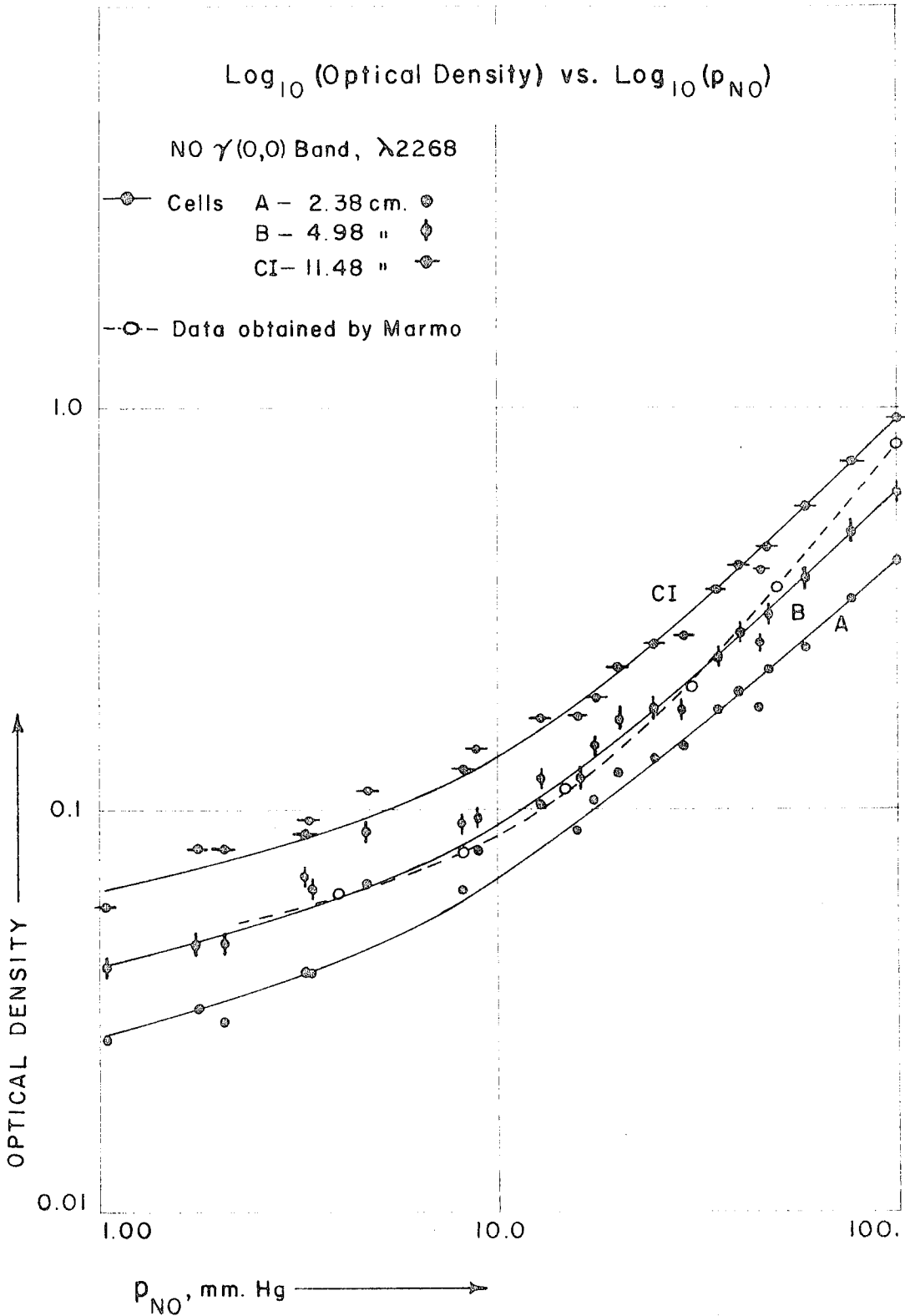


FIGURE II:

NITRIC OXIDE SELF-BROADENING

Log_{10} (Optical Density) vs. Log_{10} (Cell Path)

NO γ (1,0) Band, λ 2149.5

Each curve for constant
pressure of NO.

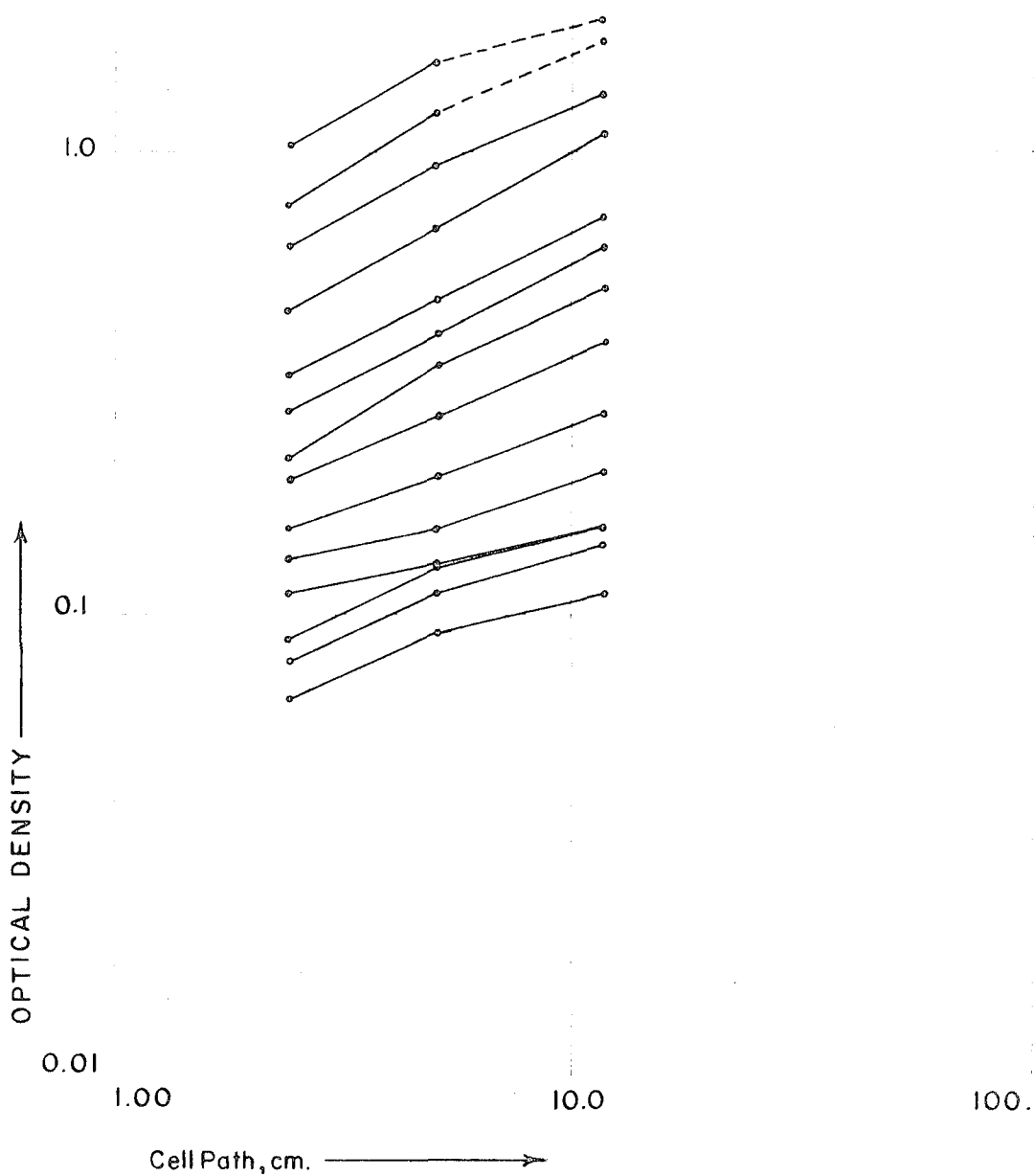
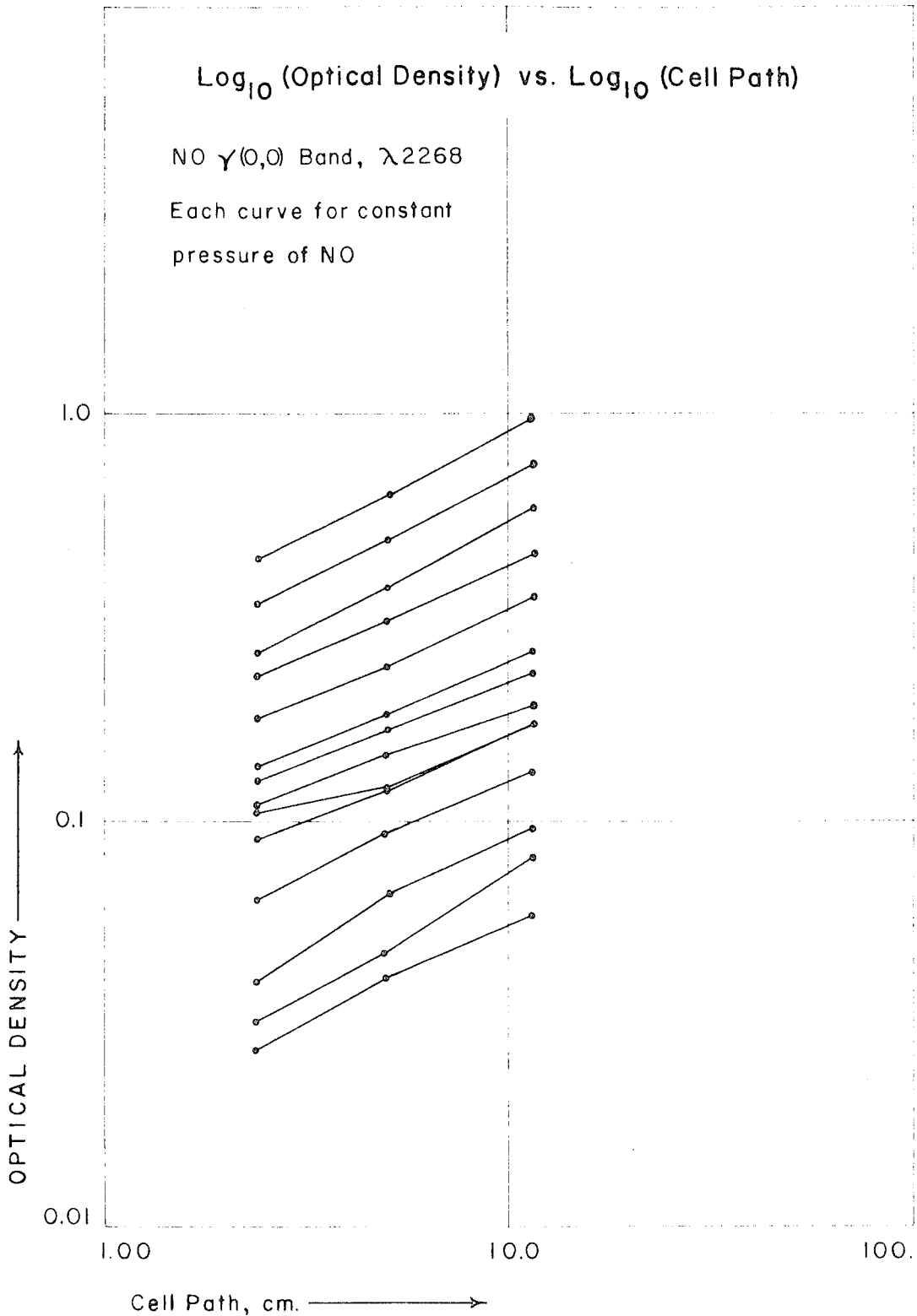


FIGURE 12:

NITRIC OXIDE SELF-BROADENING



gives the value of the power of the variable p or l to which d is proportional. Thus from Figures 11 and 12, one may deduce that d is roughly proportional to the square-root of l over the range studied (actually, the slope goes from about 0.4 to 0.6 over the range of pressures studied). The dependence of d on the cell path l is important, because it enables one to isolate the effect of optical path, x, from any true physical effects of pressure on the spectral line contour. After proper treatment of the data, one may obtain an estimate of the true effect of pressure on the spectrum. The results obtained from pressures above about 10 mm Hg are in agreement with the data of Lambrey and the conclusions reached by Mayence, namely: $d = cl^{1/2}p^{1/2}$, $d = cl^{1/2}p$ for self-broadening.

To provide a clear illustration of the self-broadening effect in NO, the data for the wavelength $\lambda 2149$ were treated as follows:

1. Third-order polynomials in $(\log_{10} p)$ were fitted by the least-square-ordinates method to the experimental curves of $\log_{10} d$ versus $\log_{10} p$. These expressions were then differentiated to give expressions for $\left(\frac{\partial \log d}{\partial \log p}\right)_l$ for each of the three cells, as a function of $\log_{10} p$.

2. At each pressure studied, there were three points giving the variation of $\log d$ with $\log l$. From these three points, two values for $\left(\frac{\partial \log d}{\partial \log l}\right)_p$ were obtained for each pressure. These were plotted versus $\log p$ and a quadratic curve

was fitted by least squares through the points. Thus the function $\left(\frac{\partial \log d}{\partial \log l}\right)_p$ as a function of $\log p$ was obtained.

3. Now, it is generally true that

$$\left(\frac{\partial \log d}{\partial \log p}\right)_{pl} = \left(\frac{\partial \log d}{\partial \log p}\right)_l + \left(\frac{\partial \log d}{\partial \log l}\right)_p \left(\frac{\partial \log l}{\partial \log p}\right)_{pl}$$

and since $\left(\frac{\partial \log l}{\partial \log p}\right)_{pl} = -1$,

$$\left(\frac{\partial \log d}{\partial \log p}\right)_{pl} = \left(\frac{\partial \log d}{\partial \log p}\right)_l - \left(\frac{\partial \log d}{\partial \log l}\right)_p ;$$

accordingly, the curve of 2 was subtracted from the three derivatives of Step 1 above, and thus was obtained $\left(\frac{\partial \log d}{\partial \log p}\right)_{pl}$ as a function of $\log p$ for each of the three cells.

4. Figure 13a shows $\left(\frac{\partial \log d}{\partial \log p}\right)_{pl}$ as a function of $\log (pl)$. This shows three curves, one for each value of l . If a line of constant (pl) is passed through the curves, three values of $\left(\frac{\partial \log d}{\partial \log p}\right)_{pl}$ are obtained, for the same pl and for three different pressures.

5. For several values of pl , these values of $\left(\frac{\partial \log d}{\partial \log p}\right)_{pl}$ were plotted versus $\log p$, and straight lines were fitted by the method of least squares to each set of three points.

6. The analytical expressions so obtained were integrated to give quadratic expressions for the logarithm of the optical density as a function of $\log p$ at constant optical path, $x = lp$, for several values of lp . The optical densities so obtained are relative only.

FIGURE 13a:
NITRIC OXIDE SELF-BROADENING

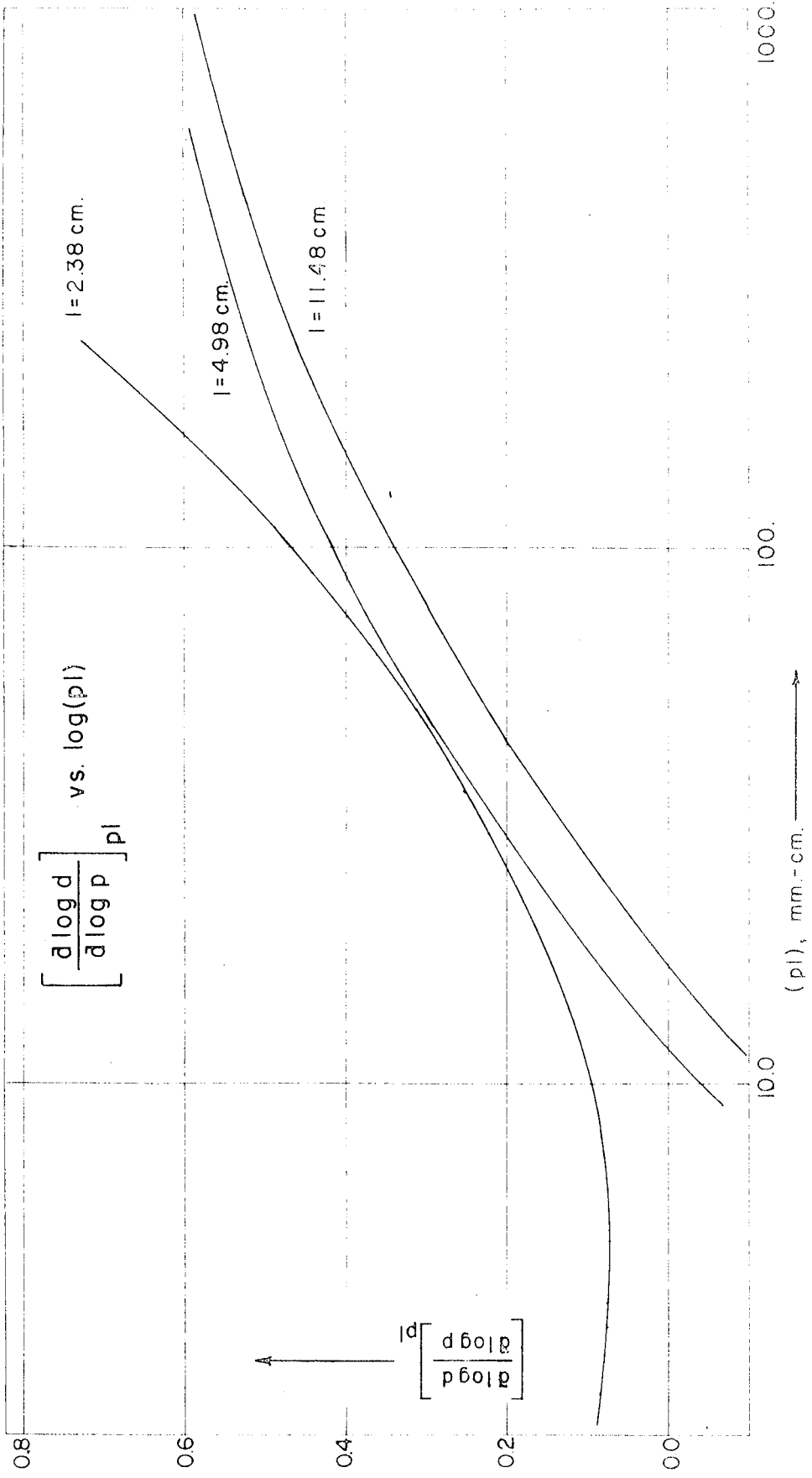
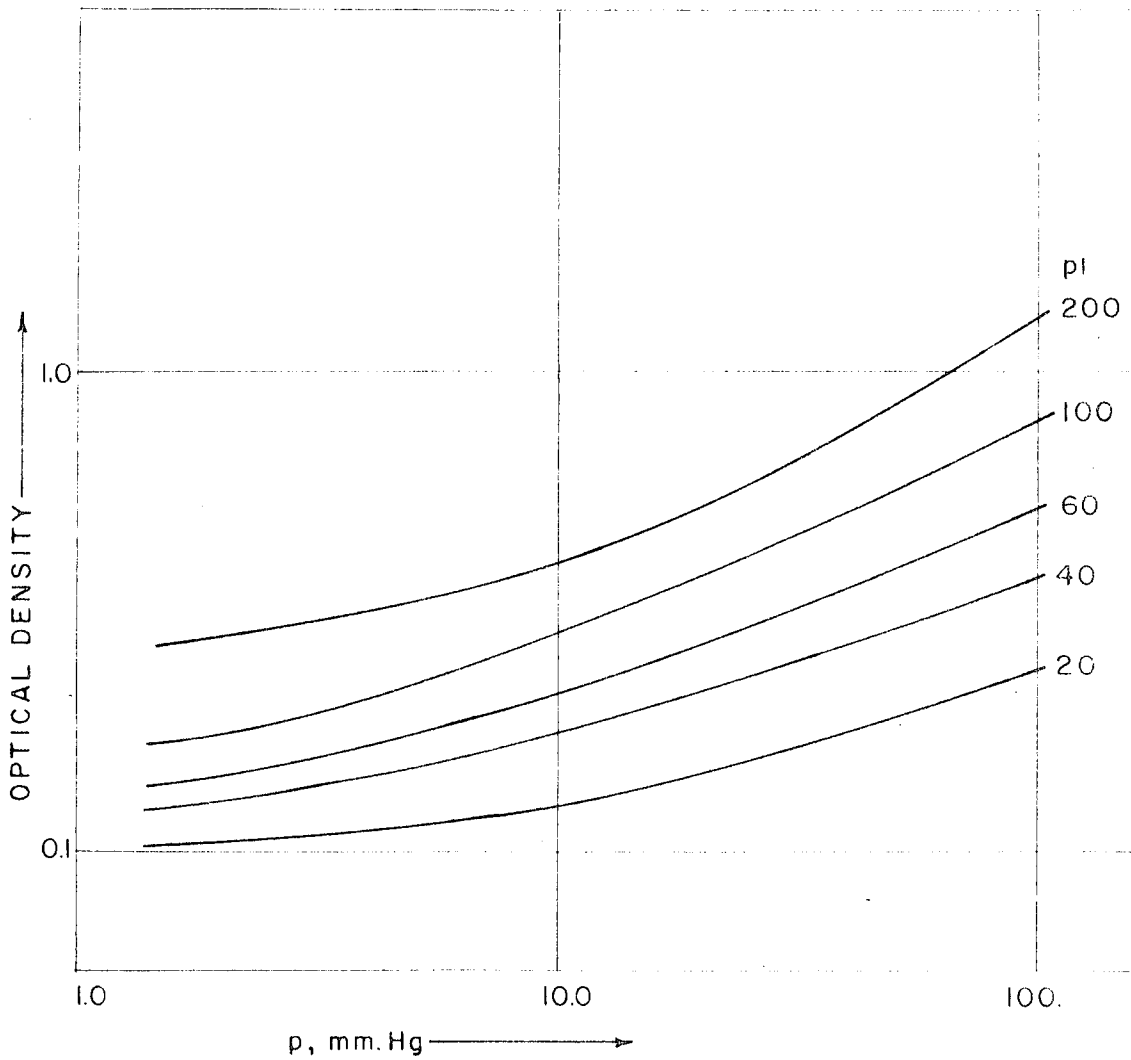


FIGURE 13b:

NITRIC OXIDE SELF-BROADENING

$\text{Log}_{10}(\text{Optical Density})$ vs. $\text{Log}_{10}(p)$, pl constant



7. In order to properly orient the curves for different values of x with respect to one another, the assumption was made that at a pressure of 10 mm Hg, d increases as the square root of x . This served to fix the relative positions of curves with respect to one another.

8. The absolute value of d for all curves was determined by an approximate match from the curve for $x=100$, with the experimental value of d at a pressure of 10 mm Hg and an optical path $x=100$. The curves are plotted in Figure 13b.

There are a few objections to this procedure which should now be discussed:

(a) Figure 13a shows a large discrepancy between the curves for 4.98 and 11.48 cm, and the curve for 2.38 cm. This results originally from the errors in the experimental data for low optical densities. In fitting straight lines through the three points from the curves which lie at any given value of $p\ell$, (Step 5) one would indeed underestimate the slopes of the straight lines in the intermediate range of $p\ell$, and overestimate them in the upper and lower ranges. However, this only affects the second derivative of the curves in Figure 13b, and since the qualitative behavior is all that is desired, the error is here neglected, in spite of the appearance of Figure 13a.

(b) A far more significant source of error is the assumption made in Step 7, that the optical density increases as \sqrt{x} at constant pressure. This is only approximately true.

Within the above limitations, one might expect to be able to predict the behavior of the experimental curves for self-broadening by the use of Figure 13b. Finally, these true pressure-effect curves may be directly compared with those from the nitrogen broadening experiments, Figures 14-20.

The nitrogen broadening experiments gave values of optical density versus total pressure P for a constant partial pressure of NO . Some curves of $\log d$ versus $\log P$, for various values of the partial pressure p of NO , and several wavelengths, are shown in Figures 14-20. Several features are important in these plots.

1. The apparent effect of increasing the total pressure with nitrogen is qualitatively the same as in the case of the self-broadening by NO (see Figure 13); if the partial pressure of nitric oxide is greater than about 15 mm, then there is not much difference apparent between the effect of adding nitrogen at constant optical path of NO , and the effect of increasing the pressure of NO at constant optical path of NO ; (compare, for instance, Figure 15 with Figure 13b). Lambrey found a slight difference in the effect of nitrogen and argon on the broadening from that of NO itself, for partial pressures of NO greater than about 15 mm; he found that the exponent of P for nitrogen broadening was 0.38 instead of 0.40 as found for the self-broadening. It is our opinion that such a distinction is not justifiable because of the poor precision of the data.

FIGURES 14-20:

NITROGEN BROADENING OF NITRIC OXIDE

$\gamma(1,0)$ AND $\gamma(0,0)$ BANDS

$\text{Log}_{10}(\text{Optical Density})$ vs. $\text{Log}_{10}(P_{\text{Total}})$

$$P_{\text{Total}} = P_{\text{NO}} + P_{\text{N}_2}$$

CELLS: A 2.38 cm.
 B 4.98 cm.
 C 9.95 cm.

(Refer to Figure 8 for Key to Wavelengths)

FIGURE 14:

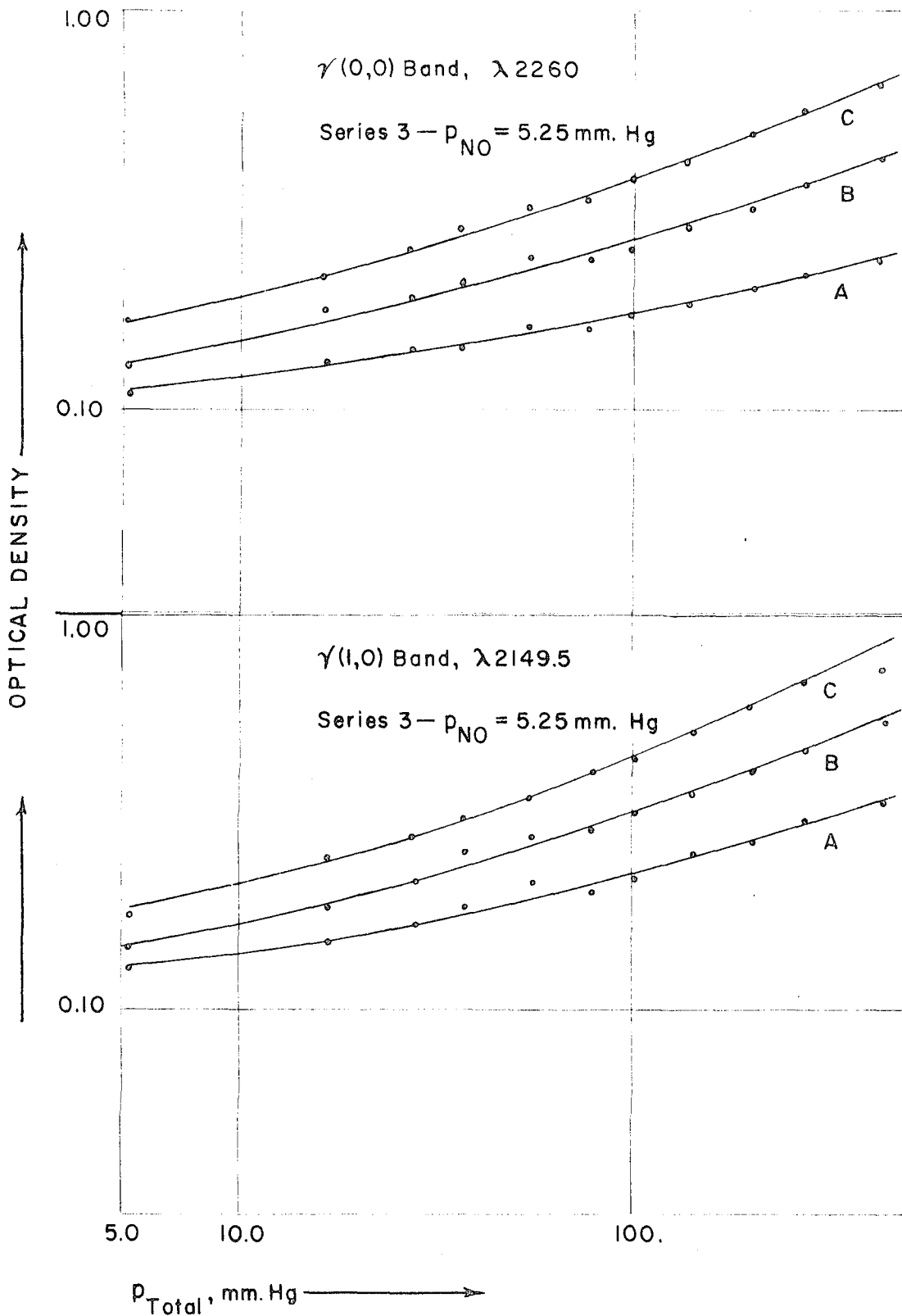


FIGURE 15:

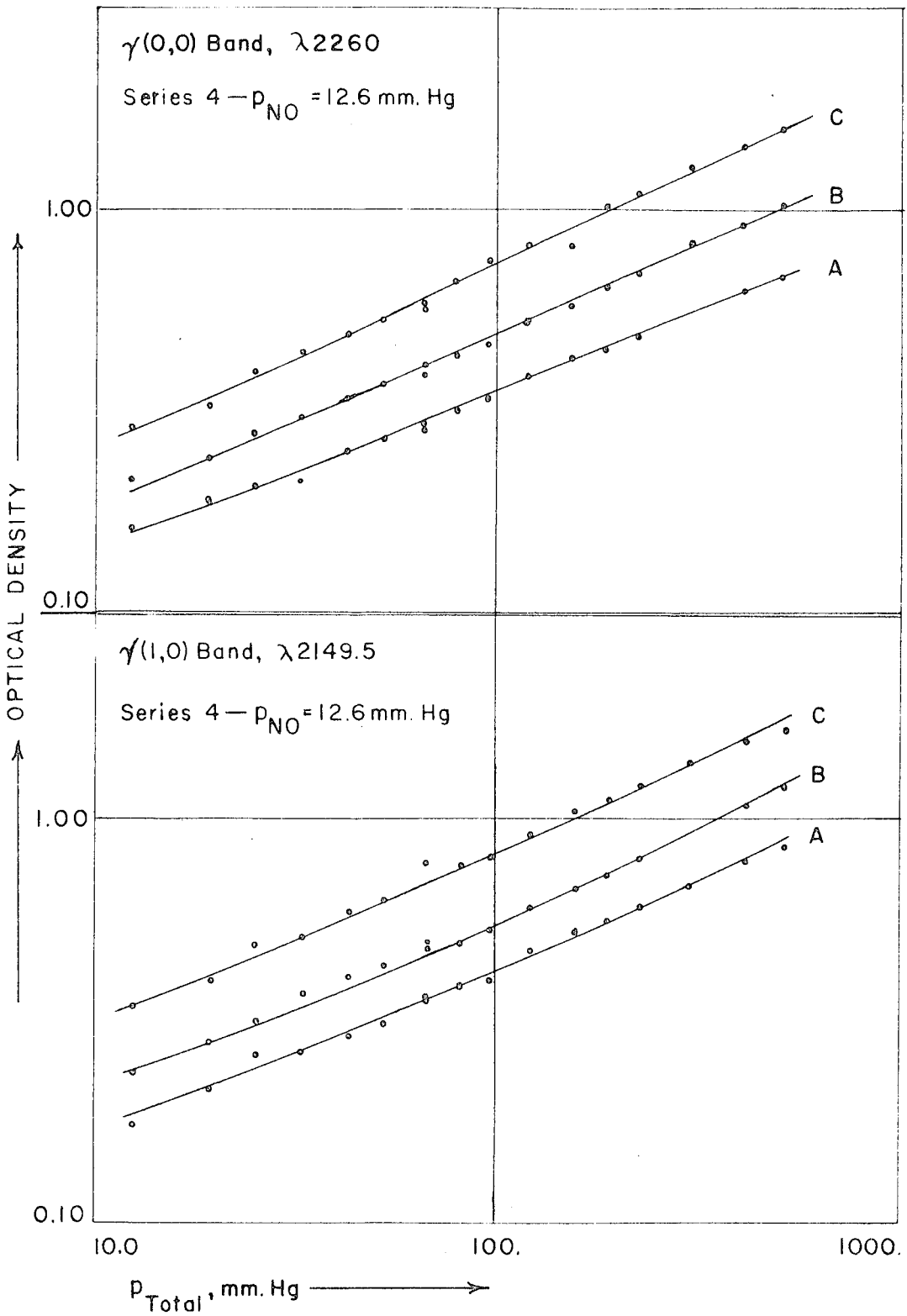


FIGURE 16:

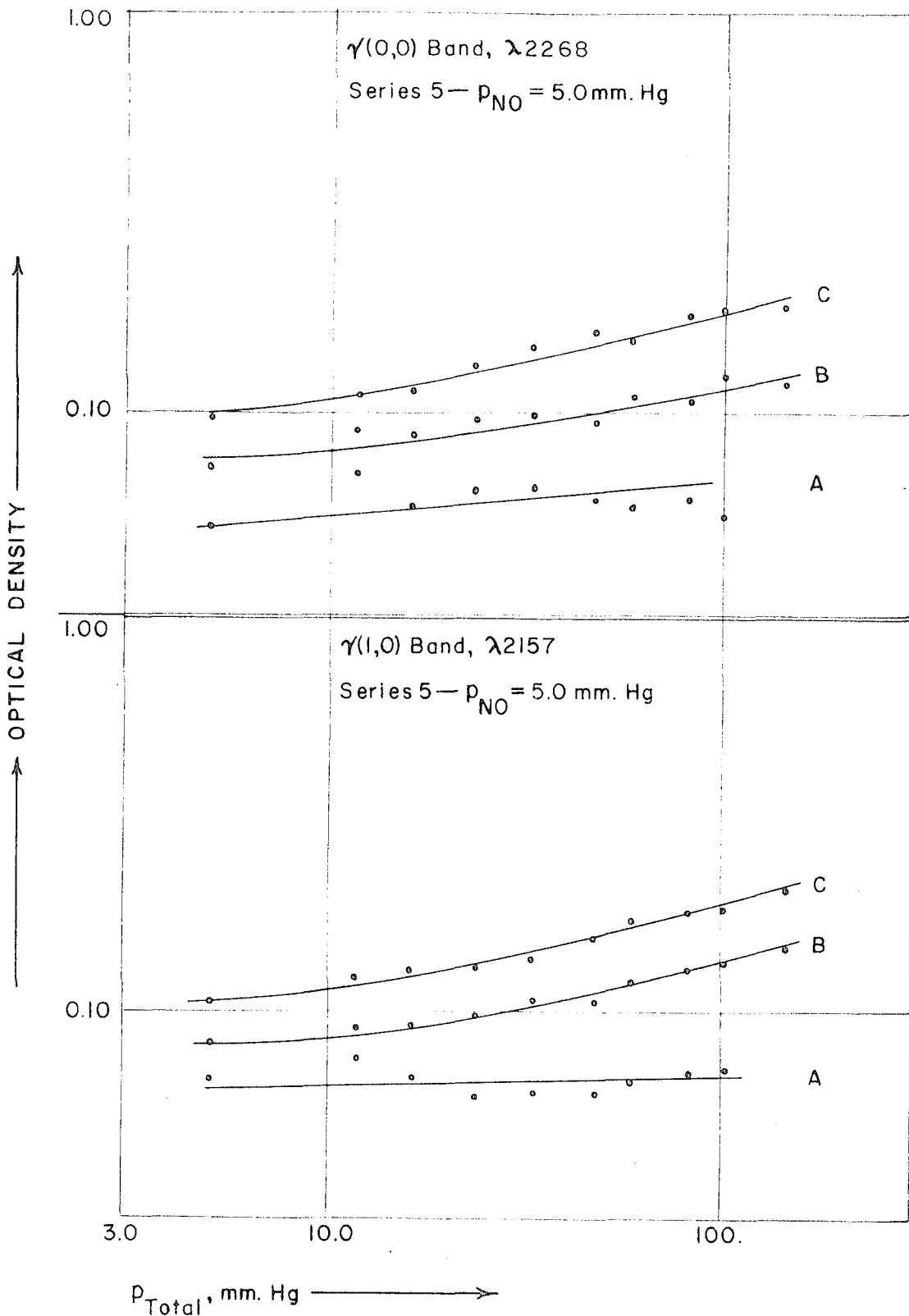


FIGURE 17:

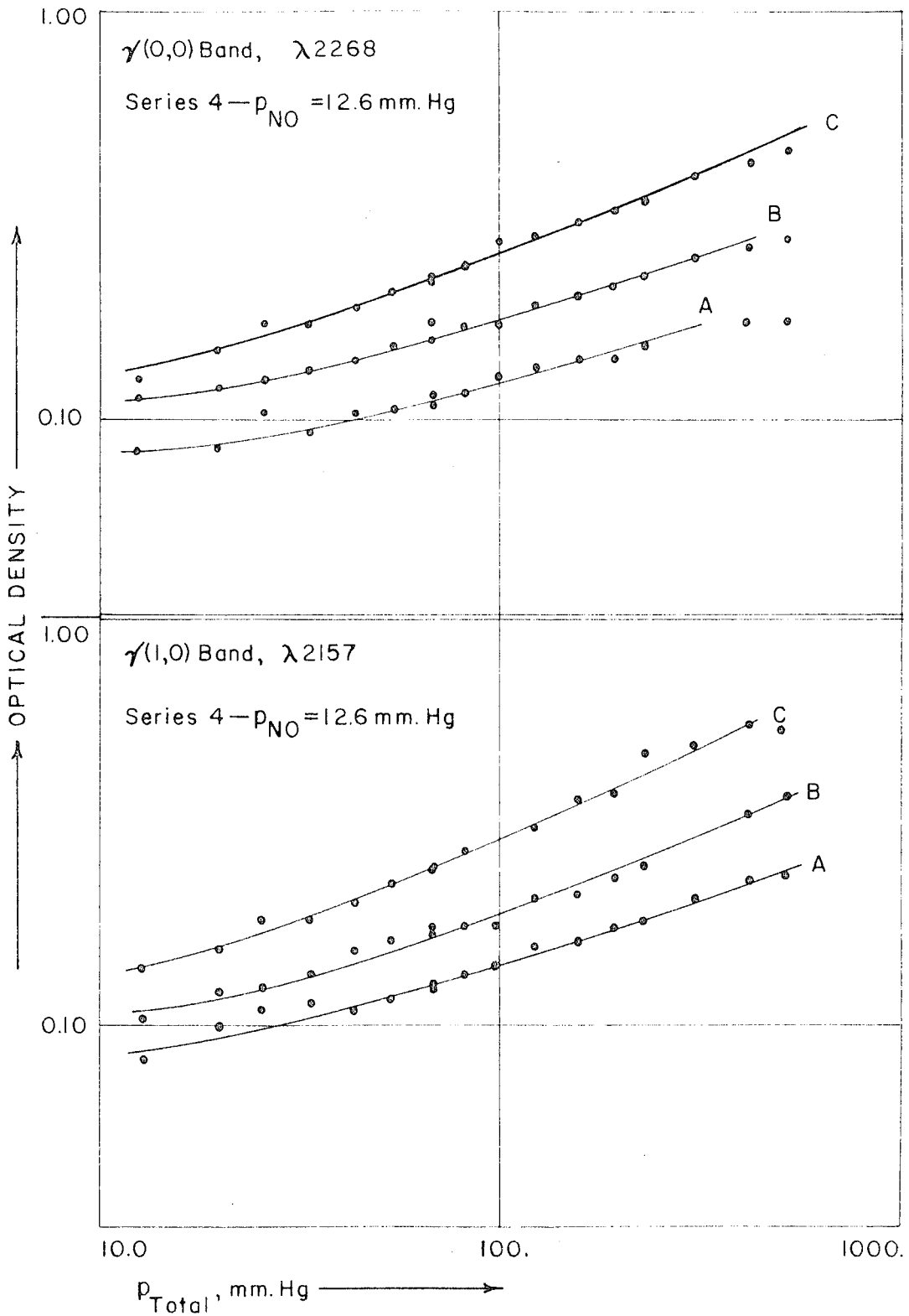


FIGURE 18:

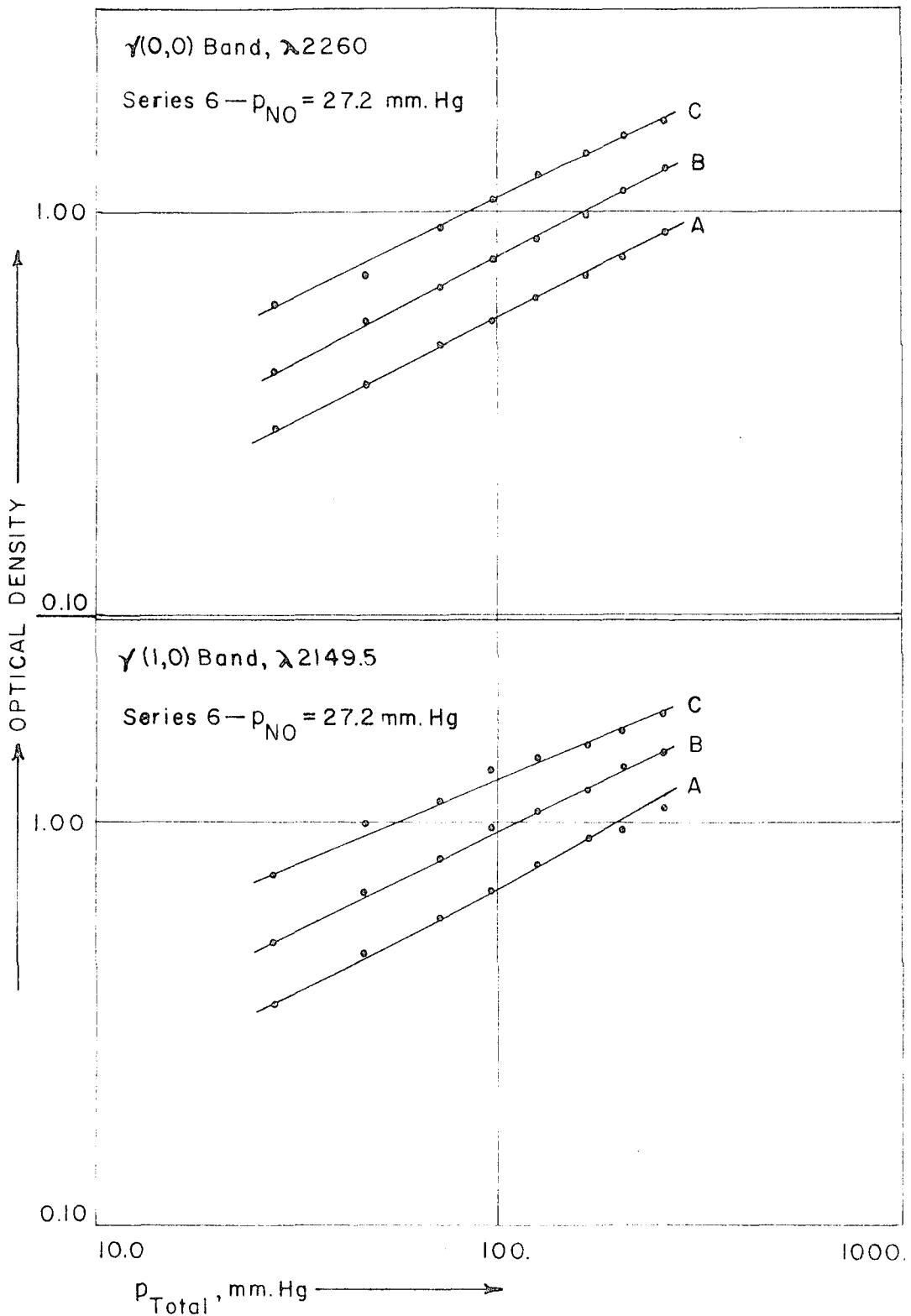


FIGURE 19:

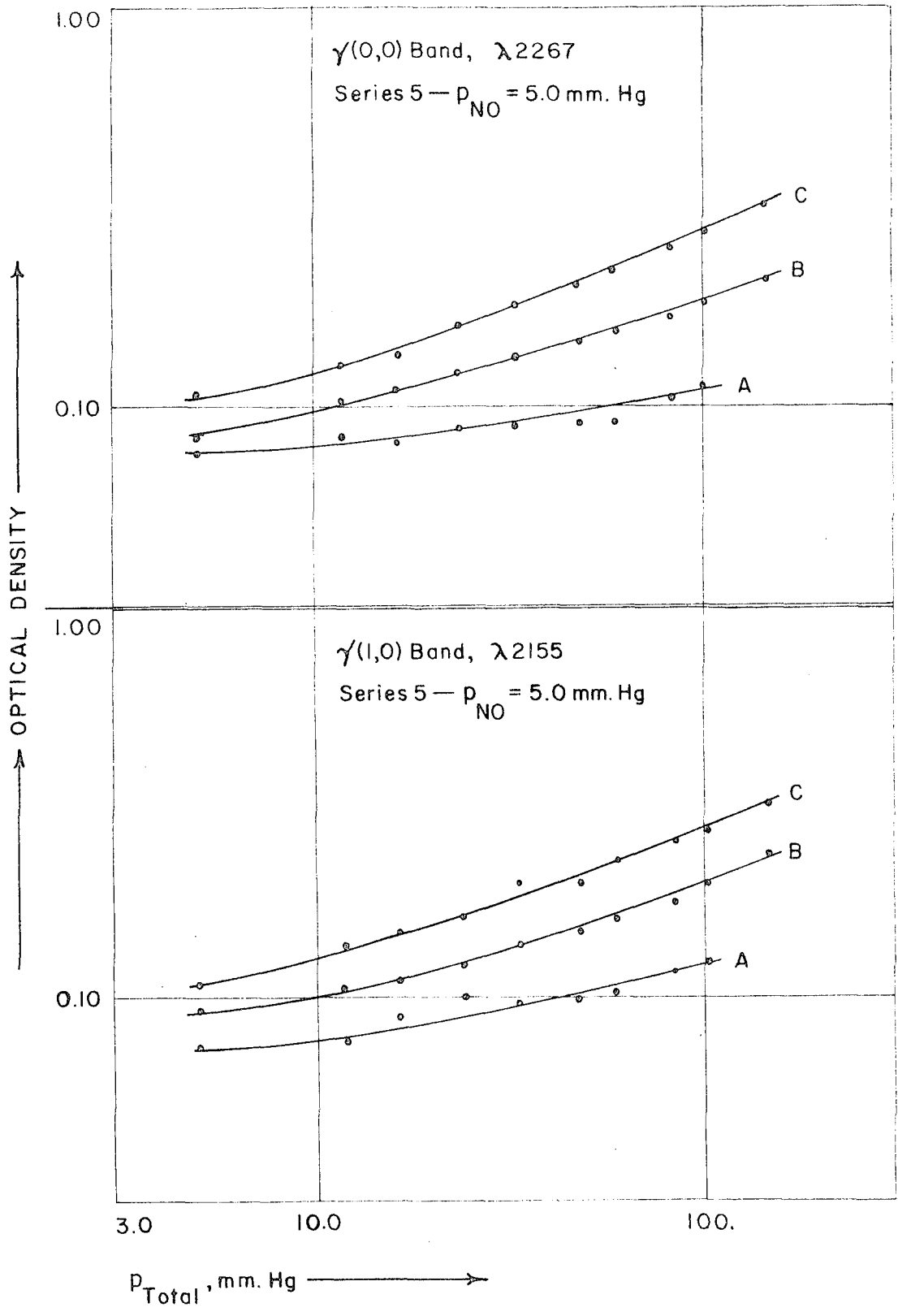
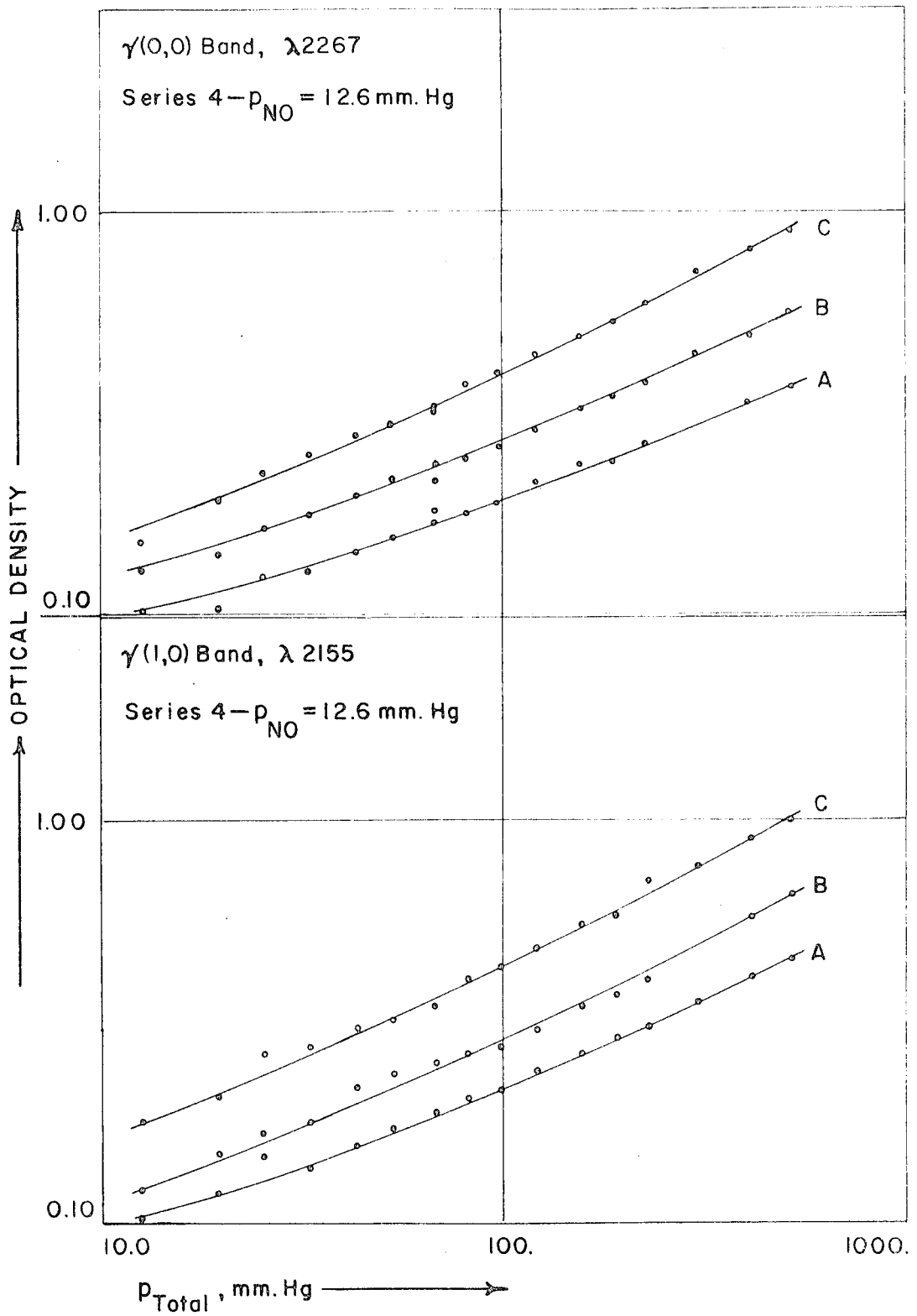


FIGURE 20:



2. If the optical path of NO is decreased sufficiently, then the apparent effect of adding nitrogen is considerably decreased; and for very short cells, and low partial pressures of NO, adding nitrogen causes little or no change in the optical density (see Figure 16). This behavior is a result of the exponential dependence of the absorption upon the optical path, and is shown by the growth curves in Figure 23.

V. THEORETICAL CALCULATIONS

As was discussed in Section III, the calculation of growth curves requires the computation of the following integral:

$$\int_{-\infty}^{\infty} \rho(z-z_0) [1 - \exp(-\chi f(z))] dz$$

where $f(z)$ is proportional to the true absorption coefficient of the spectrum. If some assumption is made concerning the contours of individual lines and the structure of the spectrum, $f(z)$ may be calculated from the known constants of the molecule. It is also assumed that the absolute intensity of an absorption line is not significantly altered by an increase in the line width. This is equivalent to the assumption of the constancy of the wave functions and their matrix elements in the first-order perturbation theory, even though the energy is shifted by the perturbation.

The calculations made were based on a model of the $\gamma(0,0)$ band of NO, but neglecting spin splitting from either the $X^2\Pi$ state, which is 120 cm^{-1} , and thus essentially splits the band into two sub-bands which are widely separated, or the $A^2\Sigma^+$ state, for which the splitting has not been observed even up to high rotational quantum numbers. The structure is therefore essentially that of a $\Sigma^+ - \Pi$ transition. The

Λ -doubling defect has also been neglected. The frequencies of the three branches P, Q, R are given by

$$R(J) = \nu_{oo} + 2B'_V + (3B'_V - B''_V)J + (B'_V - B''_V)J^2$$

$$Q(J) = \nu_{oo} + (B'_V - B''_V)J + (B'_V - B''_V)J^2$$

$$P(J) = \nu_{oo} - (B'_V - B''_V)J + (B'_V - B''_V)J^2$$

$J = J''$, the quantum number in the lower state; B''_V is the B_V for the lower state, B'_V that for the upper state. The P- and R- branches can be represented by a single Fortrat parabola,

$$\nu = \nu_{oo} + (B'_V - B''_V)m + (B'_V - B''_V)m^2$$

where m goes through all integral values plus and minus except $m = 0$ and $m = 1$. The Q-branch commences with $J = 1$. Instead of values of B_0 for the two states, the values of B_e were used: For the ${}^2\Pi$ state, $B''_e = 1.70 \text{ cm}^{-1}$; the distortion constant $\alpha''_e = 0.0178 \text{ cm}^{-1}$. For the $A^2\Sigma^+$ state, $B'_e = 1.995 \text{ cm}^{-1}$ and $\alpha'_e = 0.0164 \text{ cm}^{-1}$. Relative intensities for the lines are given approximately by the Honl-London formulae (16) coupled with the Boltzmann factor:

$$F_J^R = \frac{J}{4} e^{-E_J/kT}$$

$$F_J^Q = \frac{2J+1}{4} e^{-E_J/kT}$$

$$F_J^P = \frac{J+1}{4} e^{-E_J/kT}$$

The temperature used was 298^oK. The band structure thus computed has lines of frequencies and relative intensities which are shown approximately in Table 2.

The slit function used was a gaussian curve whose effective width was 12.80 cm⁻¹ (compare the slit width used in the experiments, page 23). It was centered at a point -9.00 cm⁻¹ from the band origin, i.e. toward the head at -11.40 cm⁻¹.

Two problems arise at this point concerning the matching of the calculated optical density with the densities measured in the experiments. It is not possible to determine exactly how the frequency setting of the calculation is related to the frequency at which the maximum of the peak λ 2268 occurs, although in choosing the setting used it was attempted to choose a location likely to be close to that maximum. The second difficulty comes from the difference of 10% in the slit widths employed in the calculation and in the experiments. Does the magnitude of optical density at a given frequency depend critically upon the slit width?

The question about the slit width can be answered by data taken with a slit width of 26.4 cm⁻¹ for the $\gamma(0,0)$ band. It was found that the optical densities for this width are only decreased about 8% to 12% at λ 2268 from the densities found for a slit width of 14.1 cm⁻¹. Consequently we may safely neglect the effect on the optical density of a 10% change in slit width.

If this effect of slit width is neglected, then it follows

Table 2

Nitric Oxide Band Model

Line	ν (cm ⁻¹)	$F_t(\nu)$		Line	ν (cm ⁻¹)	$F_t(\nu)$
P(6)	-11.40	0.50		Q(1)	0.60	0.30
P(7)	-11.20	0.51		Q(2)	1.75	0.47
P(5)	-11.00	0.47		P(13)	2.60	0.32
P(8)	-10.40	0.50		Q(3)	3.50	0.63
P(4)	-10.00	0.43		Q(4)	5.80	0.77
P(9)	- 9.00	0.48		P(14)	7.00	0.27
P(3)	- 8.40	0.36		R(1)	8.60	0.10
P(10)	- 7.00	0.45		Q(5)	8.70	0.86
P(2)	- 6.20	0.28		P(15)	12.00	0.23
P(11)	- 4.40	0.41		Q(6)	12.20	0.92
P(1)	- 3.40	0.20		R(2)	13.80	0.19
P(12)	- 1.20	0.36		Q(7)	16.25	0.95
					etc.	

that the calculated optical density is not greater than that which would be obtained for the peak $\lambda 2268$, either in a theoretical calculation, or in an experiment with an optical path corresponding to the same theoretical optical path. To prove this, one may consider the detailed structure of the model of the spectrum which was used (see Table 2). It will be evident that at the position where the slit is centered, near the band head, if one imagines that the slit center has been moved in from regions beyond the band head, toward the band origin, the optical density would have been observed to increase steadily from zero, and will certainly not have passed through any minima, certainly not the pronounced minimum between the two experimental peaks $\lambda 2268$ and $\lambda 2267$, which is the minimum lying between the P-branch band head and the Q,R-branch peak. As can be seen by inspection, this minimum must lie closer to the band origin than the slit center at -9.00 cm^{-1} . Consequently, the optical density obtained for the above location of the slit center cannot be greater than the local maximum of the region to which we have shown it is restricted, and this local maximum is just the peak at $\lambda 2268$.

The first calculation is based on the assumption that the lines have pure Lorentz contours with the same half-width. The method of calculation is a straightforward graphical one. Templates were made, for the relative intensities given above, for all lines listed within the slit width. The curves were traced and added. Then the ordinates so obtained were multi-

plied by various values of X, the theoretical optical-path factor, and the true absorptions, $[1 - \exp(-Xf(\nu))]$, were plotted versus frequency on an ordinate scale determined by the gaussian slit function at that frequency. The integrations were carried out with a planimeter. The error introduced by the planimeter was less than 2%, but the major source of errors was in the graphical estimation of line wings; even though these were very small, a large error could result when the value of X was large, since then the wings became very strongly absorbing. Still, the error involved in the overall estimate is probably not greater than 10%. Since the extreme accuracy of the calculation is not critical, no attempt will be made to estimate the error.

Table 3 shows the results of these calculations, and in Figure 21 the calculated optical density is plotted as a function of an optical path factor, X, and of half-width,

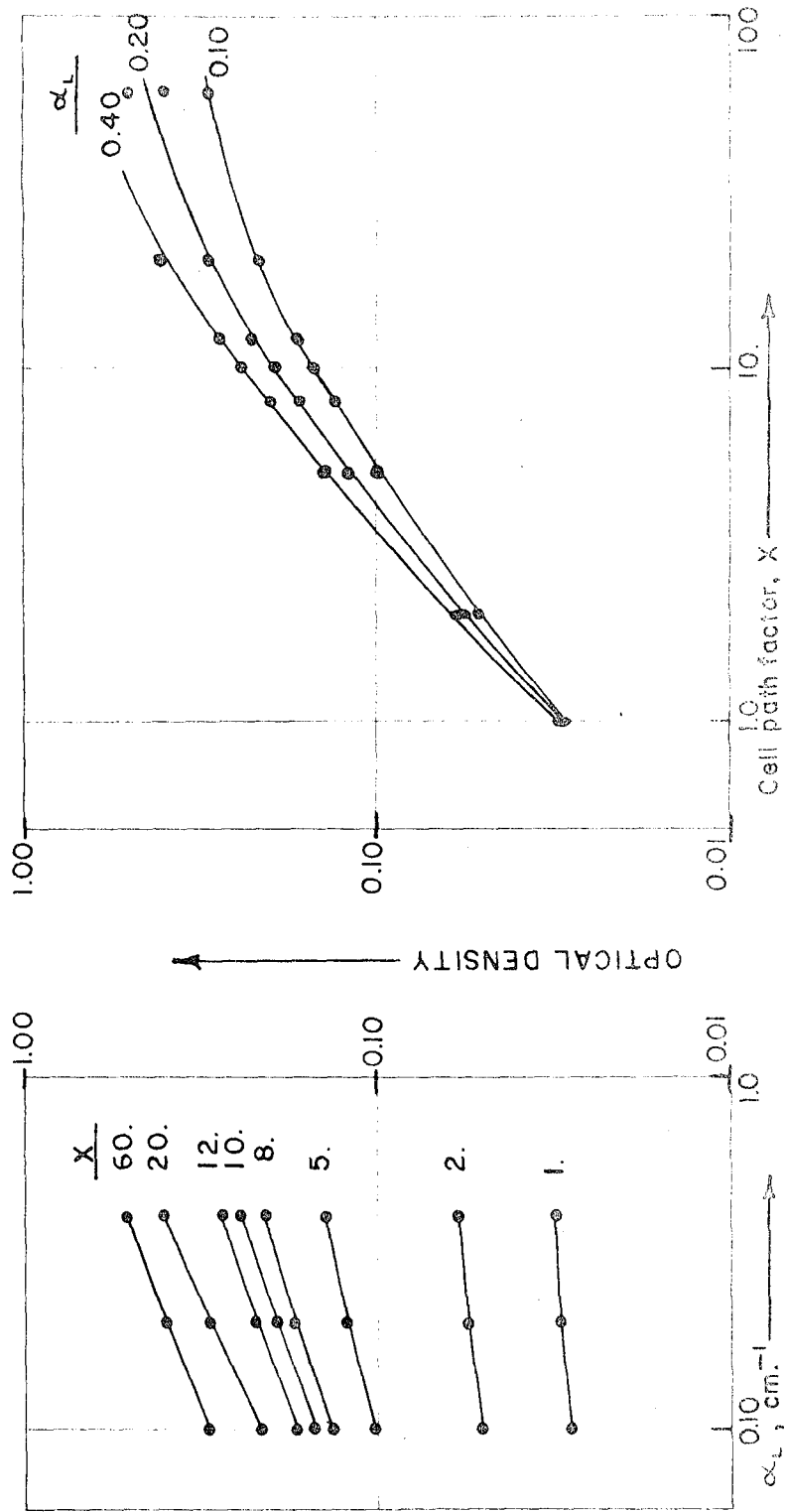
α_1 . It can be seen from the curves in this figure that the optical density at first increases almost linearly with optical path, but subsequently changes over to a square-root dependence. At high nitric oxide concentrations, one does observe what is found by these calculations for large X. It is interesting also that the linear relation which is obeyed initially was also obtained by Elsasser. Another feature of interest is that the increase in optical density with increasing α_1 is strongly dependent on the value of X, the optical path; if X is small, the effect of changing α_1 is hardly

Table 3
 Calculation of Optical Density as a Function of Path Length and Line Width,
 Assuming Lines to Have a Simple Lorentz Contour

X	0.10 cm ⁻¹		0.20 cm ⁻¹		0.40 cm ⁻¹	
	A ₀	I/I ₀	d	A ₀	I/I ₀	d
1	0.0785	0.9215	0.035	0.0822	0.9178	0.037
2	0.139	0.861	0.065	0.150	0.850	0.071
5	0.257	0.743	0.129	0.307	0.693	0.159
8	0.329	0.671	0.173	0.404	0.596	0.225
10	0.367	0.633	0.199	0.457	0.543	0.265
12	0.403	0.597	0.224	0.502	0.498	0.303
20	0.492	0.508	0.294	0.618	0.382	0.418
60	0.621	0.379	0.421	0.750	0.250	0.602
				A ₀	I/I ₀	d
				0.0854	0.9146	0.039
				0.158	0.842	0.075
				0.335	0.665	0.177
				0.466	0.534	0.272
				0.533	0.467	0.331
				0.591	0.409	0.388
				0.754	0.246	0.609
				0.862	0.138	0.860

FIGURE 21:

CALCULATED OPTICAL DENSITY FOR $\gamma(0,0)$ NEAR $\lambda 2268$
AS A FUNCTION OF X AND α_L , FOR LORENTZ CONTOUR.



noticeable; but when X becomes larger, d eventually acquires the full square-root dependence upon α_L . The explanation of this phenomenon lies in the following fact: when X is small, the line centers are not yet completely absorbed; consequently, the result of changing line contour at constant area has only a slight effect on the true absorption. When however the X-factor is large enough that the line center is completely absorbed, then widening the line will give a substantial increase in true absorption.

The failure of this calculation to account for the behavior observed at low NO concentrations arises from the naive assumption on which it is based: that the lines have purely Lorentzian contour. Actually, for instance, when the line half-width is 0.10 cm^{-1} , it must have purely a Doppler contour, at least at the line center, since that is the magnitude of the Doppler half-width at this temperature. It is unreliable, therefore, to extrapolate the curves from the above calculation into the regions of lower pressure, because it is just there that the Doppler width is of great significance. Consequently, although this first calculation gives satisfying confirmation of experimental results at NO pressures above 30 or 40 mm Hg, it is unsuitable for estimating the Lorentz half-width.

For this reason, it seemed advantageous to carry out a second calculation, in which a more realistic line contour was employed. In the opposite extreme from essentially

Lorentzian contour, is the case when the contour is mostly gaussian near the line center, and only in the wings is the Lorentzian contribution dominant. The general form for a line with both Doppler and Lorentz broadening can be accurately expressed as an integral (see for instance Penner and Kavanagh (17)):

$$f_j(\nu) = \frac{S_j a}{\pi \nu_j} \left(\frac{Mc^2}{2\pi RT} \right)^{1/2} \int_{-\infty}^{\infty} \frac{e^{-y^2} dy}{a^2 + [(\xi - \xi_j) - y]^2}$$

$$S_j = \int f_j(\nu) d\nu, \quad F_j = \frac{S_j}{\nu_j} \left(\frac{Mc^2}{2\pi RT} \right)^{1/2}; \quad a = \frac{\alpha_L}{2\nu_j} \left(\frac{Mc^2}{2RT} \right)^{1/2} = \frac{\alpha_L}{\alpha_D} \sqrt{\ln 2}$$

$$(\xi - \xi_j) = \left(\frac{\nu - \nu_j}{\nu_j} \right) \left(\frac{Mc^2}{2RT} \right)^{1/2} = \frac{z(\nu - \nu_j)}{\alpha_D} \sqrt{\ln 2}.$$

For the special case in which a is less than 0.2, the following expression is accurate to 0.2%:

$$\frac{f_j(\xi - \xi_j)}{F_j} = e^{-(\xi - \xi_j)^2} - \frac{2a}{\sqrt{\pi}} \left[1 - 2(\xi - \xi_j) e^{-(\xi - \xi_j)^2} \int_0^{\xi - \xi_j} e^{y^2} dy \right] + a^2 \left[1 - 2(\xi - \xi_j)^2 \right] e^{-(\xi - \xi_j)^2}$$

define $F(z) = e^{-z^2} \int_0^z e^{y^2} dy$ (i)

If $\frac{\xi - \xi_j}{a} \gg 1$, a good approximation is (wings of the line):

$$\frac{f(\xi - \xi_j)}{F_j} = \frac{a}{\sqrt{\pi}} \cdot \frac{1}{a^2 + (\xi - \xi_j)^2} \left[1 + \frac{3}{2(\xi - \xi_j)^2} \right] \quad (ii)$$

In the case of the nitric oxide band spectrum model which has been used, Table 2 shows that, except for the three lines at

the band head, the distance between line centers is never less than 0.40 cm^{-1} . Investigation of the magnitudes of the expressions (i) and (ii) has shown that, for $|v-v_j| \geq 0.20 \text{ cm}^{-1}$ (or $|\xi-\xi_j| \geq 3.330$), (ii) is a good approximation to (i), with error less than 1% at 0.20 cm^{-1} from the head. Consequently, near the center of any line (except the three lines near the band-head) the total true absorption coefficient, $f_t(v)$, may be expressed as follows:

$$f_t(v) = F_j \left\{ e^{-(\xi-\xi_j)^2} - \frac{2a}{\sqrt{\pi}} \left[1 - 2(\xi-\xi_j) e^{-(\xi-\xi_j)^2} \int_0^{\xi-\xi_j} e^{-y^2} dy \right] + a^2 \left[1 - 2(\xi-\xi_j)^2 \right] e^{-(\xi-\xi_j)^2} \right. \\ \left. + \sum_{k \neq j} \left(\frac{F_k}{F_j} \right) \frac{a}{\sqrt{\pi}} \left[\frac{1}{a^2 + (\xi-\xi_k)^2} \right] \left(1 + \frac{3}{2(\xi-\xi_k)^2} \right) \right\} \quad (\text{iii}).$$

where the sum over k represents the contributions of the wings. Further approximation to the expression for the wings may be made; if $a \leq 0.2$ and $|\xi-\xi_j| \geq 3.330$, an acceptable approximation will be:

$$\frac{f_k(v-v_k)}{F_k} \approx \frac{a}{\sqrt{\pi}} \frac{1}{(\xi-\xi_k)^2} \left[1 + \frac{3}{2(\xi-\xi_k)^2} \right]$$

In the actual calculation, a still rougher approximation was used, by neglecting the correction term $\frac{3}{2(\xi-\xi_k)^2}$. This would introduce an error of about 10% at $|\xi-\xi_k|=3.330$, but it becomes rapidly smaller as $|\xi-\xi_k|$ increases. The error in the estimation of wing contributions will be not greater than about 5%; and since, as we shall see, the total contri-

bution of the wings to the a-dependent term is about 35%, the total error in the a-dependent term as a result of the above approximations will be of the order of 2%, in the direction of underestimating the a-dependent term.

The problem then is to compute the integral:

$$\int_{-\infty}^{\infty} e^{-b(\xi-\xi_0)^2} [1 - e^{-\chi f_t(\xi)}] d\xi$$

where $e^{-b(\xi-\xi_0)^2}$ is the slit weighting function, and $f_t(\xi)$ has the form (iii) for $|\xi-\xi_j| \leq 3.330$ ($|v-z_j| \leq 0.20 \text{ cm}$) on either side of each line center z_j ; and has the wing form in all portions not in the above regions:

$$f_t(\xi) = \sum_k \frac{F_k a}{\sqrt{\pi}} \left(\frac{1}{(\xi-\xi_k)^2} \right) \quad (\text{iv})$$

In addition, for the three lines at the band head, (iii) is not correct, since there is overlapping of the lines to a considerable degree. These will be treated separately later.

Let us consider also the non-peak regions in which (iv) is applicable, the "non-peak" regions as they will be called. Define the centers of these regions as points z_i ; the subscript i will be used only for non-peak regions, j only for peaks at their central regions, and k for all other lines whose centers are away from the region under consideration.

The next step is to approximate the gaussian weighting

function by Taylor's expansions for each region around its center, ν_j or ν_i . This gives

$$e^{-b(\xi-\xi_0)^2} \approx e^{-b(\xi_{j(i)}-\xi_0)^2} - b(\xi_{j(i)}-\xi_0)e^{-b(\xi_{j(i)}-\xi_0)^2}(\xi-\xi_{j(i)}) \dots$$

$$\approx R_{1j(i)} + R_{2j(i)}(\xi-\xi_{j(i)})$$

It will develop that R_2 contributions will be very small; and they will be neglected.

The actual integration will involve three forms: peak regions, non-peak regions, and the band head region.

1. Peak regions. Using the form (iii) for $f_t(\xi)$, one may write:

$$f_t(\xi) = F_j \left\{ e^{-z^2} - \frac{2a}{\sqrt{\pi}} \int_0^z e^{-z^2} e^{y^2} dy \right\} + a^2 \left[1 - 2z^2 \right] e^{-z^2} + \sum_{k \neq j} \frac{F_k}{F_j} \cdot \frac{a}{\sqrt{\pi}} \frac{1}{(z - \Delta_{kj})^2}$$

$$z = \xi - \xi_j$$

$$\Delta_{kj} = (\xi_k - \xi_j)$$

The limits of the integration are $\pm z_0 = 3.330$. Expanding the exponential of $-X f_t(\xi)$ in a power series, one must then compute:

$$\int_{-z_0}^{z_0} - \sum_n \frac{(-X F_j)^n}{n!} [f_j(z)]^n (R_{1j} + R_{2j} z) dz$$

The linear term will be deferred till the n^{th} order term has been done. For terms of higher order than the first, the

binomial expansion is used to terms of quadratic order in a . The expression for wing contributions from other lines will be approximated by a Taylor series:

$$\sum_k \frac{F_k a}{\sqrt{\pi}} \frac{1}{(z - \Delta_{kj})^2} \approx \sum_k \frac{F_k a}{\sqrt{\pi}} \cdot \frac{1}{\Delta_{kj}^2} - \sum_k \frac{F_k a}{\sqrt{\pi}} \frac{1}{(-\Delta_{kj})^3} (z)$$

$$\approx K_{1j} a + K_{2j} a z ;$$

we shall also neglect the K_2 terms as trial calculations have shown them to be small.

For the n^{th} term ($n \geq 2$):

$$\frac{(-X F_j)^n}{n!} \int_{-z_0}^{z_0} \left\{ e^{-nz^2} + n e^{-(n-1)z^2} \left[-\frac{2a}{\sqrt{\pi}} (1 - 2ze^{-z^2} \int_0^z e^{y^2} dy) + \left(\frac{K_{1j}}{F_j} \right) a + a^2 (1 - 2z^2) e^{-z^2} \right] \right.$$

$$\left. + \frac{n(n-1)}{2} e^{-(n-2)z^2} \left[\left(\frac{-2a}{\sqrt{\pi}} \right)^2 (1 - 2ze^{-z^2} \int_0^z e^{y^2} dy)^2 + \frac{2a K_{1j}}{F_j} \left(\frac{-2a}{\sqrt{\pi}} \right) (1 - 2ze^{-z^2} \int_0^z e^{y^2} dy) \right] \right.$$

$$\left. + \left(\frac{K_{1j}}{F_j} \right)^2 a^2 \right\} (R_{1j} + R_{2j} z) dz ;$$

multiplying out, one obtains:

$$\frac{(-X F_j)^n}{n!} \int_{-z_0}^{z_0} \left\{ e^{-nz^2} + \left(-\frac{2a}{\sqrt{\pi}} + \frac{K_{1j} a}{F_j} \right) (n e^{-(n-1)z^2}) + \frac{4a}{\sqrt{\pi}} (n z e^{-nz^2} \int_0^z e^{y^2} dy) + a^2 n e^{-nz^2} \right.$$

$$\left. - 2a^2 n z^2 e^{-nz^2} + \frac{2a^2}{\pi} n(n-1) e^{-(n-2)z^2} + \left(\frac{8a^2}{\pi} \right) (n(n-1) z^2 e^{-nz^2} \int_0^z e^{y^2} dy \int_0^z e^{u^2} du) \right.$$

$$\left. - \left(\frac{8a^2}{\pi} \right) (n(n-1) z e^{-(n-1)z^2} \int_0^z e^{y^2} dy) - \frac{2a^2 K_{1j}}{F_j \sqrt{\pi}} (n(n-1) e^{-(n-2)z^2}) + \left(\frac{K_{1j}}{F_j} \right)^2 \frac{a^2}{2} n(n-1) e^{-(n-2)z^2} \right.$$

$$\left. + \frac{4a^2 K_{1j}}{F_j \sqrt{\pi}} (n(n-1) z e^{-(n-1)z^2} \int_0^z e^{y^2} dy) \right\} (R_{1j} + R_{2j} z) dz .$$

Since the above terms are all even functions of z , the R_2 term does not contribute; it only does contribute when multiplied with the small K_2 terms, so the result is negligible. The integrals from $-z_0$ to $+z_0$ are essentially the same as from $-\infty$ to $+\infty$, except for certain special cases. Some integrals are now evaluated:

$$\int_{-\infty}^{\infty} e^{-nz^2} dz = \frac{\sqrt{\pi}}{\sqrt{n}} \qquad \int_{-\infty}^{\infty} z^2 e^{-nz^2} dz = \frac{1}{2n} \frac{\sqrt{\pi}}{\sqrt{n}}$$

$$\begin{aligned} \int_{-z_0}^{z_0} z e^{-mz^2} \int_0^z e^{u^2} du &= \frac{e^{-mz^2}}{(-2m)} \int_0^z e^{u^2} du \Big|_{-z_0}^{z_0} + \frac{1}{2m} \int_{-z_0}^{z_0} e^{-(m-1)z^2} dz \\ &= \frac{\sqrt{\pi}}{2m\sqrt{m-1}}, m > 1; \quad = z_0 - F(z_0), m = 1 \end{aligned}$$

where

$$F(z) = e^{-z^2} \int_0^z e^{y^2} dy.$$

Finally,

$$\begin{aligned} \int_{-z_0}^{z_0} z^2 e^{-nz^2} \int_0^z e^{u^2} du \int_0^z e^{y^2} dy dz &= -\frac{1}{2n} \left\{ z e^{-(n-2)z^2} (F(z))^2 \Big|_{-z_0}^{z_0} - 2 \int_{-z_0}^{z_0} z e^{-(n-1)z^2} \int_0^z e^{u^2} du dz \right. \\ &\quad \left. - \int_{-z_0}^{z_0} e^{-nz^2} \int_0^z e^{u^2} du \int_0^z e^{y^2} dy dz \right\} \end{aligned}$$

The last term is:

$$G = \int_{-z_0}^{z_0} e^{-nz^2} \int_0^z e^{u^2} du \int_0^z e^{y^2} dy dz; \text{ now, } z \leq \int_0^z e^{y^2} dy \leq ze^{z^2}$$

so that

$$\int_{-z_0}^{z_0} ze^{-nz^2} \int_0^z e^{u^2} du dz \leq G \leq \int_{-z_0}^{z_0} ze^{-(n-1)z^2} \int_0^z e^{u^2} du dz.$$

For $n > 2$,

$$\frac{\sqrt{\pi}}{2n\sqrt{n-1}} \leq G \leq \frac{\sqrt{\pi}}{2(n-1)\sqrt{n-2}};$$

we have employed

$$G = \frac{\sqrt{\pi}}{(2n-1)\sqrt{n-2}}.$$

For $n=2$, substitute

$$G \approx \int_{-z_0}^{z_0} z^2 e^{-(n-1)z^2} dz = \frac{\sqrt{\pi}}{2}.$$

$$\int_{-z_0}^{z_0} z^2 e^{-nz^2} \int_0^z e^{u^2} du \int_0^z e^{y^2} dy dz = \begin{cases} \frac{\sqrt{\pi}}{\sqrt{n-2}} \left(\frac{1}{4n(n-1)} + \frac{1}{n(2n-1)} \right), & n > 2 \\ -\frac{z_0}{2} F^2(z_0) + z_0 - F(z_0) + \frac{\sqrt{\pi}}{8}, & n = 2. \end{cases}$$

Substituting these values into the expression for the n^{th} term, one obtains the following simplified expressions (next page):

$$\frac{(-XF_j)^n}{n!} \left\{ \frac{\sqrt{\pi}(1-a^2)}{\sqrt{n}} + \frac{\sqrt{\pi}a^2n}{\sqrt{n}} + \frac{aK_{ij}n\sqrt{\pi}}{F_j\sqrt{n-1}} - \frac{2a(n-1)}{\sqrt{n-1}} - \frac{2K_{ij}a^2n(n-2)}{F_j\sqrt{n-2}} \right. \\ \left. + \frac{2a^2}{\sqrt{\pi}} \left[\frac{n(n-1)}{\sqrt{n-2}} - \frac{2n}{\sqrt{n-2}} + \frac{2}{\sqrt{n-2}} + \frac{2(n-1)}{(2n-1)\sqrt{n-2}} \right] \right\}$$

Summing over n from 3 to ∞ :

$$= \sqrt{\pi}(1-a^2)\beta_1(XF_j) + \sqrt{\pi}a^2\beta_3(XF_j) + \frac{\sqrt{\pi}aK_{ij}}{F_j}\beta_2(XF_j) - 2a\beta_6(XF_j) \\ + \frac{2a^2}{\sqrt{\pi}} \left[\beta_5(XF_j) + 2\beta_7(XF_j) - 2\beta_4(XF_j) + 2\beta_8(XF_j) \right],$$

where the functions β are defined:

$$\beta_1(u) = -\sum_3^{\infty} \frac{(-u)^n}{n! \sqrt{n}}; \quad \beta_2(u) = -\sum_3^{\infty} \frac{(-u)^n}{n! \sqrt{n-1}}; \quad \beta_3(u) = -\sum_3^{\infty} \frac{(-u)^n}{n! \sqrt{n}}; \\ \beta_4(u) = -\sum_3^{\infty} \frac{(-u)^n}{n! \sqrt{n-2}}; \quad \beta_5(u) = -\sum_3^{\infty} \frac{(-u)^n}{n! \sqrt{n-2}}; \quad \beta_6(u) = -\sum_3^{\infty} \frac{(-u)^n}{n! \sqrt{n-1}}; \\ \beta_7(u) = -\sum_3^{\infty} \frac{(-u)^n}{n! \sqrt{n-2}}; \quad \beta_8(u) = -\sum_3^{\infty} \frac{(-u)^n}{n! (2n-1)\sqrt{n-2}}.$$

The term for n=2 is as follows:

$$-\frac{(XF_j)^2}{2} \left\{ \frac{\sqrt{\pi}(1-a^2)}{\sqrt{2}} + \frac{2\sqrt{\pi}a^2}{\sqrt{2}} + \frac{2a\sqrt{\pi}K_{ij}}{F_j} - 2a + \frac{8a^2}{\pi} \left[z_0 - z_0 F^2(z_0) + \frac{\sqrt{\pi}}{8} \right] \right. \\ \left. - \frac{8a^2K_{ij}F(z_0)}{\sqrt{\pi}F_j} \right\}.$$

The functions $\beta(u)$ were calculated for a range of values of u from 2.0 to 15.0. In the actual estimation the quadratic terms (i.e., $n = 2$) which have the same analytical form as terms $n=2$ were combined at this level with the similar terms from higher n , and the resulting functions were plotted, before graphs were used to interpolate for the specific lines. This device avoided the subtraction of two large numbers to obtain a small one, and gave the small one directly from the plot. The terms in question are the first four in each of the above expressions, for $n \geq 3$ and $n = 2$.

Finally, the term $n = 1$ may be done explicitly:

$$(XF_j) \int_{-z_0}^{z_0} \left\{ e^{-z^2} - \frac{2a}{\sqrt{\pi}} (1-2ze^{-z^2}) \int_0^z e^{y^2} dy + a^2 (1-2z^2) e^{-z^2} + \frac{a}{F_j \sqrt{\pi}} \sum_k \frac{F_k}{(z - \Delta_{kj})^2} \right\} dz$$

$$= (XF_j) \left[\sqrt{\pi} - \frac{4aF(z_0)}{\sqrt{\pi}} + \frac{2az_0}{\sqrt{\pi}} \sum_k \left(\frac{F_k}{F_j} \right) \frac{1}{(\Delta_{kj}^2 - z_0^2)} \right]$$

The value of $F(z_0)$ may be obtained from the tables of the function made by W. L. Miller and A. R. Gordon (18). $F(z_0) = .1582$.

2. Non-peak regions. Here the function to be integrated is:

$$\int_{-w_{oi}}^{w_{oi}} [1 - e^{-Xf_i(\xi - \xi_i)}] [R_{1i} + R_{2i}(\xi - \xi_i)] d\xi \quad w = \xi - \xi_i$$

$$f_i(\xi - \xi_i) = \sum_k \frac{F_k a}{\sqrt{\pi}} \frac{1}{(\omega - \Delta_{ki})^2}.$$

The quadratic term can be obtained by a Taylor series expansion:

$$\begin{aligned} \left[\sum_k \frac{F_k a}{\sqrt{\pi}} \frac{1}{(\omega - \Delta_{ki})^2} \right]^2 &\approx \left[\sum_k \frac{F_k a}{\sqrt{\pi}} \frac{1}{\Delta_{ki}^2} \right]^2 + 2 \left[\sum_k \frac{F_k a}{\sqrt{\pi}} \frac{1}{\Delta_{ki}^2} \right] \left[\sum_k \frac{F_k a}{\sqrt{\pi}} \frac{1}{\Delta_{ki}^3} \right] \omega \\ &+ \left[\sum_k \frac{2F_k a}{\sqrt{\pi}} \frac{1}{\Delta_{ki}^3} \right] \frac{\omega^2}{2} + 3 \left[\sum_k \frac{F_k a}{\sqrt{\pi}} \frac{1}{\Delta_{ki}^2} \right] \left[\sum_k \frac{F_k a}{\sqrt{\pi}} \frac{1}{\Delta_{ki}^4} \right] \omega^2 + \dots \end{aligned}$$

Now, investigation has shown that under all circumstances the linear and quadratic terms in ω in this expansion contribute less than 2% to the value of the term quadratic in a . They will be neglected. Therefore, for the total contribution of a non-peak region (R_2 -contributions are again neglected):

$$R_{ii} \left\{ \sum_k \frac{2X F_k a \omega_{oi}}{\sqrt{\pi} \Delta_{ki}^2} - \frac{X^2}{2} \left[\sum_k \frac{F_k a}{\sqrt{\pi} \Delta_{ki}^2} \right]^2 (2\omega_{oi}) \right\}$$

where $\Delta_{ki} = (\xi_k - \xi_i)$; $2\omega_{oi}$ is the width of the i^{th} non-peak region in the dimensionless units of $\xi = \frac{2z}{\alpha_0} \sqrt{\ln 2}$.

A special non-peak region is the one which is in front of the band head. This is treated the same way as the others, except that it is not extended out to infinity, but only for 2.00 cm^{-1} to the left of the band head.

3. Band head region. Here there are three lines 0.20 cm^{-1} apart from one another, and of about equal intensities (.50, .51, and .47). Expanding the exponential of $-Xf_t(\xi)$ as before, we may still do the linear term accurately. For higher order in n , the correct treatment of the problem would involve the computation of integrals which are too formidable to do without great labor. Instead, the higher order terms will be approximately computed by treating the peaks as in the case of the other peak regions. The K_{1j} used will be considerably larger here, because of the proximity of the other peaks, but otherwise no unusual problems develop. An estimate of the error incurred by this approximation will now be made.

For the n^{th} term, the correct expression is (in the region of overlap from ξ_1 to ξ_2 , between two lines):

$$(\eta_j = \xi - \xi_j)$$

(see next page)

$$\int_{\xi_1}^{\xi_2} \frac{(-X)^n}{n!} \left\{ \sum_0^n \frac{n! F_1^m F_2^{n-m}}{m! (n-m)!} e^{-m\eta_1^2} e^{-(n-m)\eta_2^2} \right.$$

$$+ \sum_0^{n-1} \frac{n! F_1^m F_2^{n-m-1}}{m! (n-m-1)!} e^{-m\eta_1^2} e^{-(n-m-1)\eta_2^2} \left[-\frac{2a}{\sqrt{\pi}} (F_1 + F_2 - 2\eta_1 F(\eta_1) - 2\eta_2 F(\eta_2)) \right.$$

$$\left. + F_1 a^2 (1 - 2\eta_1^2) e^{-\eta_1^2} + F_2 a^2 (1 - 2\eta_2^2) e^{-\eta_2^2} \right\}$$

$$+ \sum_{m=0}^{n-2} \frac{n! F_1^m F_2^{n-m-2}}{m! 2! (n-m-2)!} e^{-m\eta_1^2} e^{-(n-m-2)\eta_2^2} \left(\frac{4a^2}{\sqrt{\pi}} \right) \left[1 - 2\eta_1 F(\eta_1) \right] \left[1 - 2\eta_2 F(\eta_2) \right] F_1 F_2 \left. \right\} d\xi.$$

Consider first $\frac{n! F_1^m F_2^{n-m}}{m! (n-m)!} e^{-m\eta_1^2} e^{-(n-m)\eta_2^2}$, the form appearing in the term independent of a. When $m=0$ or $m=n$, one has simply the non-overlapping contributions. When $n-m$ or m are large or even greater than 1, this expression tends rapidly to zero everywhere, because of the extreme narrowing effect of the index n or m . The largest term, in fact, comes from the term $n=2$, and it is $2e^{-\eta_1^2} e^{-\eta_2^2}$. The maximum value occurs when $\eta_1 = \eta_2 = \frac{.10}{.05} \sqrt{\ln 2}$; the value there is $1/128$, which when integrated from ξ_1 to ξ_2 gives a result of .026, to be compared with the total result from non-overlapping terms, of the order of $\sqrt{\frac{\pi}{2}}$.

In the a-dependent term, again the quadratic ($n=2$) case will contribute the most, the higher terms will have very much smaller contributions to make, etc., exactly as above. The

term for $n=2$ can be estimated as follows: the correct term is:

$$2! \left[e^{-\eta_1^2} \left(-\frac{2a}{\sqrt{\pi}} (1-2\eta_2 F(\eta_2)) + a^2 (1-\eta_2^2) e^{-\eta_2^2} \right) + \dots \text{etc.} \right]$$

The maximum value is probably of the order of the value at 0.10 cm^{-1} , which is $1/32 (.306a-.353a^2)$. Integrating from ξ_1 to ξ_2 again, one obtains the result that the error is about $(.064 F_1)$, which again is small compared to the total a -dependency, which is of the order of $\beta_6(u)$, about 10 or better.

The last error will be from the term in a^2 which arises by a cross-product of the form:

$$F_1 F_2 \frac{4a^2}{\pi} \left[1-2\eta_1 F(\eta_1) \right] \left[1-2\eta_2 F(\eta_2) \right]$$

and, again using the value at 0.10 cm^{-1} , one obtains

$$(.306)^2 (3.33) \frac{4a^2}{\pi} F_1 F_2 \approx 0.2a^2$$

which, when compared to the total a^2 term, is negligible.

One may therefore safely conclude that the error introduced in the final answer, by the approximation made for the band head region, is less than 2% for any of the terms, constant, linear or quadratic in a .

The final answer to the computation is obtained by summing

the local integrals over all the running indices i and j , and dividing by the slit function to normalize. The result is the observed absorption at the frequency setting of the slit. The final answers have been computed for two relative optical paths, 10 and 20. The analytical functions obtained are:

$$X = 10; A_0 = 0.1253 + 0.1462a - .1485a^2$$

$$X = 20; A_0 = 0.1493 + 0.313a + .1818a^2$$

In Figure 22, the value of d as a function of a is shown on a logarithmic plot.

In the limit of large a , the curves for the optical density must asymptotically approach those found for the Lorentz line calculation, and it would be useful to correlate the curves obtained from each calculation. The cell path factors used in each calculation were purely relative, and the relation between them must be found in order to correlate the curves. In the case of the Lorentzian contour, it was assumed that a Lorentzian line had magnitude 1.000 at the line center for $A_j = 1.00$, and $\alpha_1 = 0.10 \text{ cm}^{-1}$. This means that a factor (π) (.05) was introduced into the standard normalized form,

$$\left(\frac{\alpha_1}{2\pi} \right) \left(\frac{1}{\frac{\alpha_1^2}{4} + (z - z_j)^2} \right)$$

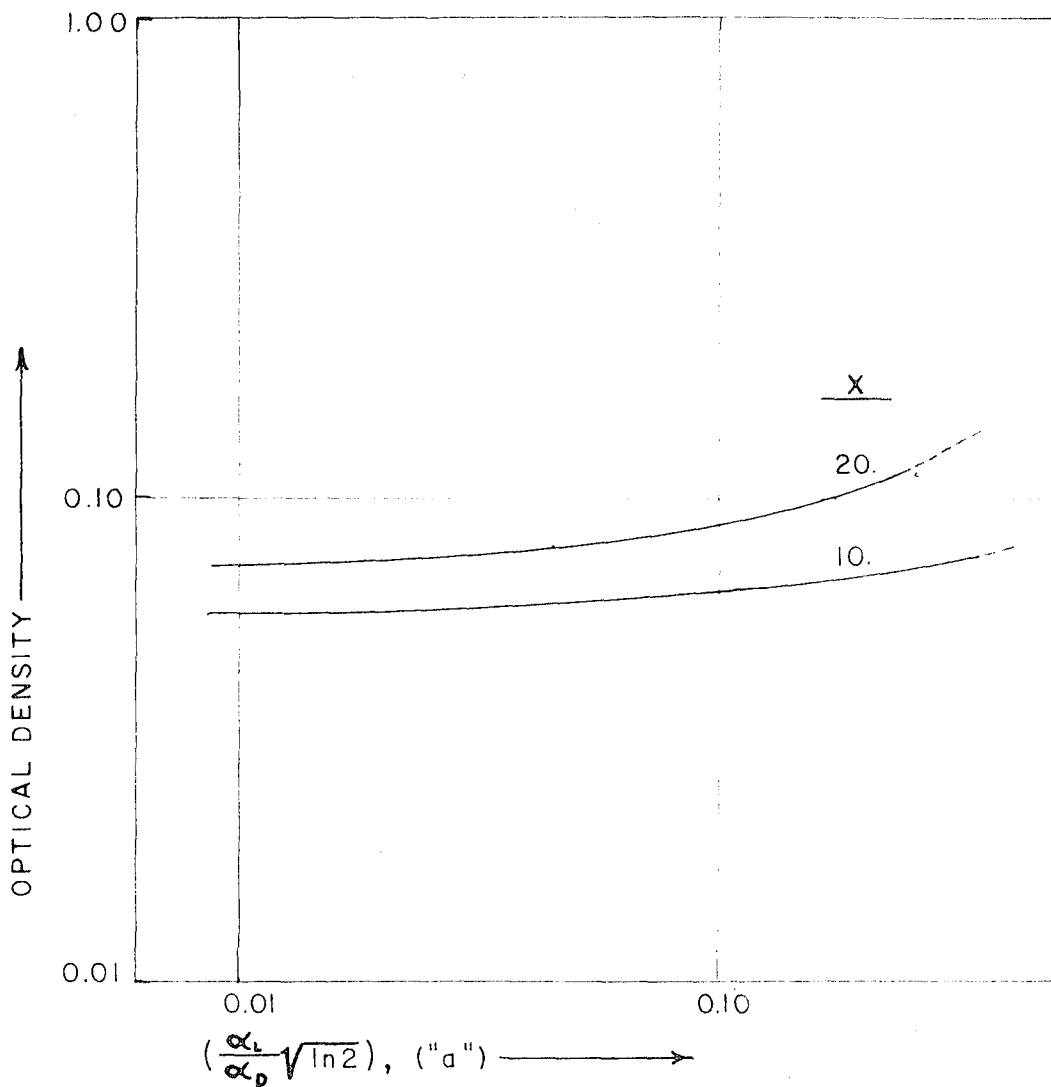
FIGURE 22:

THEORETICAL GROWTH CURVES

DOPPLER LINES WITH LORENTZ BROADENING

NO $\gamma(0,0)$ BAND, $\sim \lambda 2268$

$\text{Log}_{10}(\text{Optical Density})$ vs. $\text{Log}_{10}\left(\frac{\alpha_L}{\alpha_D} \sqrt{\ln 2}\right)$



In addition, a scale factor of 1.13 was introduced before the relative X-factors of 1,2,5,8,10,12,20, and 60 were introduced. In the case of the analytical calculations, one may easily find the factors as follows: when $\frac{\xi - \xi_j}{a} \gg 1$, the form $\frac{a}{\sqrt{\pi}} \frac{1}{a^2 + (\xi - \xi_j)^2}$ was used. In the limit of large a this is indeed a Lorentzian curve, for all values of $(\xi - \xi_j)$; but the above expression remains valid in particular. Remembering that $a = \frac{\alpha_L \sqrt{\ln 2}}{\alpha_D}$, and that $\xi - \xi_j = \frac{2(\nu - \nu_j) \sqrt{\ln 2}}{\alpha_D}$, one may see that

$$\frac{a}{\sqrt{\pi}} \left[\frac{1}{a^2 + (\xi - \xi_j)^2} \right] = \frac{\sqrt{\pi} \alpha_L \alpha_D}{4\pi \sqrt{\ln 2}} \left[\frac{1}{\frac{\alpha_L^2}{4} + (\nu - \nu_j)^2} \right]$$

since $\alpha_D = 0.10 \text{ cm}^{-1}$, the ratio of the two relative cell path factors X and X', say, is $(1.13)(\sqrt{\pi})(\sqrt{\ln 2}) = 1.667$. That is, a factor 10.00 on the X-scale of the pure-Lorentzian curves is 16.67 on the X-scale of the combined contour.

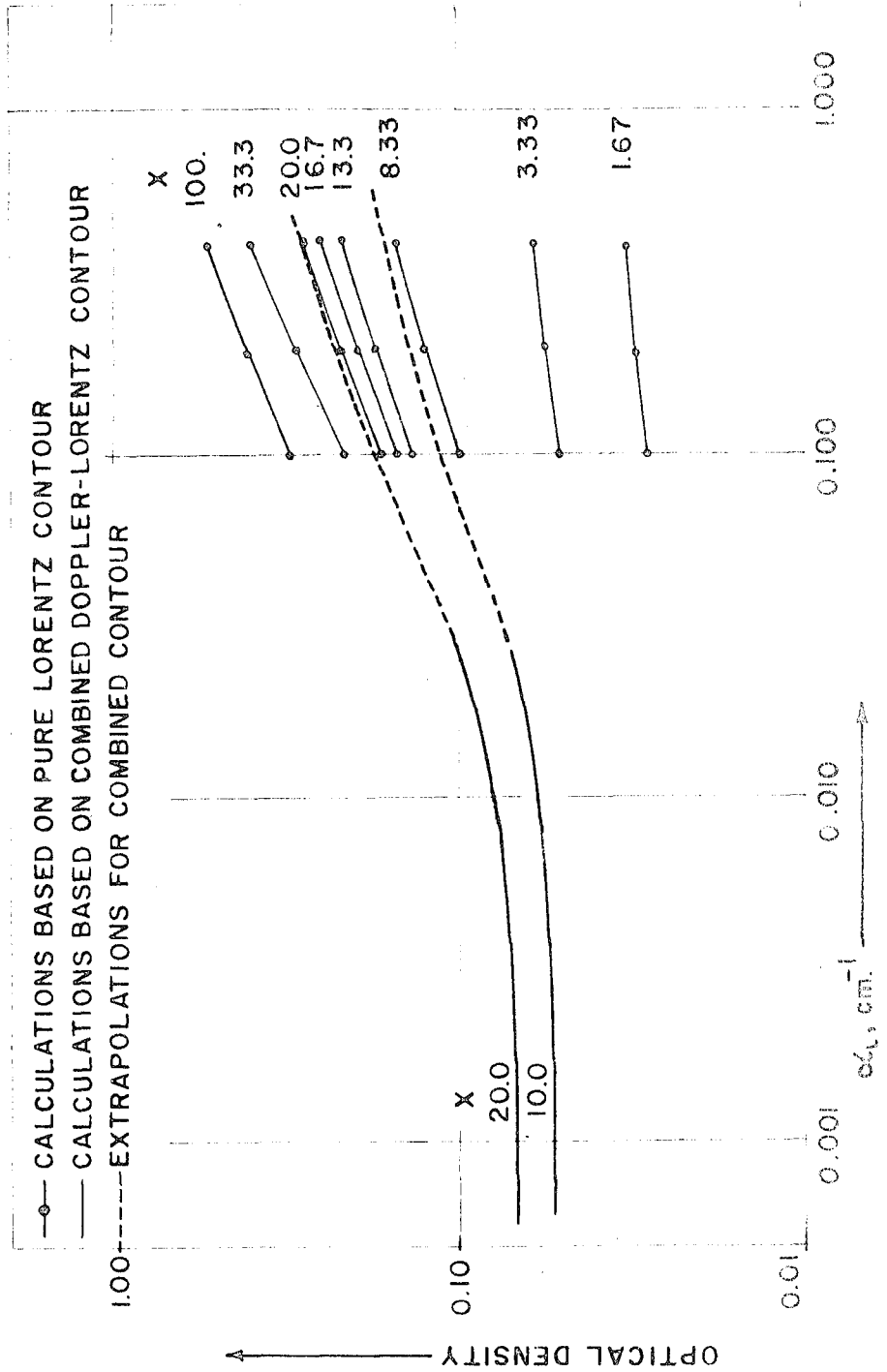
A correlation is made between the two calculations by plotting them both on a graph of $\text{Log}_{10} d$ versus $\text{Log}_{10} \alpha_L$. The curves for combined contour will at first lie slightly above those for a pure Lorentz contour because of the extra width due to the Doppler broadening, but they will asymptotically approach the Lorentz contour calculations as the half-width α_L increases.

Figure 23 shows the result of this correlation, together with a qualitative extrapolation of the actual curves. The behavior of d as a function of increasing half-width α_L is

FIGURE 23:

THEORETICAL GROWTH CURVES

$\text{LOG}_{10}(\text{OPTICAL DENSITY})$ VS. $\text{LOG}_{10}(\alpha_L)$, $\lambda 2268$



in agreement with the observed behavior of d as a function of the total pressure. Therefore it may be concluded that the simple Lorentz theory is capable of explaining the line broadening of these transitions of NO. An attempt to estimate the collision diameter will be made in the next section.

Several interesting experiments are suggested by the calculations made. One of these is to study the optical density when the path length is short but the pressure sufficiently high so that a Lorentz contour is a satisfactorily accurate description of line shape. When the optical path is varied under such conditions, it may be predicted that optical density will be nearly a linear function of the optical path x . This result was also obtained by Ladenburg and Reiche, and by Elsasser, in their more simple models which were mentioned earlier. Of course, the major difficulty inherent in such an experiment is the low optical density at which this phenomenon must necessarily be observed. Another experiment would be to obtain d for very low pressures, by using a long cell. This would help to provide information about the NO self-broadening as compared to the nitrogen broadening effect, and would help also in the estimate of the collision diameter.

VI. ESTIMATE OF THE COLLISION DIAMETER

Estimation of the collision diameter depends essentially upon the matching of the abscissa $\log_{10} \alpha_c$ of the curves of growth with the abscissa $\log_{10}(P)$ of the observed plots of $\log d$ versus $\log P$ at constant optical path x (only the nitrogen broadening data were used), at the same frequency setting, slit width, and optical density. Provided these conditions are fulfilled, the value obtained for α should be accurate to better than $\pm 0.5 \text{ \AA}$. Unfortunately, it is not possible to exactly satisfy all these conditions, and the best that can be done is to provide certain constraints upon the matching of curves.

The difference of 10% between the slit widths of theory and experiment has already been shown to have a negligible effect on the optical density obtained (see Section V, page 66).

As was also demonstrated in Section V, page 66 , the optical density obtained in the calculation cannot be greater than the optical density at the peak $\lambda 2268$ for the corresponding experimental optical path. This result leads to the following constraint: in matching the theoretical growth curves with the experimental curves, we are not permitted to displace the theoretical curves to actual densities less than their calculated values, although we are permitted a moderate

amount of freedom (say, <20%) in the displacement to actual optical densities higher than their calculated values, to obtain a match with the experimental curves.

The above constraint, however, does not determine the optical density matching, since there is no correlation between the true optical path, x , in cm-mm Hg, and the theoretical optical path factor X of the growth curves. Without some information about the absolute intensity of the $\gamma(0,0)$ band it would not be possible to obtain this correlation.

Another criterion of matching may be introduced at this point: The variation of optical density with the optical path at constant pressure is known from the experiments. At 20 mm Hg the optical density at $\lambda 2268$ is proportional to $(x)^{0.41}$ over a range of optical paths from 48 to 198 cm-mm. This implies that the optical density ratio of two curves of growth whose optical path factors X lie in a range corresponding to the above range of x must be given by the expression $(X_2/X_1)^{0.41}$ at 20 mm Hg; for $X_2/X_1 = 2.0$, the ratio of optical densities should be 1.33. The logarithm of 1.33 is 0.123; this separation occurs between the curves for $X=20$ and $X=10$ for the value of half-width $\alpha_L=0.010 \text{ cm}^{-1}$. Now, even without recourse to a correlation between the theoretical path factor X and the experimental path x in cm-mm, it seems unlikely that $X=20$ would correspond to a value for x of more than 198 cm-mm. We may therefore safely conclude that the separation between the curves of growth $X=20$ and

$X=10$ will not be greater than 0.123 at 20 mm Hg. This leads to the conclusion that the collision diameter cannot be greater than that corresponding to $\alpha_1 = 0.010 \text{ cm}^{-1}$ at 20 mm Hg, or 9 Angstroms.

Recently, the absolute integrated intensities of the γ -bands (0,0), (1,0), and (2,0) have been measured by Weber and Penner (22). By using the value they quote for $\gamma(0,0)$ it is possible to obtain the necessary correlation between the theoretical optical path factor X and the true optical path x to which it corresponds. The calculation is outlined in detail in Part II of the Appendix; it will suffice here to describe the basic steps: From the data quoted by Weber and Penner it is possible to get an expression for the integrated absorption coefficient over the band. By summing up the theoretical relative intensities of the model of the band used in the calculations for the growth curves, it is possible to get the absolute integrated absorption coefficient of a given line. From this, with the proper normalization factors the correlation ratio between x and X can be found. The result is that X/x has a value of 1.588, where X is the theoretical optical path in Figure 23 and x is the true optical path in cm-mm. Thus, for instance, $X=20$ corresponds to $x=12.6 \text{ cm mm}$. This correlation leads to an approximate match, $\alpha_1 = 0.010 \text{ cm}^{-1}$ at $P=100 \text{ mm Hg}$. The resulting value for σ is 3.8 A. The match is indicated by the heavy lines in Figures 24a and 24b.

FIGURE 24a:

COLLISION DIAMETER ESTIMATE

Match between Scales of Half-Width α_L and Pressure

$\gamma(0,0)$ Band, $\lambda 2268$ — Series 1-9

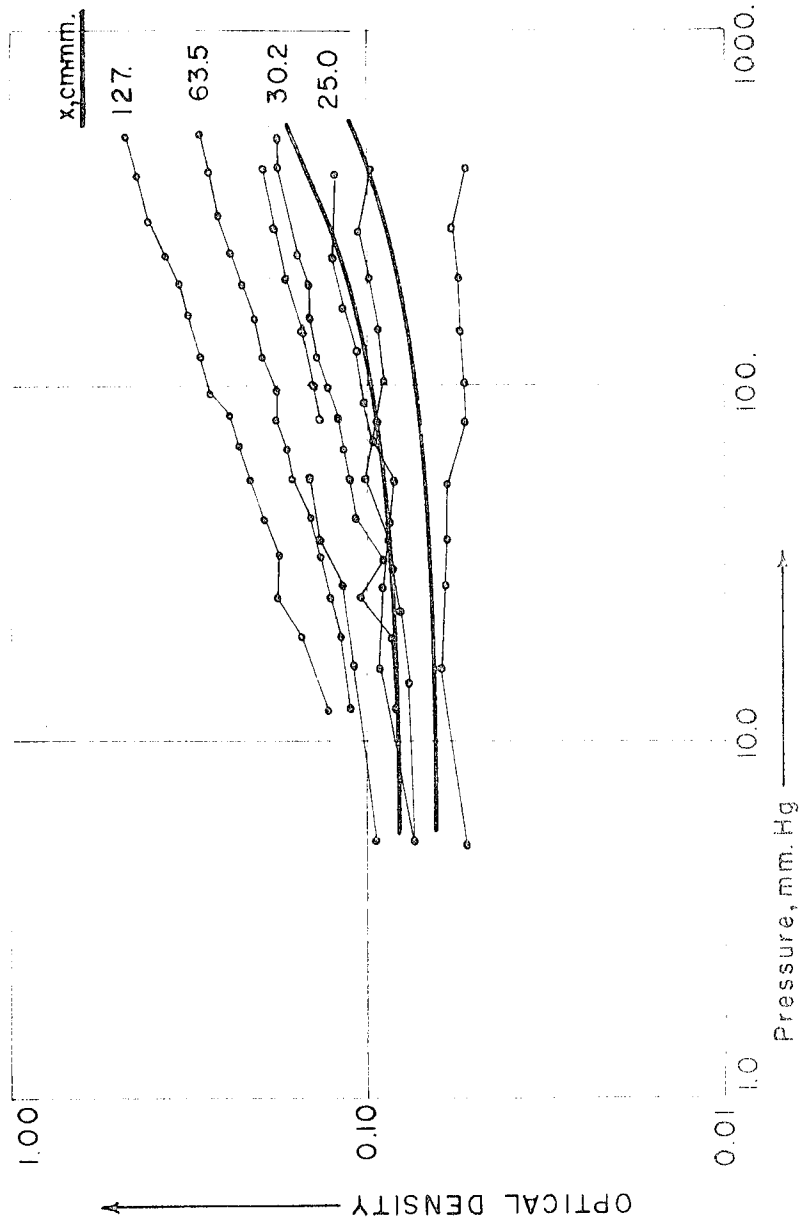
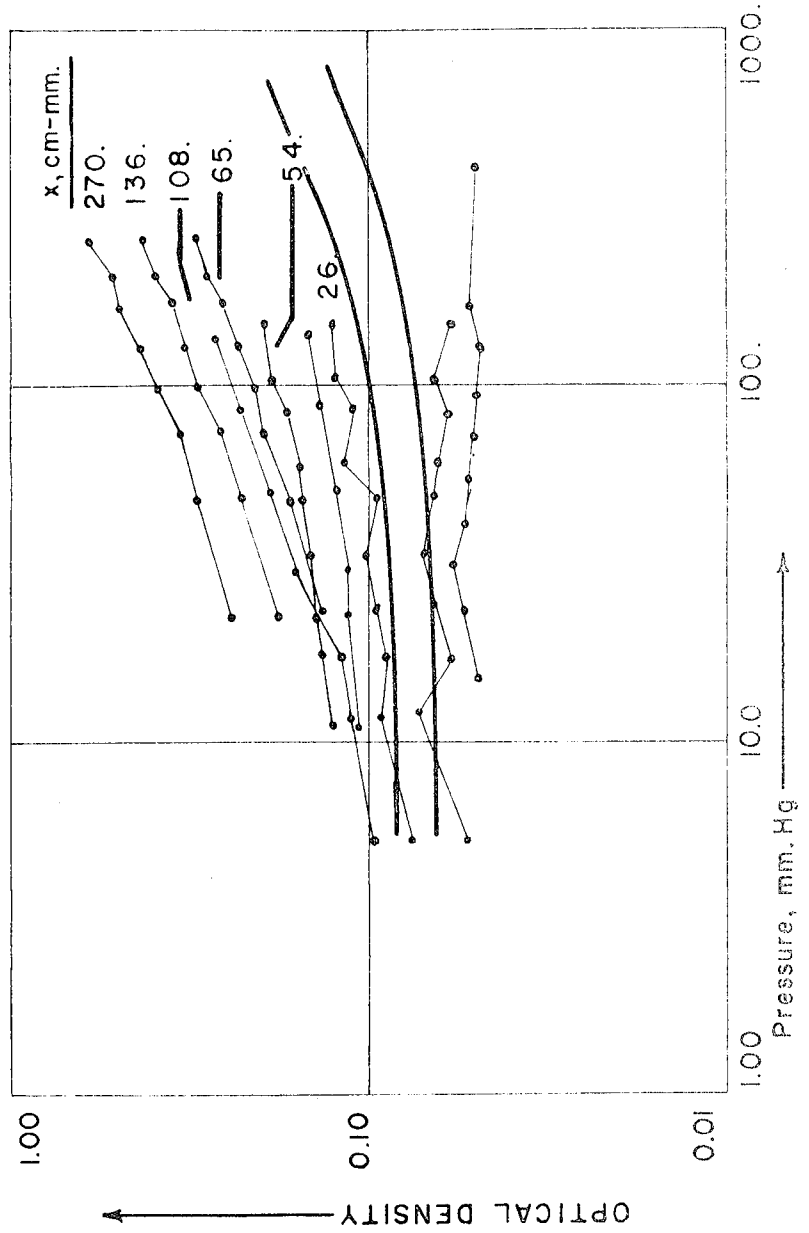


FIGURE 24b:

COLLISION DIAMETER ESTIMATE

Match between Scales of Half-Width α_L and Pressure

$\gamma(0,0)$ Band, $\lambda 2268$ — Series 1-9



In the actual estimate, only selected portions of the data have been used: tracings of optical density versus total pressure for $\lambda 2268$, in the $\gamma(0,0)$ band, at constant partial pressures of NO. Some of these data were too erratic and have not been included in Figures 24a and 24b, although they are tabulated in Table B of the Appendix.

It is unfortunate that the calculated curves do not lie in the same region of optical path as the more reliable experimental data, but this was not foreseen because the value of the absolute intensity was not available at the time the calculations were made. The value $X=20$ was a sort of upper limit for which the calculation was feasible for a combined contour, since the functions called $\beta(X)$ in the calculation (see page 80) are alternating series, most of whose terms are many orders of magnitude larger than the sum. The calculations were made on a 10-place calculator, and a typical function β for the argument $X=20$ involves approximately 60 terms, 30 of which are of the order of 10^8 or larger, while the sum is less than 400; so the capabilities of the calculating machine are a limiting factor for higher X . Calculations for larger X could be made by using the IBM computer available here or by a numerical integration, but the labor involved in either step would probably not be justified by the value of the results obtained. The estimate of σ is sufficiently well determined if the intensity measurement used is a reliable one.

VII. ERRORS

The accuracy of the spectrophotometer tracings is affected by a great number of sources of error, of which the most important will now be discussed. It is evident from inspection of Figures 9-20 that these errors are of considerable magnitude. It will be shown, however, that they will not strongly affect the collision diameter estimate; correction for the systematic deviations observed would tend to slightly increase the value obtained for σ .

Evidences of errors in the experimental data are of three types:

1. Scatter of points in any single series with a given cell. This includes most of the "random" errors, and will be only briefly mentioned.

2. If one compares plots for the nitrogen broadening experiments from different series, then it will be found that certain discrepancies occur between plots. These discrepancies are only detectable for the strongest peaks of the bands, $\lambda 2149.5$ and $\lambda 2260$; in the other cases, they lie within the scatter of any one plot. If one assumes that nitrogen is as effective as NO in causing broadening, then it follows that the optical density observed with a given path of nitric oxide, x , at a given total pressure P , ought to be the same, regardless of what the partial pressure of NO is. However,

comparison of Figures 14, 15, and 18 reveals that this is not quite true. In Figure 14, for which the partial pressure of NO is 5.3 mm, the optical path for the 10 cm cell is 53 mm-cm; for Figure 15, the partial pressure of NO is 12.6 mm, so that for the 5 cm cell and the 2.4 cm cell the optical paths are 63 and 30, respectively. But superposition of the plots shows that, although the first few points from the curve for the 10 cm cell in Figure 14 lie correctly in place in Figure 15, the slope of that curve is noticeably less than those for the curves of Figure 15, and the end-points lie far too low, in fact superposing on the curve for optical path 30 at higher pressures (2.4 cm cell). A similar, although not so pronounced, deviation may be observed by comparison of Figures 15 and 18.

3. Occasionally sharp "breaks" may be observed at one point for all three cells in a series of measurements. In some of the data this is a very obvious systematic deviation. The clearest example in the plots shown is in Series 3.

The possible sources of error may be classified according to their origin in the spectrophotometer, the cells, or the gas-filling system.

A. Spectrophotometer Errors:

1. Noise: This is a significant contributor to random errors when the optical density falls below 0.10; its approximate magnitude can be estimated visually by reference to Figure 8. The erratic behavior of curves

for such low densities is attributed to this cause.

2. Variations in slit width and balance control: If the zero level of the balance control is altered, there is a corresponding alteration in the slit width; this does not affect the optical density obtained by more than 5%, except for optical densities less than 0.10.

3. Variations in slit width with time: The slit width has a tendency to change over periods of time of the order of two or three days, even for constant setting of the other controls. Unfortunately, this fact was unknown when most of the measurements were made; but again this will not profoundly alter the values of optical density resulting.

4. As has been already mentioned on page 43, there is a tendency for the instrument to underestimate optical densities above a magnitude of about 1.5.

B. Cell Errors:

1. Leakage: In most of the series of measurements, the cells were first tested for vacuum; a pressure of 5×10^{-5} mm of Hg at the beginning of a series was considered sufficient to indicate that the leak rate was negligible. After the use of "Araldite" cement for the windows was adopted, little difficulty with leaks was experienced; although there was occasional evidence of decomposition of nitric oxide after

a series was completed, this decomposition is not ascribed to leaks. The stopcocks were reground twice during the experimental work.

C. Gas-Filling System Errors:

1. Pressure Measurements: The pressure gauge used for most of the nitrogen broadening experiments showed a slight discrepancy from readings given by the open-end manometer when the two were compared; but unfortunately, this gauge was broken before an accurate recalibration could be made. It is possible, however, to estimate the error, if one assumes the manometer to be correct; the result obtained is that the pressure readings given by the gauge are not more than 3% too high. The pressure gauge was used up to about 40 mm, and for higher pressures the manometer was used. This correction has not been applied to the pressures quoted.

2. Leakage of the system during a series of measurements: This was not discovered or suspected during most of the experimental work; but the deviations observed and mentioned above may be completely explained by assuming that the nitrogen added to the cells contained oxygen as a contaminant. After the commencement of a series, no further checks were made on the vacuum system for leaks; so that it is quite possible that the oxygen might have entered by that means. One series of measurements, Series 5, was terminated because of an

obvious leakage of the system after standing overnight.

3. Impurity in the nitrogen: The remaining possibility concerning the contamination of the nitrogen was that the oxygen had entered during the processes of purifying and storing the tank nitrogen. This would appear unlikely, since the amount of oxygen necessary to effect the observed deviations would be of the order of 2% of the total gas pressure added. However, since there is no way of determining the facts at this time, the possibility is suggested.

It was stated above that the presence of oxygen as a contaminant in the nitrogen is able to account for all the deviations observed. This can be shown as follows: Suppose that the nitrogen added to the cells contains a small percentage of oxygen, which we may assume to react completely with NO to form nitrogen dioxide. This will serve to reduce the effective optical path of nitric oxide, and thus cause the points for increasing total pressure to be successively and proportionately lowered--in effect, to lower the slope of a given curve from what it would otherwise be. This effect would be more pronounced for lower partial pressures of NO, since a greater percentage of nitric oxide would be destroyed for the addition of a given amount of oxygen. Thus we see that the lower slopes and low values of series for which the partial pressure of nitric oxide is smaller can be accounted

for in terms of a constant concentration of oxygen in the nitrogen; but the sharp breaks observed must be the result of leakage in the system. This becomes obvious when it is found that these breaks often occurred when the system had been standing overnight between the two measurements, as was the case in Series 3.

It might be suggested that the deviations observed are physically real. If such a hypothesis is accepted, it leads to results which are incredible on a physical basis. The strongest assumption that is physically acceptable is that nitric oxide is more effective in broadening than nitrogen. If this be granted, it is clear that as the pressure of added nitrogen increases, the difference in half-width due to different partial pressures of nitric oxide will be obliterated by the preponderant number of collisions with nitrogen, so that curves with the same optical path of nitric oxide ought to approach one another asymptotically with increasing nitrogen pressure, regardless of what the partial pressure of nitric oxide might be. Since there is no evidence of such an asymptotic approach in the curves observed, but rather an increasing separation, it must be concluded either that the difference in effect is extremely large, so that the region of asymptotic approach is not observable in the range studied, or that this mechanism is incapable of producing the observed effect. The first of these possibilities has been definitely ruled out by a photographic com-

parison of the self-broadening and the broadening by nitrogen (see Section VIII). The kind of assumption that must be made to produce the observed effect would involve interactions of so high an order as to be completely unlikely; the very least that is necessary is the assumption of 100% dimerization or extensive clustering of the NO molecules in the gas at low pressures.

It must now be considered whether or not these errors seriously affect the collision diameter estimate. To answer this question, it must be pointed out that the discrepancies lie within the experimental scatter of points for all wavelengths except the strong peaks $\lambda 2149.5$ and $\lambda 2260$. The wavelength $\lambda 2268$ only was used for estimate of the collision diameter. If one looks at Figures 24a and 24b, it is evident that there is considerable scatter in the slopes of curves having the same optical density at a given total pressure. However, the quantitative value of the slope is not a critical factor in determining the collision diameter. What is important is the pressure at which a definite trend upward commences. It can be seen by inspection that the correction to be applied in raising the slopes of the curves might result in a slight increase in the value estimated for σ .

VIII. PHOTOGRAPHIC INVESTIGATION OF EARLIER RESULTS AND COMPARISON

It must be emphasized that the effect of pressure broadening on the appearance of a spectrum is critically dependent upon a large number of specific variables of the molecule, the experimental conditions, and the analytical apparatus; and many simple criteria which have been used are really only applicable under very limited conditions. The paper by Naudé has already been referred to (page 4). He compared two photographs of the $\gamma(1,0)$ band: the first cell contained 21 mm NO in a path of 92 cm. The second photograph had exactly the same amount of NO, but 440 mm of nitrogen was added to the cell. Naudé observed that for rotational lines of the order of one Angstrom separation, in the first case there was a considerable region between the line centers in which the absorption was low, probably not more than 0.05, and the line centers were completely absorbed out; in the second picture, as Naudé put it, "every rotational line is broadened so much that the absorption becomes complete." Gaydon and Fairbairn (7) have pointed out, however, the feature of Naudé's experiment that invalidates his conclusion as to the magnitude of the pressure effect; namely, that the optical path he used was so great that a change in just the wings of the lines might account for such a phenomenal

alteration in the total absorption. This argument is correct in principle, but must be quantitatively checked to assure its validity.

In order to demonstrate that no "abnormal" pressure broadening occurs in these bands, Gaydon and Fairbairn exhibited a photograph of the $\gamma(0,0)$ band, taken with 2 mm of NO in a 15 cm path, with one atmosphere of added nitrogen. Their picture shows lines which are certainly narrow compared to the 0.7-0.8 A separation. The line centers are nearly completely absorbed, while there is no appreciable absorption at a point halfway between them. There is a factor of $92 \times 21 / 2 \times 15$, or 64.4, between the optical paths used by Gaydon and Fairbairn and by Naudé. To provide a check on the consistency of these results of Gaydon with those of Naudé, various contours were assumed, Lorentz, Doppler, and combinations of the two, and the value of the absorption coefficient was computed for frequencies near the line center and also at the point halfway between two lines of equal intensity, separated 15.4 cm^{-1} (1 A) apart. Then the following constraints were applied:

(1) A suitable value of optical path factor X was assumed, subject to the requirement that the absorption of a line be appreciable for a total width of about 0.5 cm^{-1} (Gaydon and Fairbairn case).

(2) This value of X was multiplied by 64.4, and the requirement made that the resulting absorption halfway be-

tween lines be 95%.

It proved impossible to satisfy these conditions for any contour chosen from the above forms. If a Lorentz contour of moderately great half-width is used, and criterion 2 satisfied, then the width of the lines under the conditions shown in Gaydon and Fairbairn's case would be better than 2.0 cm^{-1} ; while if condition 1 is satisfied the absorption corresponding to Naudé's photograph falls far short of what it should be; and no compromise contour was found for which the two conditions could even be approximately satisfied.

Two conclusions are possible: either one of the conflicting photographs is not representative of the true appearance of the bands; or else the inconsistency arises from the different conditions not taken account of, namely that in Gaydon and Fairbairn's photograph the partial pressure of NO was 2 mm, while in that of Naudé its partial pressure was 21 mm. If the broadening effect of the NO self-interaction were considerably greater than that of the N_2 -NO interaction, then the two photographs might be reconcilable.

In order to decide which of the two alternatives be correct, it was decided to take photographs of the $\gamma(0,0)$ band with conditions similar to those of each case, and also additional spectrograms which ought to reveal whether or not the NO self-broadening were stronger than the nitrogen-broadening.

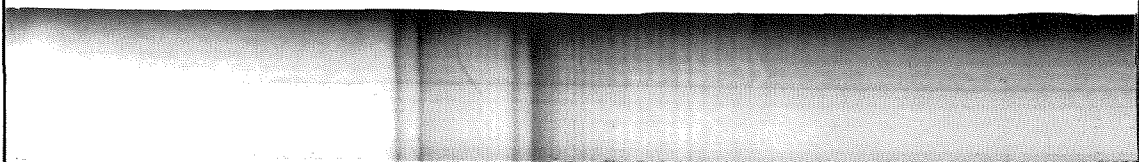
A Bausch and Lomb Quartz Littrow spectrograph, with dispersion 1.7 Å per mm at $\lambda 2270$, was used for all the photographs. A hydrogen discharge at about 1 mm pressure, 1800-2000 volts, 60 cycles, and 300 m.a., was used as source for the absorption photographs, and a Pfund iron arc as the comparison. The slit width used was 0.010 mm. Five photographs were made:

- (1) NO, 3.3 mm pressure, 10 cm path
- (2) NO, 3.3 mm pressure, 10 cm path, plus 675 mm N₂
- (3) NO, 603 mm pressure, 0.05 cm path
- (4) NO, 47.5 mm pressure, 40 cm path
- (5) NO, 47.5 mm pressure, 40 cm path, plus 511 mm N₂.

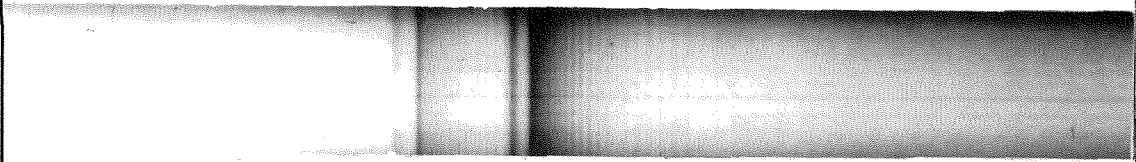
Conditions in #2 closely simulated those in Gaydon and Fairbairn's photograph. #1 was taken in order to show the effect of the nitrogen in broadening. #3 had the same optical path of NO as the first two, and shows the self-broadening effect. #4 and #5 had the same optical path of NO as Naudé's photograph, but the partial pressure of NO was about twice as great as in his case, so that broadening ought to be even more pronounced if NO self-broadening were important.

As may be seen in Plate I, the results definitely establish that Naudé's photograph is at fault. While there is a slight strengthening of the absorption lines upon the addition of nitrogen, the lines still appear moderately sharp, and there is very definite fine structure remaining

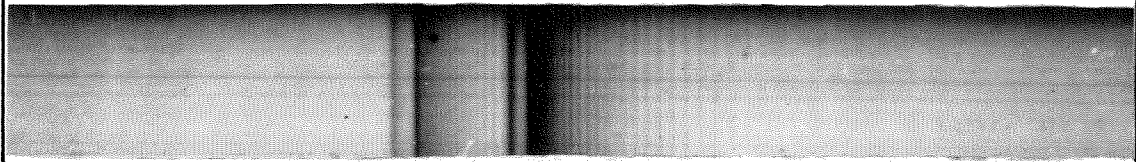
PLATE I



1. NO: PATH 10.0 cm., $P_{\text{NO}} = 3.3 \text{ mm.Hg}$



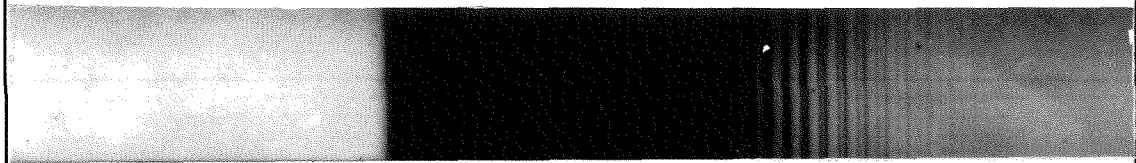
2. NO: PATH 10.0 cm., $P_{\text{NO}} = 3.3 \text{ mm.Hg}$; N_2 : $P_{\text{N}_2} = 675. \text{mm.Hg}$



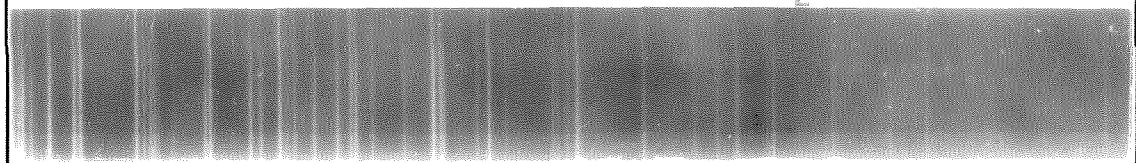
3. NO: PATH 0.053 cm., $P_{\text{NO}} = 603. \text{mm.Hg}$



4. NO: PATH 40.0 cm., $P_{\text{NO}} = 47.5 \text{ mm.Hg}$



5. NO: PATH 40.0 cm., $P_{\text{NO}} = 47.5 \text{ mm.Hg}$; N_2 : $P_{\text{N}_2} = 511. \text{mm.Hg}$



2284. 2276. 2271. 2267.5 2259.

6. IRON ARC

NITRIC OXIDE $\gamma(0,0)$ BAND, HEAD $\lambda 2269.4$

QUARTZ LITTROW, SLIT 0.010 mm.; SOURCE, H_2 DISCHARGE

in the band. Unfortunately, some of the fine structure in the original print was lost in the process of reproduction.

Photographs 2 and 3, which compare the effect of nitrogen with that of NO in broadening, show no perceptible difference. This reinforces the hypothesis made earlier that NO and nitrogen are equally effective in producing broadening in the γ -bands of NO.

It should be remarked that the band head of $\gamma(0,0)$, which really lies at $\lambda 2269.4$, has been referred to in the spectrophotometric work as $\lambda 2268$, because that was the wavelength indicated by the spectrophotometer.

IX. CONCLUSIONS AND DISCUSSION

The answer to the question of whether or not there is "abnormal" pressure broadening in the γ -bands of NO depends a great deal upon what one's criteria of abnormality are. If, for instance, it were desirable to analyze mixtures of gases for their nitric oxide content by measuring the absorption in these bands, then it is clear that there is an "abnormality" in the pressure effect which makes such a procedure completely useless.

As the investigation of the preceding section has shown, the use of simple qualitative criteria to determine the magnitude of a pressure effect may not be either conclusive or even indicative of the truth. One must make a detailed investigation to be sure.

There are other criteria possible for determining whether a pressure effect may be termed "abnormal," and they are of somewhat more fundamental character than the apparent effects over which so much discussion has been held.

1. The collision diameter is a sort of standard for comparing the effective range for collisions on an optical basis in these bands, with similar quantities for infrared and microwave spectra and with measurements of size obtained by kinetic theory measurements. A number of theoretical questions are raised by such a simple principle, primarily be-

cause the collision diameter for an electronic spectrum essentially describes the sensitivity of rotational states of the excited electronic configuration to external perturbations; and this may well be more delicate than the ground state, since presumably the electron in the excited state has a larger mean expectation value for its distance from the nucleus, and interaction with other molecules will consequently occur at a greater distance than in the ground state.

2. A specific abnormality criterion that might be advanced is the conclusion made by Lambrey that in nitric oxide this pressure effect is a unique property of the γ -band system. Some experiments carried out by Marmo indicated a true pressure effect in the β - and δ -systems of NO as well as in the γ -system. It is clear from the calculations that have been made in this work that the reason Lambrey did not observe a pressure effect in $\beta(2,0)$ is that it could not be observed even if present, because of the weak absorption of the band. It could very well be broadened just as much as the γ -bands observed.

3. Another criterion which may be used is the comparison of the pressure broadening with that observed in electronic transitions of other molecules. It is an unfortunate fact that there are few diatomic molecules for which sufficiently sharp band structure is obtained in absorption to permit convenient study of the pressure effect. If one allows more complex molecules, a study was made by Teves (19)

of o-dichloro-, p-dichloro-, and benzene itself; in some of the transitions, rotational fine structure is obtained. Teves cites values for σ which are in agreement with kinetic theory values.

SO₂ in the region from λ 3450 to λ 2800 shows pressure broadening; as has been discussed by Franck, Sponer, and Teller (20), the broadening could not be due to predissociation, because the energy of the excited state involved is far too low. The above authors noted that even at 2 mm SO₂ pressure, the fine structure appears completely blurred out; they estimate that σ is more than 15 times the kinetic theory value. This general result has been confirmed by us in a brief study of the SO₂ spectrum with the same spectrometer used for NO. SO₂ above 1.3 mm pressure obeys Beer's law, and there is no effect observed on adding nitrogen to the gas. This indicates that the fine structure has been almost entirely blurred out. Franck, Sponer, and Teller attribute this broadening effect to a radiationless transition made by the molecule into another stable excited electronic state. The close spacing and extensive overlapping of levels in a polyatomic rotor would permit such a transition with greater ease than in the case of a diatomic molecule. The primary importance of this information about SO₂ to our problem is to show that a pressure effect which has been definitely connected with only a radiationless transition into discrete levels gives a value of σ which is an

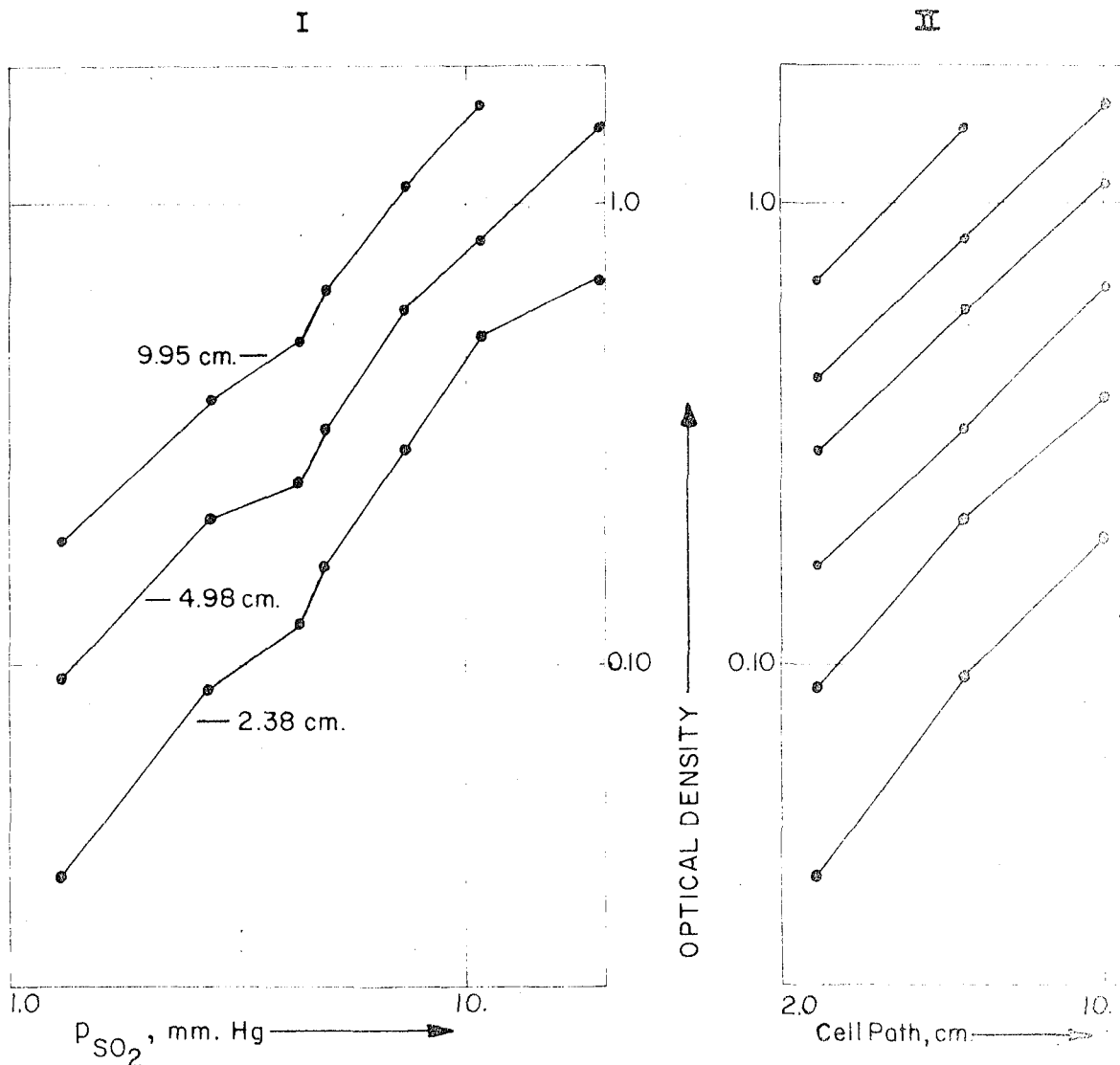
FIGURE 25:

SO₂ SELF-BROADENING

Log₁₀ (Optical Density) vs. $\begin{cases} \text{Log}_{10} (p_{\text{SO}_2}) & \text{I} \\ \text{Log}_{10} (\text{Cell Path}) & \text{II} \end{cases}$

Beer's law is obeyed, indicating absence of unresolved fine structure.

No pressure effect occurs
above 1. mm.Hg.



order of magnitude larger than kinetic theory values. While smaller values of σ would not preclude the possibility of radiationless transitions to either a continuum or to discrete levels as the cause of broadening, less importance must be attached to such an explanation if the value of σ is not large. In any case, it is never wise to use pressure broadening as an unsupported proof of such transitions.

In the study which Marmo made of the NO absorption bands, the true pressure effect in NO self-broadening can be discerned in the data which he has published. The apparent absorption coefficient k decreases at first as $(\frac{1}{\sqrt{p_{NO}}})$, but after the pressure reaches 20 to 30 mm, the values of k level off and remain approximately constant (indicating that d is a linear function of p_{NO}). The Schumann-Runge bands of oxygen in the vacuum ultraviolet have been studied by Watanabe, Inn, and Zelikoff (21), using the same instrument and methods as Marmo employed. In a recent communication, Dr. K. Watanabe sent to us some values of k for those bands. The data extend over pressures from 7.2 to 491.0 mm oxygen in a 4.70 cm path, and the intensities of the bands are almost as large as those of NO. In this whole range, the absorption coefficient decreases steadily as $(\frac{1}{\sqrt{p_{O_2}}})$, and shows no trace of the deviations which NO exhibits. The study of the pressure broadening effect in the Schumann-Runge bands of oxygen would therefore make an extremely interesting investigation, and would provide an interesting complement to the value of σ for NO.

The results which have been obtained in this investigation give no evidence for a strong radiationless transition. The most reasonable conclusion is that the molecule does not show unusual or "abnormal" pressure broadening when the criteria of a quantitative description are applied. The remote possibility of a collision diameter as large as 9 Å remains if the absolute intensity measurement is not used. However, a simple explanation can be made of even a diameter as large as 9 Å:

If one uses the united atom description of the NO molecule, then all the excited states of the system involve promotion of an electron to an orbit of higher principal quantum number. The resulting increase in the effective radius of sensitivity would account for the increase in σ .

From the standpoint of the general problem presented by unresolved fine structure, this work has shown that the specialized analysis we have used to determine σ is in principle reliable, provided an estimate of the absolute intensity is available. However, it must be remembered that the line intensities and spacing, the resolving power, and the optical path, while they may not drastically affect the general type of relationship obtained for the observed optical density, will delicately control its magnitude, and the displacement of the curve of growth relative to the experimental and theoretical parameters; so that it is not reliable to treat a general case with a model derived for a specific spectrum.

This may be an explanation of the reason why the Schumann-Runge bands of oxygen do not show a pressure effect at the pressure range where it appears in nitric oxide; the Schumann-Runge transition is ${}^3\Sigma_u^- - {}^3\Sigma_g^+$ and would be expected to have a radically different structure.

There is another method of obtaining collision diameters which has been used especially in the infrared region (23). This involves the determination of the absolute intensity just as our method does, but does not contain the problems of calculating the optical density at a specific frequency, since it deals with the behavior of the integrated absorption. On the other hand, it requires a knowledge of the integrated absorption over a considerable range of pressures, and in particular must involve data from the region where the contour is essentially that due to Lorentz broadening; and secondly, it has been applied up to the present only to spectra which are simpler in their structure than the bands we have studied. Therefore, while the method which has been used to estimate the collision diameter in this investigation is less certain, it does exist as an alternate method of analysis to that which has been commonly employed.

The example of nitric oxide has in any case demonstrated that it is well to use caution in the interpretation of apparent pressure effects in molecular spectra.

APPENDIX, PART I

DATA TABLE A: SELF-BROADENING IN NITRIC OXIDE

Values of optical density, d , versus pressure of NO, for paths 2.38, 4.98, 11.48 cm. Resolution 0.57 A at $\lambda 2157$, 0.32 A at $\lambda 2268$.

DATA TABLE B: NITROGEN BROADENING OF NITRIC OXIDE

Values of optical density versus total pressure for paths 2.38, 4.98, 9.95 cm. Resolution the same as above.

APPENDIX, PART I

TABLE A

NITRIC OXIDE SELF-BROADENING

Values of optical density, \bar{d} , versus p_{NO}
 A--2.38 cm cell; B--4.98 cm cell; CI--11.48 cm cell

p_{NO} , mm	1.04	1.76	2.05	3.27	3.37	4.75
cell, λ						
$\lambda 2149.5$						
A	0.066	0.080	0.082	0.089	0.111	0.131
B	0.091	0.111	0.103	0.126	0.127	0.153
CI	0.110	0.141	0.127	0.156	0.156	0.203
$\lambda 2152$						
A	0.010	0.016	0.019	0.010	0.022	0.033
B	0.023	0.020	0.029	0.033	0.030	0.047
CI	0.022	0.039	0.032	0.044	0.056	0.060
$\lambda 2155$						
A	0.042	0.049	0.050	0.056	0.064	0.073
B	0.059	0.062	0.072	0.073	0.071	0.084
CI	0.071	0.080	0.073	0.090	0.097	0.115
$\lambda 2157$						
A	0.027	0.039	0.038	0.043	0.052	0.063
B	0.046	0.053	0.053	0.068	0.070	0.089
CI	0.058	0.072	0.070	0.087	0.096	0.111
$\lambda 2260$						
A	0.063	0.071	0.075	0.080	0.083	0.110
B	0.079	0.099	0.097	0.111	0.119	0.144
CI	0.108	0.134	0.130	0.150	0.150	0.179
$\lambda 2262$						
A	0.047	0.040	0.047	0.049	0.063	0.065
B	0.051	0.059	0.052	0.067	0.076	0.079
CI	0.065	0.073	0.070	0.090	0.102	0.103
$\lambda 2264$						
A	0.002	0.003	0.004	0.006	0.012	0.017
B	0.002	0.012	0.012	0.017	0.014	0.024
CI	0.014	0.023	0.019	0.028	0.022	0.021
$\lambda 2267$						
A	0.041	0.054	0.041	0.059	0.062	0.079
B	0.060	0.074	0.063	0.077	0.078	0.096
CI	0.073	0.089	0.080	0.097	0.103	0.122
$\lambda 2268$						
A	0.027	0.032	0.030	0.040	0.040	0.065
B	0.041	0.047	0.053	0.069	0.064	0.090
CI	0.058	0.080	0.079	0.087	0.095	0.114

DATA TABLE A--Continued

NITRIC OXIDE SELF-BROADENING

Values of optical density, d , versus p_{NO}

p_{NO} , mm	8.20	8.80	12.72	15.80	17.15	19.90
cell, λ						
$\lambda 2149.5$						
A	0.140	0.152	0.198	0.217	0.240	0.279
B	0.195	0.200	0.266	0.304	0.345	0.405
CI	0.260	0.272	0.388	0.459	0.512	0.629
$\lambda 2152$						
A	0.030	0.034	0.051	0.060	0.055	0.067
B	0.056	0.054	0.073	0.090	0.092	0.110
CI	0.080	0.090	0.120	0.145	0.155	0.187
$\lambda 2155$						
A	0.088	0.086	0.110	0.120	0.130	0.150
B	0.110	0.111	0.147	0.163	0.184	0.221
CI	0.139	0.150	0.210	0.244	0.285	0.336
$\lambda 2157$						
A	0.064	0.079	0.098	0.096	0.111	0.129
B	0.091	0.100	0.124	0.125	0.150	0.173
CI	0.119	0.133	0.177	0.179	0.210	0.248
$\lambda 2260$						
A	0.141	0.148	0.177	0.191	0.215	0.240
B	0.169	0.186	0.239	0.259	0.287	0.347
CI	0.236	0.251	0.338	0.409	0.430	0.529
$\lambda 2262$						
A	0.076	0.080	0.108	0.106	0.124	0.135
B	0.100	0.100	0.131	0.143	0.173	0.209
CI	0.131	0.150	0.201	0.237	0.255	0.324
$\lambda 2264$						
A	0.025	0.022	0.033	0.032	0.030	0.029
B	0.033	0.028	0.039	0.041	0.045	0.054
CI	0.034	0.050	0.047	0.065	0.068	0.068
$\lambda 2267$						
A	0.085	0.096	0.121	0.119	0.130	0.142
B	0.102	0.119	0.147	0.163	0.179	0.217
CI	0.144	0.155	0.214	0.232	0.250	0.307
$\lambda 2268$						
A	0.063	0.080	0.103	0.089	0.106	0.123
B	0.094	0.095	0.120	0.119	0.145	0.169
CI	0.129	0.142	0.170	0.170	0.190	0.229

DATA TABLE A--Continued

NITRIC OXIDE SELF-BROADENING

Values of optical density, d , versus p_{NO}

p_{NO} , mm	24.13	29.00	35.05	39.85	45.3	47.00
cell, λ						
$\lambda 2149.5$						
A	0.330	0.359	0.460	0.548	0.554	0.624
B	0.481	0.540	0.697	0.832	0.855	0.950
CI	0.729	0.852	1.105	1.331	1.334	1.340
$\lambda 2152$						
A	0.085	0.098	0.120	0.133	0.149	0.150
B	0.134	0.154	0.180	0.210	0.240	0.240
CI	0.210	0.243	0.300	0.346	0.389	0.380
$\lambda 2155$						
A	0.172	0.192	0.236	0.299	0.286	0.315
B	0.260	0.274	0.357	0.435	0.444	0.493
CI	0.383	0.452	0.587	0.706	0.732	0.780
$\lambda 2157$						
A	0.140	0.136	0.184	0.205	0.200	0.232
B	0.190	0.198	0.266	0.312	0.306	0.343
CI	0.287	0.320	0.399	0.479	0.488	0.530
$\lambda 2260$						
A	0.274	0.304	0.377	0.448	0.462	0.500
B	0.401	0.457	0.582	0.680	0.730	0.780
CI	0.610	0.737	0.950	1.088	1.199	1.180
$\lambda 2262$						
A	0.156	0.169	0.222	0.269	0.267	0.300
B	0.240	0.250	0.340	0.403	0.400	0.468
CI	0.363	0.413	0.548	0.671	0.637	0.685
$\lambda 2264$						
A	0.038	0.040	0.055	0.065	0.070	0.070
B	0.060	0.079	0.077	0.084	0.110	0.108
CI	0.089	0.111	0.130	0.148	0.180	0.169
$\lambda 2267$						
A	0.168	0.179	0.230	0.260	0.252	0.286
B	0.235	0.252	0.328	0.390	0.400	0.440
CI	0.348	0.402	0.520	0.627	0.672	0.700
$\lambda 2268$						
A	0.135	0.145	0.178	0.193	0.180	0.225
B	0.180	0.179	0.240	0.278	0.261	0.305
CI	0.260	0.272	0.355	0.414	0.397	0.450

DATA TABLE A--Continued

NITRIC OXIDE SELF-BROADENING

Values of optical density, d , versus p_{NO}

p_{NO} , mm		58.3	75.5	100.4
cell, λ				
$\lambda 2149.5$	A	0.780	1.063	1.420
	B	1.227	1.597	1.903
	CI	1.763	1.97	-----
$\lambda 2152$	A	0.185	0.238	0.330
	B	0.298	0.395	0.542
	CI	0.486	0.670	0.923
$\lambda 2155$	A	0.403	0.569	0.765
	B	0.639	0.906	1.203
	CI	1.063	1.424	1.743
$\lambda 2157$	A	0.289	0.365	0.485
	B	0.432	0.581	0.780
	CI	0.670	0.937	1.250
$\lambda 2260$	A	0.636	0.884	1.208
	B	0.991	1.389	1.750
	CI	1.565	1.897	1.950
$\lambda 2262$	A	0.394	0.520	0.687
	B	0.591	0.792	1.015
	CI	0.954	1.222	1.498
$\lambda 2264$	A	0.089	0.117	0.152
	B	0.130	0.187	0.253
	CI	0.218	0.322	0.452
$\lambda 2267$	A	0.354	0.496	0.670
	B	0.552	0.789	1.090
	CI	0.942	1.299	1.653
$\lambda 2268$	A	0.259	0.340	0.434
	B	0.376	0.494	0.628
	CI	0.579	0.747	0.960

APPENDIX, PART I

DATA TABLE B

NITROGEN BROADENING OF NITRIC OXIDE

Values of optical density, d , versus P_{total}

A--2.38 cm cell; B--4.98 cm cell; C--9.95 cm cell

Series	1.0	1.1	1.2	1.3 *	3.0	3.1
P_{NO} , mm	4.20	4.20	4.20	4.20	5.25	5.25
$P_{\text{NO+N}_2}$, mm	4.20	15.00	26.25	36.2	5.25	16.45
$\lambda 2149.5$	A 0.117 B 0.128 C 0.162	0.123 0.166 0.204	0.128 0.175 0.242	0.097 0.150 0.230	0.126 0.144 0.177	0.148 0.178 0.247
$\lambda 2152$	A 0.022 B 0.040 C 0.054	0.032 0.038 0.057	0.024 0.034 0.060	0.015 0.028 0.050	0.030 0.042 0.054	0.040 0.050 0.072
$\lambda 2155$	A 0.073 B 0.070 C 0.090	0.074 0.093 0.115	0.078 0.096 0.134	0.057 0.073 0.130	0.068 0.082 0.098	0.087 0.110 0.132
$\lambda 2157$	A 0.060 B 0.063 C 0.078	0.060 0.070 0.100	0.050 0.067 0.090	0.030 0.052 0.086	0.055 0.078 0.100	0.062 0.085 0.108
$\lambda 2260$	A 0.092 B 0.120 C 0.140	0.111 0.140 0.181	0.110 0.152 0.218	0.088 0.140 0.227	0.108 0.130 0.168	0.128 0.172 0.216
$\lambda 2262$	A 0.060 B 0.063 C 0.080	0.060 0.080 0.124	0.070 0.092 0.130	0.056 0.088 0.137	0.060 0.077 0.091	0.072 0.097 0.124
$\lambda 2264$	A 0.006 B 0.022 C 0.028	0.015 0.020 0.032	0.024 0.022 0.042	0.015 0.037 0.052	0.012 0.022 0.030	0.015 0.028 0.038
$\lambda 2267$	A 0.068 B 0.083 C 0.098	0.078 0.088 0.110	0.070 0.097 0.130	0.054 0.090 0.135	0.074 0.080 0.103	0.077 0.104 0.124
$\lambda 2268$	A 0.047 B 0.067 C 0.090	0.047 0.066 0.090	0.038 0.077 0.100	0.038 0.053 0.093	0.052 0.074 0.095	0.062 0.094 0.106

DATA TABLE B--Continued

NITROGEN BROADENING OF NITRIC OXIDE

Values of optical density, d, versus P_{total}

Series	3.2	3.3	3.4	3.5	3.6	3.7
P_{NO}, mm	5.25	5.25	5.25	5.25	5.25	5.25
P_{NO+N_2}, mm	27.75	37.05	55.2	79.1	101.4	141.3
$\lambda 2149.5$						
A	0.163	0.182	0.207	0.198	0.210	0.245
B	0.210	0.250	0.272	0.282	0.313	0.342
C	0.273	0.304	0.340	0.398	0.428	0.510
$\lambda 2152$						
A	0.032	0.042	0.040	0.042	0.050	0.050
B	0.042	0.057	0.060	0.070	0.075	0.070
C	0.070	0.070	0.070	0.104	0.104	0.116
$\lambda 2155$						
A	0.087	0.103	0.108	0.108	0.120	0.140
B	0.110	0.127	0.140	0.150	0.156	0.182
C	0.143	0.158	0.175	0.206	0.227	0.248
$\lambda 2157$						
A	0.062	0.074	0.072	0.---	0.---	0.---
B	0.084	0.098	0.098	0.100	0.110	0.110
C	0.105	0.118	0.125	0.145	0.160	0.160
$\lambda 2260$						
A	0.140	0.140	0.158	0.156	0.175	0.178
B	0.186	0.203	0.240	0.238	0.250	0.284
C	0.251	0.284	0.320	0.337	0.367	0.414
$\lambda 2262$						
A	0.078	0.087	0.102	0.094	0.107	0.107
B	0.103	0.122	0.144	0.128	0.147	0.173
C	0.147	0.177	0.188	0.193	0.228	0.286
$\lambda 2264$						
A	0.026	0.020	0.022	0.022	0.024	0.022
B	0.034	0.025	0.035	0.035	0.035	0.035
C	0.052	0.064	0.064	0.044	0.060	0.058
$\lambda 2267$						
A	0.088	0.097	0.100	0.090	0.097	0.106
B	0.105	0.127	0.140	0.140	0.148	0.169
C	0.155	0.174	0.192	0.204	0.210	0.243
$\lambda 2268$						
A	0.060	0.058	0.058	0.050	0.052	0.054
B	0.090	0.087	0.100	0.094	0.090	0.092
C	0.115	0.133	0.144	0.130	0.140	0.146

DATA TABLE B--Continued

NITROGEN BROADENING OF NITRIC OXIDE

Values of optical density, d , versus P_{total}

Series	3.8	3.9	3.10	4.0	4.1	4.2
P_{NO} , mm	5.25	5.25	5.25	12.6	12.6	12.6
$P_{\text{NO+N}_2}$, mm	200.7	272.5	429.9	12.6	19.6	25.3
$\lambda 2149.5$ A B C	0.267 0.397 0.590	0.300 0.452 0.670	0.335 0.540 0.818	0.174 0.237 0.340	0.212 0.280 0.397	0.261 0.316 0.480
$\lambda 2152$ A B C	0.060 0.090 0.120	0.056 0.095 0.150	0.058 0.110 0.162	0.050 0.070 0.113	0.057 0.088 0.123	0.070 0.082 0.140
$\lambda 2155$ A B C	0.142 0.204 0.297	0.162 0.240 0.348	0.173 0.278 0.420	0.102 0.120 0.180	0.118 0.148 0.207	0.144 0.165 0.260
$\lambda 2157$ A B C	0.075 0.125 0.180	0.080 0.124 0.200	0.080 0.188 0.235	0.082 0.103 0.138	0.099 0.121 0.156	0.110 0.124 0.187
$\lambda 2260$ A B C	0.198 0.318 0.490	0.218 0.353 0.552	0.235 0.420 0.666	0.162 0.216 0.293	0.190 0.247 0.330	0.208 0.282 0.398
$\lambda 2262$ A B C	0.118 0.190 0.270	0.178 0.202 0.305	0.140 0.240 0.377	0.092 0.118 0.157	0.098 0.138 0.191	0.132 0.162 0.226
$\lambda 2264$ A B C	0.026 0.040 0.080	0.030 0.044 0.083	0.030 0.052 0.090	0.028 0.043 0.051	0.030 0.041 0.053	0.034 0.037 0.053
$\lambda 2267$ A B C	0.114 0.180 0.270	0.117 0.208 0.308	0.127 0.234 0.360	0.103 0.130 0.153	0.106 0.147 0.196	0.127 0.168 0.228
$\lambda 2268$ A B C	0.054 0.098 0.167	0.056 0.103 0.176	0.050 0.098 0.190	0.082 0.113 0.127	0.084 0.120 0.148	0.104 0.124 0.177

DATA TABLE B--Continued

NITROGEN BROADENING OF NITRIC OXIDE

Values of optical density, d , versus P_{total}

Series	4.3	4.4	4.5	4.6	4.7	4.8
P_{NO} , mm	12.6	12.6	12.6	12.6	12.6	12.6
$P_{\text{NO+N}_2}$, mm	33.1	43.2	52.7	67.3	67.3	80.4
$\lambda 2149.5$ A	0.264	0.287	0.312	0.358	0.338	0.380
B	0.362	0.403	0.431	0.485	0.468	0.485
C	0.500	0.582	0.632	0.672	0.674	0.760
$\lambda 2152$ A	0.065	0.070	0.076	0.077	0.082	0.088
B	0.092	0.106	0.110	0.110	0.120	0.113
C	0.140	0.151	0.160	0.170	0.169	0.200
$\lambda 2155$ A	0.137	0.155	0.170	0.182	0.183	0.200
B	0.178	0.216	0.231	0.251	0.240	0.260
C	0.272	0.299	0.317	0.340	0.348	0.400
$\lambda 2157$ A	0.113	0.108	0.116	0.122	0.124	0.131
B	0.136	0.157	0.164	0.175	0.218	0.177
C	0.182	0.204	0.227	0.240	0.240	0.272
$\lambda 2260$ A	0.214	0.254	0.270	0.294	0.283	0.320
B	0.306	0.342	0.370	0.419	0.390	0.437
C	0.443	0.497	0.541	0.587	0.580	0.673
$\lambda 2262$ A	0.130	0.162	0.157	0.174	0.170	0.172
B	0.175	0.200	0.210	0.234	0.218	0.240
C	0.238	0.284	0.300	0.337	0.318	0.368
$\lambda 2264$ A	0.033	0.036	0.034	0.047	0.042	0.050
B	0.053	0.050	0.058	0.067	0.053	0.080
C	0.072	0.079	0.080	0.088	0.100	0.110
$\lambda 2267$ A	0.130	0.146	0.158	0.181	0.170	0.180
B	0.180	0.200	0.220	0.239	0.217	0.248
C	0.253	0.280	0.300	0.325	0.320	0.378
$\lambda 2268$ A	0.092	0.103	0.107	0.114	0.108	0.118
B	0.132	0.140	0.152	0.172	0.153	0.170
C	0.176	0.192	0.210	0.223	0.220	0.240

DATA TABLE B--Continued

NITROGEN BROADENING OF NITRIC OXIDE

Values of optical density, d , versus P_{total}

Series	4.9	4.10	4.11	4.12	4.13	4.14	
P_{NO} , mm	12.6	12.6	12.6	12.6	12.6	12.6	
$P_{\text{NO+N}_2}$, mm	97.3	120.3	154.5	188.7	227.3	300.7	
$\lambda 2149.5$	A	0.400	0.471	0.520	0.560	0.600	0.678
	B	0.530	0.597	0.673	0.723	0.796	-----
	C	0.810	0.910	1.040	1.111	1.200	1.380
$\lambda 2152$	A	0.092	0.108	0.112	0.124	0.130	0.140
	B	0.122	0.132	0.144	0.159	0.174	-----
	C	0.205	0.220	0.290	0.260	0.285	0.320
$\lambda 2155$	A	0.210	0.237	0.258	0.280	0.303	0.347
	B	0.270	0.298	0.340	0.362	0.393	-----
	C	0.423	0.475	0.542	0.574	0.690	0.758
$\lambda 2157$	A	0.140	0.157	0.160	0.173	0.180	0.210
	B	0.177	0.205	0.210	0.235	0.250	-----
	C	0.270	0.310	0.370	0.375	0.480	0.498
$\lambda 2260$	A	0.340	0.390	0.437	0.458	0.492	-----
	B	0.472	0.524	0.580	0.648	0.700	0.840
	C	0.758	0.813	0.920	1.024	1.110	1.293
$\lambda 2262$	A	0.197	0.217	0.239	0.256	0.282	-----
	B	0.264	0.296	0.317	0.352	0.380	0.450
	C	0.393	0.428	0.482	0.530	0.580	0.668
$\lambda 2264$	A	0.048	0.053	0.060	0.063	0.068	-----
	B	0.079	0.088	0.094	0.104	0.110	0.124
	C	0.112	0.125	0.132	0.140	0.160	0.188
$\lambda 2267$	A	0.190	0.216	0.240	0.242	0.270	-----
	B	0.262	0.291	0.328	0.348	0.381	0.447
	C	0.400	0.440	0.496	0.543	0.597	0.717
$\lambda 2268$	A	0.127	0.136	0.140	0.141	0.150	-----
	B	0.171	0.190	0.200	0.216	0.230	0.255
	C	0.278	0.288	0.310	0.331	0.350	0.408

DATA TABLE B--Continued

NITROGEN BROADENING OF NITRIC OXIDE

Values of optical density, d , versus P_{total}

Series	4.15	4.16	5.0	5.1	5.2	5.3
P_{NO}, mm	12.6	12.6	5.0	5.0	5.0	5.0
P_{NO+N_2}, mm	408.9	514.1	5.0	11.8	16.2	23.7
$\lambda 2149.5$ A	0.783	0.850	0.120	0.149	0.148	0.150
B	1.078	1.197	0.148	0.188	0.208	0.224
C	1.565	1.652	0.188	0.245	0.265	0.300
$\lambda 2152$ A	0.158	0.165	0.035	0.042	0.032	0.030
B	0.224	0.292	0.050	0.048	0.050	0.050
C	0.370	0.395	0.060	0.068	0.073	0.072
$\lambda 2155$ A	0.400	0.440	0.075	0.077	0.088	0.097
B	0.562	0.637	0.093	0.105	0.110	0.120
C	0.890	0.976	0.108	0.136	0.147	0.160
$\lambda 2157$ A	0.230	0.235	0.068	0.077	0.068	0.062
B	0.338	0.370	0.085	0.092	0.093	0.098
C	0.560	-----	0.108	0.122	0.128	0.129
$\lambda 2260$ A	0.630	0.678	0.103	0.123	0.132	0.137
B	0.920	1.040	0.132	0.158	0.171	0.190
C	1.472	1.595	0.158	0.204	0.228	0.254
$\lambda 2262$ A	0.348	0.377	0.070	0.080	0.078	0.081
B	0.505	0.551	0.078	0.094	0.103	0.113
C	0.760	0.848	0.090	0.125	0.137	0.158
$\lambda 2264$ A	0.088	0.100	0.020	0.020	0.022	0.024
B	0.140	0.149	0.024	0.024	0.030	0.032
C	0.216	0.245	0.028	0.032	0.040	0.040
$\lambda 2267$ A	0.340	0.362	0.076	0.083	0.080	0.088
B	0.497	0.562	0.082	0.103	0.110	0.122
C	0.813	0.913	0.110	0.130	0.136	0.162
$\lambda 2268$ A	0.173	0.177	0.052	0.071	0.058	0.063
B	0.270	0.282	0.073	0.091	0.088	0.096
C	0.440	0.470	0.097	0.111	0.113	0.132

DATA TABLE B--Continued

NITROGEN BROADENING OF NITRIC OXIDE

Values of optical density, d , versus P_{total}

Series	5.4	5.5	5.6	5.7	5.8	5.9	
P_{NO} , mm	5.0	5.0	5.0	5.0	5.0	5.0	
$P_{\text{NO+N}_2}$, mm	33.3	47.9	59.3	82.8	101.2	145.0	
$\lambda 2149.5$	A	0.160	0.170	0.180	0.200	0.216	-----
	B	0.244	0.282	0.291	0.325	0.363	0.436
	C	0.350	0.390	0.408	0.488	0.527	0.630
$\lambda 2152$	A	0.027	0.036	0.037	0.040	0.044	-----
	B	0.053	0.047	0.057	0.070	0.073	0.078
	C	0.085	0.085	0.090	0.098	0.092	0.115
$\lambda 2155$	A	0.097	0.100	0.103	0.117	0.123	-----
	B	0.136	0.148	0.160	0.172	0.194	0.233
	C	0.197	0.196	0.224	0.252	0.262	0.313
$\lambda 2157$	A	0.063	0.062	0.067	0.070	0.071	-----
	B	0.108	0.106	0.120	0.130	0.131	0.147
	C	0.136	0.152	0.169	0.180	0.186	0.205
$\lambda 2260$	A	0.142	0.143	0.153	0.164	0.162	-----
	B	0.210	0.230	0.248	0.275	0.297	0.329
	C	0.290	0.322	0.350	0.412	0.445	0.514
$\lambda 2262$	A	0.087	0.089	0.090	0.103	0.112	-----
	B	0.138	0.147	0.153	0.170	0.180	0.210
	C	0.185	0.204	0.220	0.258	0.280	0.311
$\lambda 2264$	A	0.022	0.030	0.030	0.025	0.030	-----
	B	0.023	0.042	0.048	0.050	0.052	0.036
	C	0.050	0.060	0.062	0.063	0.072	0.072
$\lambda 2267$	A	0.087	0.088	0.097	0.108	0.106	-----
	B	0.134	0.148	0.165	0.161	0.190	0.203
	C	0.180	0.200	0.206	0.242	0.262	0.278
$\lambda 2268$	A	0.063	0.060	0.057	0.061	0.055	-----
	B	0.098	0.095	0.110	0.108	0.124	0.120
	C	0.147	0.160	0.153	0.177	0.183	0.187

DATA TABLE B--Continued

NITROGEN BROADENING OF NITRIC OXIDE

Values of optical density, d , versus P_{total}

Series	6.0	6.1	6.2	6.3	6.4	6.5
P_{NO} , mm	27.2	27.2	27.2	27.2	27.2	27.2
$P_{\text{NO+N}_2}$, mm	27.2	46.0	70.3	95.0	123.0	162.0
$\lambda 2149.5$ A	0.349	0.476	0.578	0.666	0.777	0.912
B	0.500	0.670	0.810	0.962	1.050	1.172
C	0.730	0.984	1.122	1.347	1.425	1.556
$\lambda 2152$ A	0.086	0.116	-----	0.144	0.163	0.177
B	0.140	0.167	0.182	0.208	0.225	0.287
C	0.212	0.256	0.263	0.300	0.337	0.374
$\lambda 2155$ A	0.200	0.255	0.300	0.346	0.394	0.490
B	0.270	0.358	0.430	0.490	0.534	0.605
C	0.333	0.517	0.585	0.702	0.778	0.880
$\lambda 2157$ A	0.142	0.190	0.205	0.238	0.268	0.320
B	0.197	0.256	0.293	0.332	0.348	0.383
C	0.278	0.356	0.387	0.450	0.491	0.550
$\lambda 2260$ A	0.291	0.377	0.468	0.533	0.614	0.688
B	0.402	0.540	0.654	0.767	0.858	0.984
C	0.597	0.802	0.920	1.088	1.240	1.403
$\lambda 2262$ A	0.173	0.225	0.278	0.304	0.347	0.404
B	0.287	0.314	0.370	0.432	0.482	0.536
C	0.354	0.463	0.517	0.605	0.683	0.762
$\lambda 2264$ A	0.048	0.060	0.069	0.072	0.082	0.102
B	0.063	0.072	0.084	0.102	0.112	0.133
C	0.100	0.112	0.128	0.162	0.180	0.204
$\lambda 2267$ A	0.174	0.227	0.259	0.301	0.342	0.384
B	0.231	0.297	0.367	0.420	0.467	0.540
C	0.338	0.450	0.500	0.607	0.698	0.797
$\lambda 2268$ A	0.130	0.153	0.190	0.200	0.222	0.250
B	0.172	0.217	0.247	0.286	0.316	0.338
C	0.238	0.300	0.325	0.383	0.424	0.480

DATA TABLE B--Continued

NITROGEN BROADENING OF NITRIC OXIDE

Values of optical density, d , versus P_{total}

Series	6.6	6.7	
P_{NO} , mm	27.2	27.2	
P_{NO+N_2} , mm	198.6	253.4	
$\lambda 2149.5$ A B C	0.946 1.362 1.682	1.077 1.481 1.827	
$\lambda 2152$ A B C	0.196 0.285 0.402	0.210 0.306 0.448	
$\lambda 2155$ A B C	0.478 0.720 1.022	0.567 0.807 1.134	
$\lambda 2157$ A B C	0.307 0.454 0.621	0.340 0.502 0.712	
$\lambda 2260$ A B C	0.763 1.143 1.548	0.892 1.290 1.705	
$\lambda 2262$ A B C	0.438 0.627 0.835	0.498 0.701 0.958	
$\lambda 2264$ A B C	0.100 0.153 0.223	0.114 0.184 0.254	
$\lambda 2267$ A B C	0.417 0.620 0.899	0.480 0.710 1.037	
$\lambda 2268$ A B C	0.264 0.385 0.518	0.287 0.414 0.582	

DATA TABLE B--Continued

NITROGEN BROADENING OF NITRIC OXIDE

Values of optical density, d , versus P_{total}

Series	7.0	7.1	7.2	7.3	7.4	7.5	
P_{NO} , mm	2.21	2.21	2.21	2.21	2.21	2.21	
$P_{\text{NO+N}_2}$, mm	2.21	4.35	10.7	17.9	32.3	63.3	
$\lambda 2268$	A	.042	.041	.038	.038	.029	.029
	B	.053	.059	.061	.057	.047	.044
	C	.072	.085	.093	.087	.085	.089
Series	7.6	7.7	8.0	8.1	8.2	8.3	
P_{NO} , mm	2.21	2.21	5.3	5.3	5.3	5.3	
$P_{\text{NO+N}_2}$, mm	98.7	203.7	5.3	14.4	22.9	29.3	
$\lambda 2268$	A	.029	.029	.061	.048	.052	.056
	B	.044	.046	.075	.075	.082	.086
	C	.097	.102	.096	.095	.100	.111
Series	8.4	8.5	8.6	8.7	8.8	8.9	
P_{NO} , mm	5.3	5.3	5.3	5.3	5.3	5.3	
$P_{\text{NO+N}_2}$, mm	38.9	53.5	68.2	90.3	125.1	165.2	
$\lambda 2268$	A	.051	.050	.048	.048	.049	.047
	B	.085	.082	.095	.099	.105	.111
	C	.119	----	.124	.138	.148	.162
Series	8.10	8.11	9.0	9.1	9.2	9.3	
P_{NO} , mm	5.3	5.3	10.8	10.8	10.8	10.8	
$P_{\text{NO+N}_2}$, mm	222.3	393	10.8	22.0	30.6	49.3	
$\lambda 2268$	A	----	.048	.083	.082	.082	.090
	B	.120	.119	.100	.105	.109	.117
	C	.176	.192	.122	.131	.149	.180

DATA TABLE B--Continued

NITROGEN BROADENING OF NITRIC OXIDE

Values of optical density, d , versus P_{total}

Series	9.4	9.5	
p_{NO} , mm	10.8	10.8	
$P_{\text{NO+N}_2}$, mm	87.1	138.5	
$\lambda 2268$ A	.091	.093	
B	.128	.140	
C	.220	.250	

* Series 2 was discarded.

APPENDIX, PART II

CALCULATION OF THE CORRELATION FACTOR BETWEEN
THEORETICAL AND EXPERIMENTAL OPTICAL PATHS

Weber and Penner (22) give the value of a quantity S , which has the units $\text{cm}^{-2}\text{atm}^{-1}$, and is defined as follows:

$$S = (\ln 10) \frac{d}{dx} \int_{\text{band}} d \, dz \quad \begin{array}{l} \nu \text{ in cm}^{-1} \\ x \text{ in cm-atm.} \end{array}$$

When the lines are broadened into one another, as is the case in the experiments of Weber and Penner, S has a very simple interpretation; it is just the integral of the absorption coefficient over the band,

$$S = \int_{\text{band}} f_{\epsilon}(\nu) \, d\nu$$

The value given by Weber and Penner for S is $8,830 \text{ cm}^{-2}\text{atm}^{-1}$.

Now,

$$\int_{\text{band}} f_{\epsilon}(\nu) \, d\nu = C_1 \sum_{\text{band}} S_j e^{-\frac{E_j}{kT}} \int_{\text{line}} f(\nu) \, d\nu$$

here $S_j e^{-\frac{E_j}{kT}}$ are the relative intensities of the lines, C_1 is an "absolute intensity constant" whose value is to be determined, and the remaining factor comes from the integral of line contour. To find the correlation we shall use

Lorentz contours and the Lorentz calculations. We normalize

$\int_{line} f(\nu) d\nu$ to the value 1.00 cm^{-1} , and C_1 is accordingly adjusted. The sum $\sum_J S_J e^{-\frac{E_J}{kT}}$ is carried out using the same model as was used for the calculations, namely that spin splitting for the ${}^2\Sigma^+$ state and the Λ -type doubling are negligibly small. The sum of the S_J for a given J is $2J+1/2$ for each of the sub-bands, ${}^2\Sigma^+ - {}^2\Pi_{1/2}$ and ${}^2\Sigma^+ - {}^2\Pi_{3/2}$. The energy levels can be written as follows:

$$E_J = hc[B_{01}J(J+1) - 3/4 B_{01}], \text{ referred to } J=\frac{1}{2} \text{ of } {}^2\Pi_{1/2}$$

$$E_J = hc[B_{02}J(J+1) + 120.77 - 3/4 B_{02}], \text{ referred to}$$

$$J=\frac{1}{2} \text{ of } {}^2\Pi_{1/2}$$

$$B_{01} = 1.67 \text{ cm}^{-1}, B_{02} = 1.72 \text{ cm}^{-1}; T = 300^\circ\text{K}.$$

The sum computed is then the following:

$$\sum_J S_J e^{-\frac{E_J}{kT}} = \frac{1}{2} \left[\sum_{J=\frac{1}{2}}^{\infty} (2J+1) e^{-\frac{E_J({}^2\Pi_{1/2})}{kT}} + \sum_{J=\frac{3}{2}}^{\infty} (2J+1) e^{-\frac{E_J({}^2\Pi_{3/2})}{kT}} \right] = 95.6$$

from which we obtain $C_1 = 92.4$.

Then for a single Lorentz line, the integrated absorption coefficient is

$$\int_{line} f_t(\nu) d\nu = (92.4) S_J e^{-\frac{E_J}{kT}} \text{ cm}^{-2} \text{ atm}^{-1}.$$

The relative intensities given in Table 2, Section V, for the band model are given by $\frac{S_J e^{-\frac{E_J}{kT}}}{1.392}$ (the factor 1.392

was introduced for graphical simplicity). The line used was normalized to a value 1.00 at its center for a half-width $\alpha_L = 0.10 \text{ cm}^{-1}$. This means that the integral is

$$\int_{\text{line}} f'(v) dz = \frac{\pi(0.10)}{2} \text{ cm}^{-1}$$

Finally, before multiplying by the path factors X' of the Lorentz calculation, the absorption coefficient was multiplied by a second graphical factor 1.13.

We may then state the following equality:

$$(x, \text{cm-atm.}) (92.4 S_J e^{-\frac{E_J}{kT}}) = X' \frac{\pi(0.10)}{2} \frac{1.13}{1.39} S_J e^{-\frac{E_J}{kT}}$$

from which we deduce that $X'/x = 723$. The X' spoken of here is related to the X of Figure 23 by a factor of 1.667 (Section V, page 88). Therefore, the correlation factor is $X/x = 1.588$, where X is the theoretical optical path of Figure 23, and x is in the units cm-mm.

REFERENCES

1. R. S. Mulliken, Revs. Mod. Phys. (1932) 4, 1-86.
2. M. Lambrey, Comptes Rendues (1929) 189, 574-575;
(1930) 190, 261-263; Annales de Physique (1930) 14,
95-183.
3. J. Mayence, Ann. de Physique (1952) 7, 453-505.
4. F. F. Marmo, Ph.D. Dissertation, Harvard 1952.
5. (a) O. R. Wulf, Phys. Rev. (1934) 46, 316.
(b) G. Herzberg, "Spectra of Diatomic Molecules"
(1950), 432.
6. S. M. Naudé, Phys. Rev. (1930) 36, 333-346.
7. A. G. Gaydon and A. R. Fairbairn, Proc. Phys. Soc.
(London) (1954) A LXVII, 474-476.
8. H. Margenau and W. W. Watson, Revs. Mod. Phys. (1936)
8, 22-53.
9. J. Holtzmark, Phys. Zeits. (1924) 25, 73-84.
10. R. Karplus and J. Schwinger, Phys. Rev. (1948) 73,
1020-1026.
11. J. H. Van Vleck and V. F. Weisskopf, Revs. Mod. Phys.
(1945) 17, 227-236.
12. R. Ladenburg and F. Reiche, Annalen der Physik (1913)
42, 181-210.
13. D. M. Dennison, Phys. Rev. (1928) 31, 503-519.
14. W. M. Elsasser, Harvard Meteorological Studies Bulletin
(1938) #6, Part II.

15. S. S. Penner and H. S. Tsien, J. Chem. Phys. (1952) 20, 827-828.
16. G. Herzberg, "Spectra of Diatomic Molecules" (1950), 205.
17. S. S. Penner and R. W. Kavanagh, J. Opt. Soc. Am. (1953) 43, 385-388.
18. W. L. Miller and A. R. Gordon, J. Phys. Chem. (1931) 35, 2877-2884.
19. M. C. Teves, Zeits. fur Phys. (1928) 48, 244-258.
20. J. Franck, H. Sponer, and E. Teller, Zeits. Physik. Chem. (1932) B 18, 88-101.
21. K. Watanabe, E. C. Y. Inn, and M. Zelikoff, J. Chem. Phys. (1953) 21, 1026-1030.
22. D. Weber and S. S. Penner, to be published (J. Chem. Phys.)
23. S. S. Penner and D. Weber, J. Chem. Phys. (1951) 19, 807-816, 817-818, 974-975.

PROPOSITIONS

1. L. J. Bellamy (1) has found a linear correlation between the out-of-plane C-H bending frequencies of 1,3 disubstituted- and 1,3,5 trisubstituted-benzenes and the Hammett m - σ -values of the substituents. He found that best agreement for halogen substituents is obtained if the σ -values assigned to them are about zero instead of the values of 0.35 quoted by Hammett. A tentative explanation of this deviation is proposed.

2. In their investigation of the infrared spectrum of N_2O_3 , d'Or and Tarte (2) failed to consider the pressure broadening of the nitrogen dioxide bands. Their frequency assignments are consequently doubtful, and it is proposed that a reinvestigation of the spectrum be made taking account of the broadening.

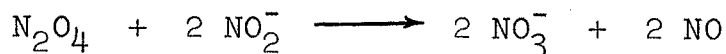
3. It is suggested that the ionic structure proposed by Mayence, Robin, and Vodar (3) for the molecular association between nitrogen and nitric oxide at high pressures is an unreasonable one, and a more simple description is offered.

4. Laurene, Campbell, Wiberley, and Clark (4) have suggested that the hydronium ion which is extracted with the ferric chloride complex from hydrochloric acid solutions by isopropyl ether has a preferential coordination of four water molecules.

(a) It is proposed that the co-extraction of water with other materials extractable by isopropyl ether be studied. Examples might be: other metal complex anions such as AuCl_4^- and SbCl_4^- , and oxygen acids like H_3PO_4 and HClO_4 .

(b) The solubilities of hydrochloric acid and water together in isopropyl ether are much greater than either of their independent solubilities. It is proposed that an attempt be made to determine the amount of HCl which is unsolvated by water in the ether phase, by means of the infrared spectrum.

5. It is proposed that at least one of the steps in the involved arguments of Szabo, Bartha, and Lakatos (5) for the bridge structure of N_2O_4 is incorrect, namely their claim that the reaction



does not take place in a neutral iodide solution. Their data to show this are interpreted in another way, and a clear method of proving which is correct is set forward.

6. It is proposed that the correlation made by Kross and Fassel (6) between the A_1 "X-sensitive" frequency of substituted benzenes and the substituent electronegativity is purely fortuitous.

7. The approximate infrared fundamental frequencies of the methylene and amino radicals are predicted with the use of the valence force approximation:

	cm ⁻¹	cm ⁻¹	cm ⁻¹
CH ₂	2903	1379	2947
NH ₂	3350	1498	3400

A somewhat larger splitting (~ 100 cm⁻¹) between the stretching frequencies may be expected as the result of interactions.

8. McMahon (7) presents evidence for the complete preferential orientation of certain polar aromatic compounds by solidification in a magnetic field. He implies that this is accomplished by the individual orientation of the molecules because of their diamagnetic anisotropy.

(a) It is proposed that a cooperative effect must be postulated to explain the orientation.

(b) It is suggested that the materials so solidified be analyzed by x-ray diffraction for evidence of preferred orientation of the molecules, and that the diamagnetic anisotropy be studied. Information obtained from single crystals of the same compounds would provide interesting comparisons.

9. The use of the standard micro-pycnometric method to determine the densities of the small crystals of Ag-Sr compounds now under investigation in this laboratory is not conveniently feasible because of rapid oxidation by the air. Flotation methods are ineffective because of the high density. A method for reasonably accurate density determinations is proposed for the special case of crystals containing silver.

10. Little is known about the state of N₂O₃ (liq.). The intense blue color has been attributed to the dimer (8) but

there is no convincing evidence of the existence of such a dimer. The color may arise from a charge-transfer interaction between the two components of N_2O_3 .

(a) It is proposed that the nuclear magnetic resonance spectrum of the liquid in a very slight excess of N_2O_4 be studied. If paramagnetic electron broadening may be avoided, the presence of chemical shifts will throw light on the structure of N_2O_3 .

(b) If paramagnetism of the electrons is detected, the electron resonance should provide information about the dissociation of the liquid into NO and NO_2 .

11. A labor saving method is pointed out for determining whether a number is prime when tables are not available. Its simplicity makes it worth remembering for mental computation.

REFERENCES FOR PROPOSITIONS

1. L. J. Bellamy, J. Chem. Soc. (1955), 2818-2822.
2. L. d'Or and P. Tarte, Bull. Soc. Roy. Sci. de Liege (1953), 22, 276-284.
3. J. G. Mayence, S. Robin, and P. Vodar, Comptes Rend. (1952), 234, 1357-1359.
4. A. H. Laurene, D. E. Campbell, S. E. Wiberley, and H. M. Clark, J. Phys. Chem. (1956), 60, 901-904.
5. Z. Szabo, L. Bartha, and B. Lakatos, J. Chem. Soc. (1956), 1784-1795.
6. R. D. Kross and V. A. Fassel, J.A.C.S. (1955) 77, 5858-5859.
7. W. McMahon, J.A.C.S. (1956), 78, 3290-3294.
8. B. M. Jones, J. Chem. Soc. (1914) 105, 2310-2322.